Process Development for Manufacturing Stochastic Peptide Microarrays

Zur Erlangung des akademischen Grades eines
DOKTORS DER INGENIEURSWISSENSCHAFTEN (Dr.-Ing.)
von der KIT-Fakultät für Maschinenbau des
Karlsruher Instituts für Technologie (KIT)
angenommene

DISSERTATION

von

M.Sc. Roman Popov

Tag der mündlichen Prüfung:	20. März 2018
Hauptreferent:	apl. Prof. Dr. Alexander Nesterov-Müller
Korreferenten:	Prof. Dr. Jan Korvink
	Prof. Dr.-Ing. Matthias Franzreb

Abstract

Tackling the challenges of developing therapies for cancer, infections, or immune system disorders requires understanding and manipulation of the metabolic pathways related to a disease state or a pathogen. An essential role in the corresponding biochemical cascades is played by proteins of various types, whose functions are manifested through their interactions with other molecules. In basic and applied research, the functionality and binding properties of proteins are more often studied using peptide microarrays, which are collections of protein fragments displayed on a solid support in a spot array format.

Commercially available peptide microarrays are manufactured using various methods, which result in different spot densities and costs per spot. While being relatively simple and straightforward to implement, the wide-spread SPOT-technique provides less than a thousand of peptides on a standard size substrate, which is not sufficient for many biological applications. At the other extreme, the lithographic method enables the synthesis of several million spots per substrate, however, at high manufacturing costs, which makes them unaffordable for many researchers. Thereby, the market need for high-density peptide microarrays at a moderate price remains still unmet.

Within the framework of the present work, a new method for manufacturing low-cost high-density peptide microarrays was developed and optimized. Successful project implementation resulted in a novel type of peptide microarray, which is referred in the present dissertation as a stochastic peptide microarray. It contains nearly 3 million synthetic peptides per substrate at material costs of around €250. This was made possible by combining the basic principles and methods of microstructure technology, solid-phase peptide synthesis, and the phenomenon of self-organization of microbeads on a microstructured substrate.

Kurzfassung

Um die Herausforderungen der Entwicklung von Therapien gegen Krebs, Infektionen oder Störungen des Immunsystems zu bewältigen, müssen die Stoffwechselwege, die mit einem Krankheitszustand oder einem Krankheitserreger in Zusammenhang stehen, verstanden und manipuliert werden. Eine wesentliche Rolle in den entsprechenden biochemischen Kaskaden spielen Proteine verschiedener Art, deren Funktionen sich in Wechselwirkungen mit anderen Molekülen manifestieren. In der Grundlagen- und angewandten Forschung werden die Funktionalität und die Bindungseigenschaften von Proteinen immer häufiger unter Verwendung von Peptidmikroarrays untersucht, bei denen es sich um Sammlungen von Proteinfragmenten handelt, die auf einem festen Träger in einem Spot-Array-Format immobilisiert werden.

Auf dem Markt erhältliche Peptidmikroarrays werden mit verschiedenen Methoden hergestellt, die zu unterschiedlichen Spotdichten und Kosten pro Spot führen. Obwohl sie relativ einfach und unkompliziert zu implementieren ist, liefert die weit verbreitete SPOT-Technik weniger als tausend Peptide auf einem Objektträger, was für viele biologische Anwendungen nicht ausreichend ist. Im anderen Extrem ermöglicht das lithographische Verfahren die Synthese von mehreren Millionen Spots pro Substrat, jedoch bei hohen Herstellungskosten, was sie für viele Forscher unerschwinglich macht. Dadurch bleibt der Marktbedarf nach hochdichten Peptidmikroarrays zu einem moderaten Preis unerfüllt.

Im Rahmen der vorliegenden Arbeit wurde ein neues Verfahren zur Herstellung von kostengünstigen hochdichten Peptidmikroarrays entwickelt und optimiert. Die erfolgreiche Projektrealisierung führte zu einem neuartigen Peptidmikroarray, das in der vorliegenden Arbeit als stochastisches Peptidmikroarray bezeichnet wird. Es enthält fast 3 Millionen synthetische Peptide pro Substrat bei Materialkosten von rund 250 €. Möglich wurde dies durch die Kombination der Grundlagen und Methoden der Mikrostrukturtechnik und der Festphasen-Peptidsynthese, sowie auch des Phänomens der Selbstorganisation von Mikropartikeln auf einem mikrostrukturierten Substrat.

Table of Contents

List of Figures

List of Tables

List of Abbreviations and Symbols

Abbreviations

AFM	atomic force microscopy
Ala	alanine
Arg	arginine
Asn	asparagine
Asp	aspartic acid
a.u.	arbitrary unit
Boc	*tert*-butoxycarbonyl moiety
bromine silane	2-bromo-*N*-(3-triethoxysilyl propyl) isobutyramide
CMOS	complementary metal-oxide-semiconductor
CV	coefficient of variation
Cys	cysteine
DBSCAN	density-based spatial clustering of applications with noise
DCM	dichloromethane
DIPEA	*N*,*N*-diisopropylethylamine
DMD	digital micromirror device
DMF	*N*,*N*-dimethylformamide
DPF	*N*,*N*-diphenylformamide
DSLR	digital single-lens reflex (camera)
EM	expectation-maximization (clustering)
Fmoc	9-fluorenylmethoxycarbonyl moiety
Fmoc-Gly-OPfp	Fmoc-glycine pentafluorophenyl ester
FWHM	full width at half maximum
Gln	glutamine
Glu	glutamic acid
Gly	glycine
His	histidine
HPLC	high-performance liquid chromatography

HTS	high-throughput screening
Ile	isoleucine
IMT	Institute of Microstructure Technology
KIT	Karlsruhe Institute of Technology
LED	light-emitting diode
Leu	leucine
Lys	lysine
MEA	*N*-methylethylamine
Met	methionine
MMA	methyl methacrylate
NHS	*N*-hydroxysuccinimide
OPfp	orthopentafluorophenyl moiety
Pbf	2,2,4,6,7-pentamethyl-2,3-dihydrobenzofuran-5-sulfonyl
PBS-T	phosphate buffer saline with TWEEN 20
PEG	poly(ethylene glycol)
PEGMA	poly(ethylene glycol) methacrylate
Phe	phenylalanine
PMMA	poly(methyl methacrylate)
PMT	photomultiplier tube
10:90-poly(PEGMA-co-MMA)	graft copolymer film consisting of 10 % (n/n) PEGMA and 90 % (n/n) PMMA
Pro	proline
PTFE	polytetrafluoroethylene
QD	quantum dot
RIE	reactive ion etching
SAM	self-assembled monolayer
SD	standard deviation
SEM	scanning electron microscopy
Ser	serine
siATRP	surface-initiated atom transfer radical polymerization
SPG	Shirasu Porous Glass
SPPS	solid-phase peptide synthesis
TAMRA	5(6)-carboxytetramethyl rhodamine

*t*Bu	*tert*-butyl moiety
TFA	trifluoroacetic acid
Thr	threonine
TIBS	triisobutilsilane
Trp	tryptophan
Trt	trityl moiety
TWEEN 20	polyoxyethylene (20) sorbitan monolaurate
Tyr	tyrosine
UV	ultraviolet
Val	valine

Symbols

A	Hamaker constant
C	concentration
c	speed of light
D	diffusion constant
d	diameter
E	energy
F	force
H	gap width
h	Planck constant
k	Boltzmann constant
m	mass
P	pressure
q	charge
R	universal gas constant
r	radius
T	temperature
T_B	boiling point
V_m	molar volume
v	velocity
γ	surface tension

ε_r	relative permittivity
ε_0	vacuum permittivity
ε_c	neighborhood radius
η	dynamic viscosity
θ	contact angle
λ	wavelength
μ	coefficient of friction
Ø	diameter
% (m/m)	mass fraction
% (n/n)	mole fraction
% (v/v)	volume fraction

1 Introduction

1.1 Background and Context

Research and development of new pharmaceuticals requires significant investments of capital, time, and labor. On average, it takes 10 to 15 years and $2.6 billion to bring a new drug to the market [1]. At the same time, less than 10 % of discovered drug candidates result in an approved medicine [2].

Advancing the understanding of the disease and drug action mechanisms has the potential for reducing the costs and risks of drug discovery. Of a particular importance in the regulation of biological processes are protein-protein interactions. The study of these interactions reveals new approaches for rational drug design [3].

1.1.1 Proteins and Peptides

Proteins are essential components of all living organisms. They play an important role in metabolism, cell signaling, immune response, and cell cycle. The functionality of proteins is substantially defined by their composition and structure.

The majority of proteins are built from continuous series of 20 different types of proteinogenic amino acids linked together via peptide bonds (Figure 1). Depending on the biological species, the median length of the protein chains ranges between 300 and 400 amino acid residues [4]. The amino acid sequence determines the folding of

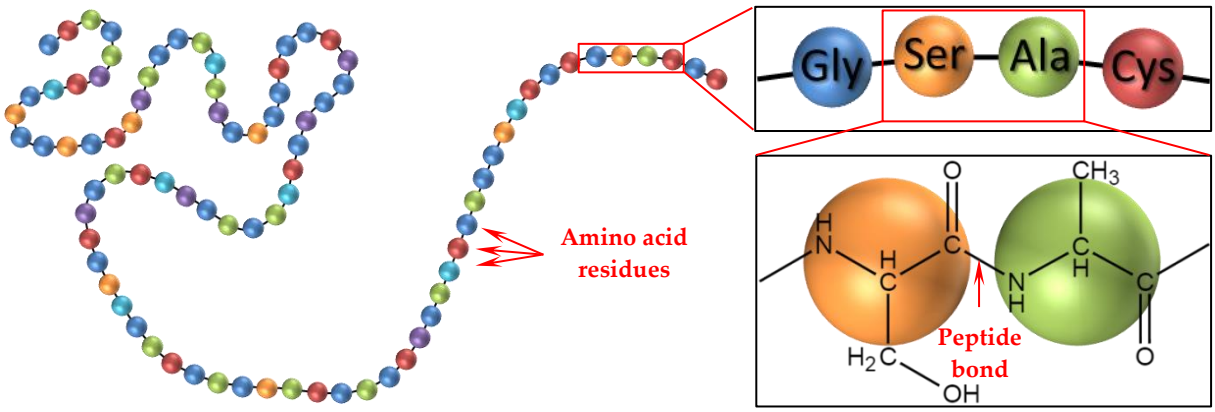

Figure 1. Schematic illustration of the protein structure. Amino acid residues, arranged in a specific linear sequence and linked together via peptide bonds, form the primary structure of a protein.

the protein into its distinct three-dimensional structure (Figure 2). Only in its native spatial conformation, the protein is capable to demonstrate its biological activity.

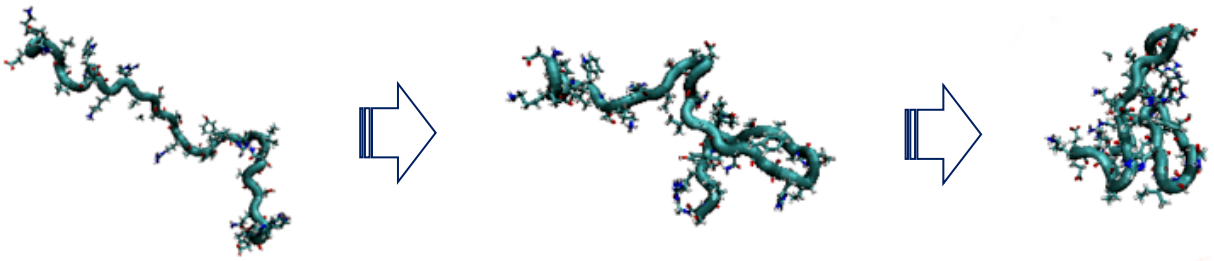

Figure 2. Schematic illustration of the protein folding. The primary structure of a protein (left) undergoes a sequence of conformational transitions (middle) resulting in a biologically active native configuration (right) ("Schematic representation of a protein folding pathway", adapted from **[5]** by F. Faccioli under a CC BY-NC-SA license, https://creativecommons.org/licenses/by-nc-sa/4.0/deed.en).

The functions of a protein are manifested through its interactions with other molecules, which occur via surface accessible interaction sites (Figure 3). The interaction site can involve a linear segment of the protein chain (a linear epitope) or it can consist of two or more segments brought together by the folded structure of the molecule (a conformational epitope). The study of the interaction sites of a protein is crucial for understanding the mechanism of its action and influencing its functionality.

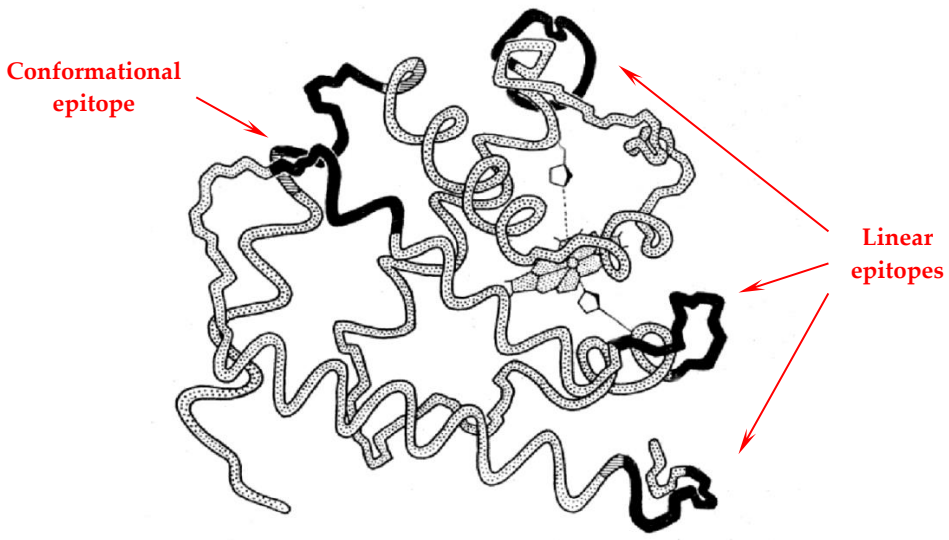

Figure 3. Schematic illustration of the surface accessible interaction sites of a protein. Linear epitopes are formed by a continuous fragment of the protein chain, while conformational epitopes are composed of two or more segments brought together by the folded structure of the protein (adapted from **[6]** with permission of Springer Nature).

The localization of the interaction sites in a protein can be predicted using computational methods [7]. However, these methods rely on background information on both the amino acids sequence and the structure of the protein, which are not available at the same time in most cases. Moreover, the simulation results are associated with high uncertainties and often require experimental validation.

Experimental methods allow for prediction and characterization of the protein binding sites without preliminary knowledge of the protein structure. To simplify the problem, quite complex protein-protein interactions can be reduced to peptide-protein interactions. In this approach, one of the proteins is replaced by a multitude of its short fragments (peptides), some of which mimic the protein interaction sites responsible for binding with another protein (Figure 4).

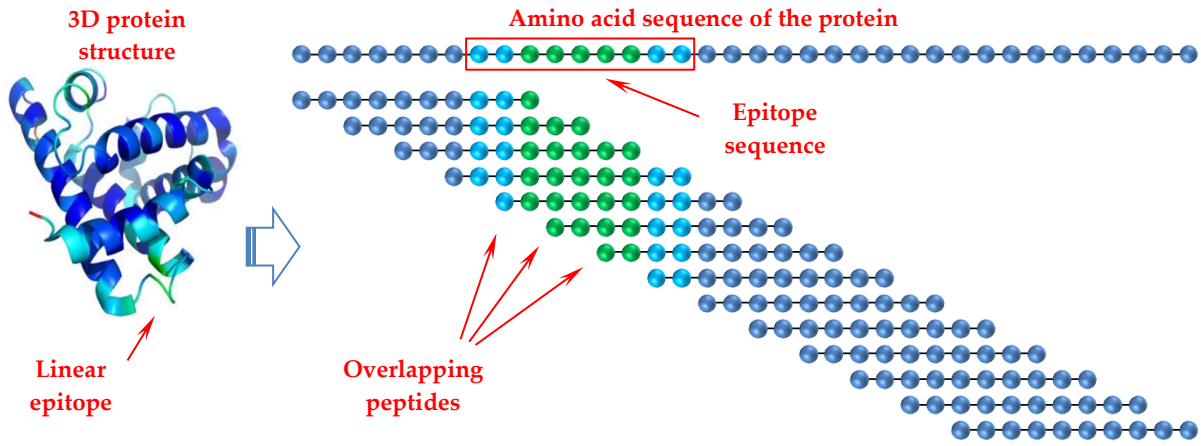

Figure 4. Representation of a protein as a multitude of its overlapping short fragments. The protein in its tertiary structure is represented by a set of peptides derived from its amino acid sequence. The peptides containing the epitope sequence can mimic surface accessible interaction sites of the protein.

Peptides are relatively short linear molecules consisting of less than 50 amino acid residues linked by peptide bonds [8]. They can be synthesized using standard chemistry and tested in terms of their affinity to a certain binder. The results of such studies can be used for characterization of the protein-protein interactions.

Identifying the binding sites implies synthesis and characterization of a multitude of peptides derived from the protein sequence. Addressing this task in a timely and cost-effective manner requires continuous development and implementation of novel high-throughput screening (HTS) tools. One of the most prominent screening tools for protein-protein interaction studies are peptide microarrays.

1.1.2 Peptide Microarrays

A peptide microarray, also referred to as a peptide chip, is a collection of various amino acid sequences arranged on a solid support in a spot array format (Figure 5). Each spot of the microarray represents a multitude of identical peptides, whereas various spots generally contain different peptides. The amino acid sequence in each spot is defined during peptide microarray fabrication, while the information on their spatial allocation constitutes a molecular library of a given peptide microarray. Since the molecules are covalently bound the substrate, a parallel high-throughput screening of their chemical, biological, or functional activity becomes possible.

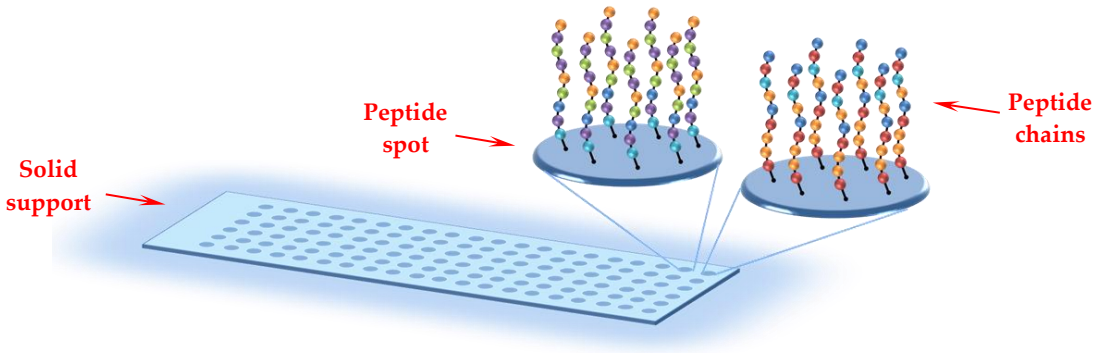

Figure 5. Schematic illustration of a peptide microarray. A multitude of identical peptides is confined within each spot on a solid support, while various spots generally contain different peptides.

The bioassay concept based on peptide microarrays is shown in Figure 6. A peptide chip containing a known molecular library is incubated with a biological sample, which can be patient or animal sera, enzymes, antibodies, cells, or cell lysates. The analyte components interact with the peptides displayed on the substrate and bind to those molecules that demonstrate sufficient affinity. The non-bound analyte components are removed during subsequent washing steps. In order to visualize the spots containing the peptides with high affinity to the biological sample, the analyte can be fluorescently labelled prior to the incubation. Alternatively, the analyte components bound to the peptides can be tagged with fluorescently labelled antibodies in an additional staining step. Both approaches enable visualization of the remaining analyte on the microarray by fluorescence readout techniques. By collating the resulting fluorescence spot pattern with the peptide microarray library, both binding and non-binding amino acid sequences can be identified.

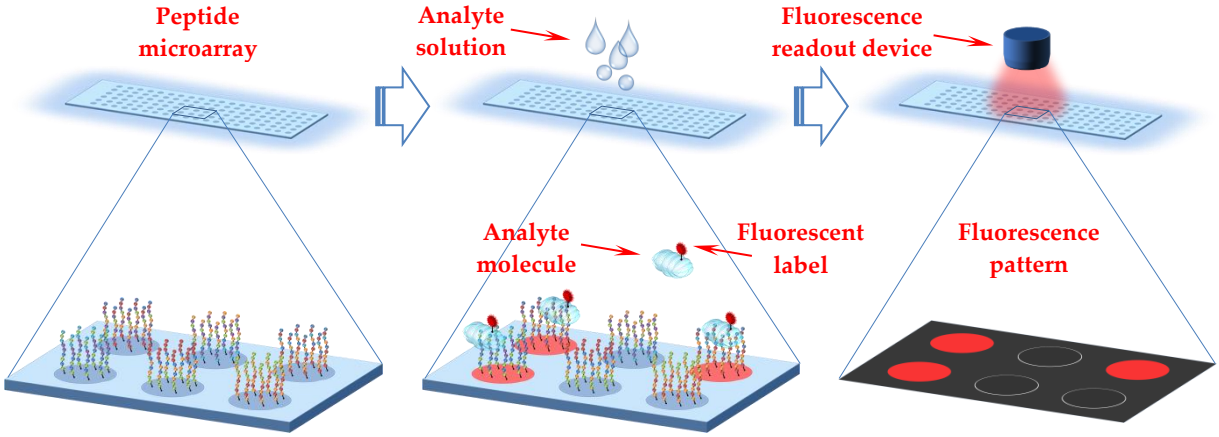

Figure 6. Principle of the bioassay using peptide microarrays. A peptide microarray with a defined molecular library (left) is incubated with an analyte. Fluorescently labelled analyte components selectively interact with the peptides displayed on the substrate (middle), which can be visualized using fluorescence readout techniques (right).

Using peptide microarrays for high-throughput screening assays enables the parallel testing of thousands of peptides in terms of their interaction with a certain analyte. It makes them suitable for diverse applications in the fields of immunology and proteomics, such as antibody epitope mapping [9, 10, 11], seromarker discovery [12, 13], enzyme profiling [14, 15], etc. Data acquired with peptide microarrays can lead to the discovery of new drugs, vaccines, and diagnostic tools. The scope and the quality of the acquired data depend on the type of the peptide microarray and its main characteristics.

There are several features that distinguish peptide microarrays from each other. The primary parameter is the composition of the molecular library, which can be specific, random, or combinatorial. The latter two types are used to screen for active peptides without preliminary information on the biological system to be studied. Combinatorial libraries are supposed to cover all possible amino acid sequence variations, which is practically impossible in most cases. For instance, the theoretical number of 10-mer peptides that can be generated out of 20 proteinogenic amino acids results in 20^{10} combinations, which exceeds the capacity of modern peptide microarrays by 7 orders of magnitude. Random peptide libraries, containing randomized peptide sequences, allow for much higher sequence variation within a limited microarray capacity, thus increasing the chance to find a molecule with a high biological activity.

Peptides differentiate from each other not only by their amino acid sequence but also by their length and structure. Most frequently, the peptides synthesized directly on a planar substrate consist of 10 to 15 amino acid residues [16]. Shorter amino acid sequences are usually not of an interest since they rarely demonstrate biological or chemical activity. Longer peptides cannot be quantitatively synthesized due to the limitations of their on-surface synthesis. In terms of their structure, the peptides displayed on the substrate can be linear or cyclic. The latter are of a great interest in many applications since their rigid cyclic structure facilitates binding, which results in higher affinity of cyclic peptides compared to linear amino acid sequences.

Another important attribute of a peptide microarray is the size of its molecular library, which is defined by the number of peptide spots displayed on a substrate. This parameter determines how many binding interactions can be tested in parallel within a single experiment. The size of the microarray library depends on the spot density, which in turns is limited by the capabilities of the manufacturing method.

The quality of a peptide microarray is crucial for evaluation and interpretation of the experimental results. It can be defined by the purity and identity of the amino acid sequences displayed in each spot. Depending on the manufacturing method, the peptides are either synthesized directly on the surface or pre-synthesized using standard bead-based synthesis. Both approaches are limited by reaction yields in each synthesis step resulting in contamination of the desired end-product by numerous by-products. To avoid false positive results, additional steps of peptide purification are required, which is impossible in case of on-surface peptide synthesis.

1.1.3 Solid-Phase Peptide Synthesis

Virtually all the methods of peptide microarray manufacturing are based on the principles of the solid-phase peptide synthesis (SPPS) developed in the early 1960s by R. B. Merrifield [17]. Compared to the classical liquid-phase approach, the solid-phase technique greatly simplified the process of peptide synthesis and significantly improved the product yield. Due to its advantages and possibility to be automated, SPPS became a standard method for low, medium and large-scale production of synthetic peptides. Using excessive amounts of reagents, it allows for a routine assembly of an arbitrary peptide with the length of up to 40 amino acid residues [18].

The method of solid-phase peptide synthesis is based on a stepwise assembling of peptides on an insoluble functionalized polymeric material. Being anchored to the solid support, peptide chains are synthesized by sequential coupling of each amino acid to the terminal end of the growing oligomer. To avoid any unintended reactions during coupling, the amino acids are protected at their amino group and, if applicable, at their side chain group. Immobilization of the molecules on the solid support enables their simple filtering and intermediate washing to remove the excess of the reagents and the process by-products after each chemical step.

Porous polymer microbeads are commonly used as a solid support for peptide synthesis. They are preliminary functionalized with a special "linker" that serves as a starting point for the growth of a peptide chain. Despite the fact the peptides are synthesized on the solid-phase material, the reagents are supplied to the reaction sites from the liquid phase. To maintain the physical state of the microbeads, they are made of a cross-linked polymer, which is resistant to the chemicals used during SPPS. In an appropriate solvent, the microbeads swell forming a gel-like medium, which facilitates the diffusion of the reagents inside the solid support. Since the chemical reactions take place in a microheterogeneous system, it enhances the process kinetics and results in a higher product yield.

The general scheme of the solid-phase peptide synthesis is shown in Figure 7. A polymer microbead is functionalized with a "linker" **L** bearing a hydroxyl group (**-OH**) and serves as a solid support for peptide synthesis. The amino acids are protected at the α-amino group (**-NPG**) and, if applicable, at the side chain group (**-SPG**). The activated α-carboxyl group of the first amino acid reacts with the hydroxyl group of the "linker" resulting in a covalent attachment of the amino acid residue to the solid support. The excess of the reagents and the reaction by-products are removed in a subsequent washing step. Thereafter, the *N*-α-protecting group is cleaved in a deprotection process revealing the α-amino group (**-NH$_2$**) of the first amino acid residue. After the washing step is performed, the second amino acid couples to the α-amino group of the first amino acid residue. The cycle of deprotection, washing, coupling, and washing is repeated multiple times until the desired amino acid sequence is synthesized. Thereafter, the remaining protecting groups are removed from the peptide chain. In a subsequent cleavage step, the peptide is released from the solid support resulting in the final product.

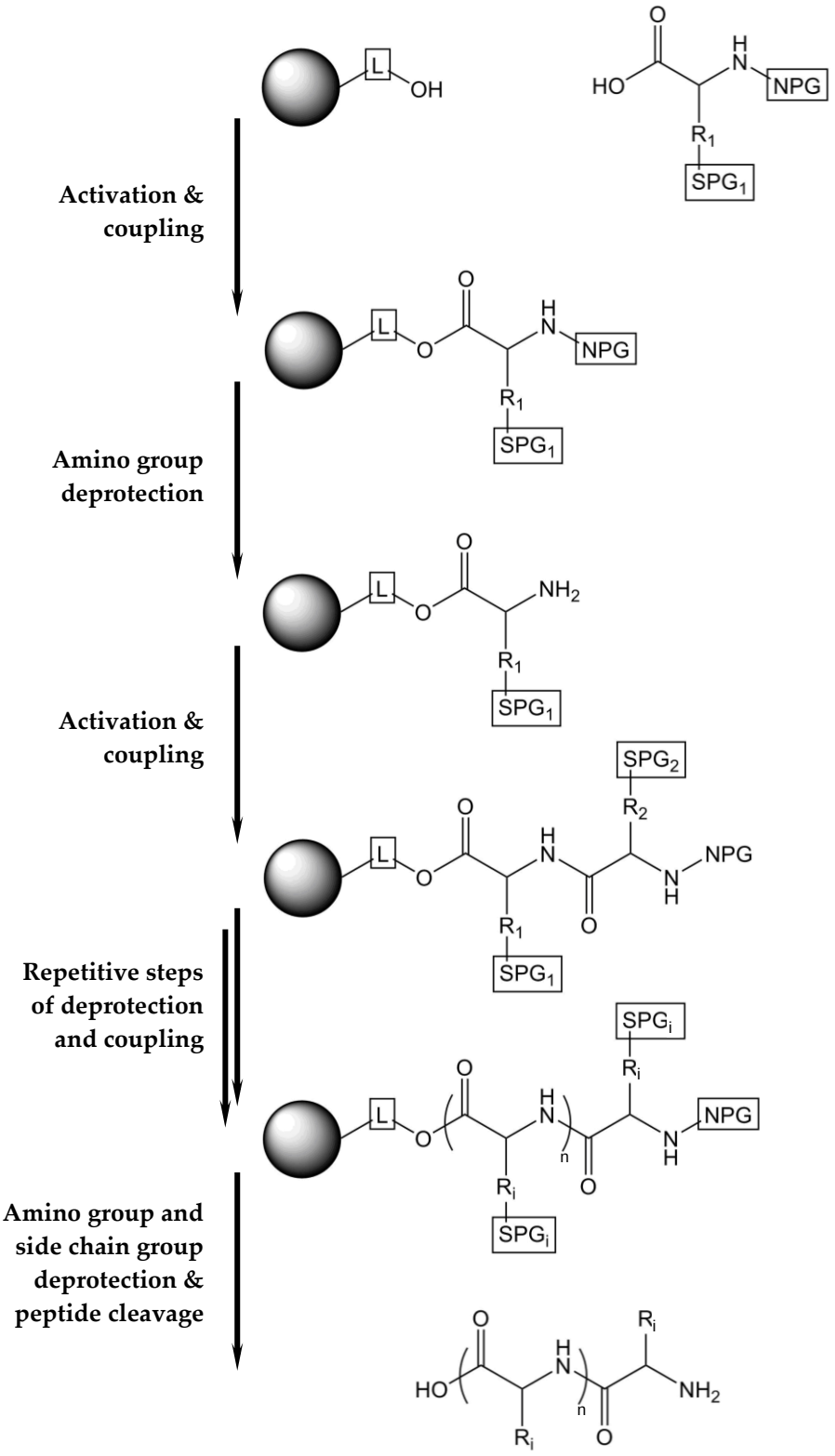

Figure 7. Schematic illustration of solid-phase peptide synthesis. Peptides are synthesized on polymer microbeads by sequential coupling of the amino acid derivatives, activated at α-carboxyl group and protected at α-amino group (-NPG) and side chain group (-SPG), with intermediate deprotection of the terminal α-amino group (washing steps are not shown).

The chemical steps of coupling and deprotection are characterized by their yield, which is generally lower than 100 %. This circumstance imposes limitations on SPPS in terms of the maximum length of the peptide chain that can be synthesized with a required product output. As depicted in Figure 8, the product yield depends on the number of repetitive process cycles performed during peptide synthesis. The green, blue and red curves demonstrate the exponential decrease of the longer-chain product output under the assumption that each process cycle results in a yield of 99 %, 95 %, and 90 %, respectively. For example, in case of the 99 % yield per process cycle, the synthesis of a 20-mer peptide would result in 82 % product output, whereas in case of the 95 % yield the product output would be 36 %. The product output of 12 % would result from the peptide synthesis with the 90 % yield in each process cycle. In each case, the final product will be contaminated by undesired amino acid sequences.

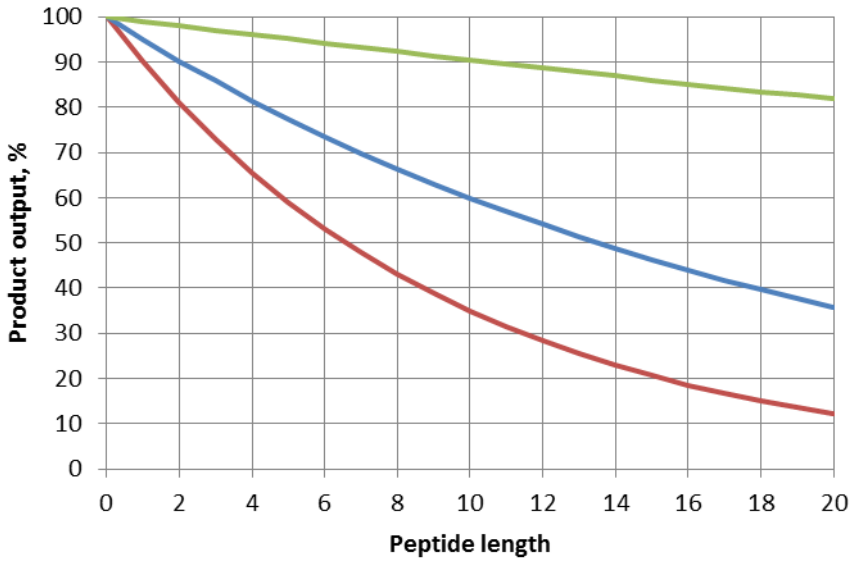

Figure 8. Relative product output as a function of the peptide chain length (in number of amino acid residues). The curves are built under assumption that each synthesis cycle results in a coupling yield of 99 % (green), 95 % (blue), and 90 % (red).

SPPS can be routinely performed with special synthesizers that automate and simplify the process of peptide synthesis. They enable generation of peptide libraries within a short period of time. The synthesized peptides can be further applied in peptide microarray manufacturing using the spotting method.

1.1.4 State-of-the-Art Manufacturing Methods

Constant development of novel technologies improves the features of peptide microarrays with an aim to make them more competitive against the microarrays of the previous generations. Currently, there is no generally accepted industrial standard for peptide microarray manufacturing. Each manufacturing strategy demonstrates its own strengths and weaknesses.

There are two main approaches for manufacturing peptide microarrays. A set of peptides can be synthesized in advance and then immobilized on a substrate in a spot array format. An alternative approach involves peptide synthesis directly on the surface of the substrate. The manufacturing methods based on the second approach differ from each other mainly by the means of generating an amino acid deposition pattern prior to each coupling step.

Spotting method

The spotting method involves the preliminary synthesis of a set of peptides and their direct transfer and coupling to the substrate in a spot array format. The pool of peptides is pre-synthesized using automated peptide synthesizers that employ standard SPPS. Thereafter, the peptides are spotted onto the substrate by an automated arrayer (Figure 9). To enable immobilization of the spotted peptides, the substrate is suitably derivatized. Functionalized glass or membrane substrates are commonly used as solid supports for the spotted peptide microarrays.

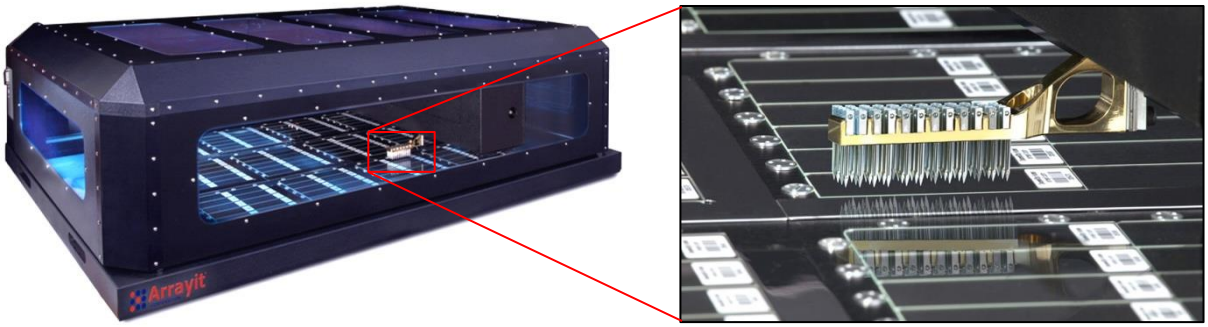

Figure 9. Microarrayer for high-throughput microarray manufacturing. Pre-synthesized peptides are printed on substrate slides in a spot array format (image credit: Arrayit Corporation).

The spotted microarrays possess several advantages compared to the microarrays with *in situ* synthesized peptides. Since each peptide is pre-synthesized in big quantities, it can be spotted multiple times being implemented within various

peptide microarray libraries. It results in more efficient and cheaper manufacturing of peptide microarray replicas. Using standard SPPS allows for longer peptide chains to be synthesized with a good product yield, which are later immobilized on a solid support. Moreover, the pre-synthesized peptides can be purified and validated prior to their transfer onto the substrate. This results in better quality of the spotted microarrays and ensures the reliability of the screening results.

The main limitation of the spotting method is the lack of flexibility and the high costs associated with the manufacturing of a custom microarray containing peptides that are not available in the pre-synthesized library. With the minimum synthesis time of one week and the price starting at €25 for a 10-mer peptide, the manufacturing of a single spotted peptide microarray can turn out to be quite expensive and time-consuming [16].

Another disadvantage of the spotting method is a very small size of the peptide library that can be displayed on a single chip. Since the peptides are transferred onto the substrate in a dissolved form, they tend to spread over the substrate surface prior to their immobilization. Generally, a spot size of approximately 1 mm in diameter can be achieved using the spotting method. It results in the average spot density of 25 spots/cm^2, which corresponds to around 400 spots per standard 75 mm x 25 mm substrate.

SPOT-method

The SPOT-synthesis, first presented by R. Frank in 1990, employs an alternative approach for manufacturing peptide microarrays [19]. Instead of spotting pre-synthesized peptides onto the substrate, they are assembled directly on a planar support in a spot array format using simultaneous parallel solid-phase peptide synthesis. The principle of the SPOT-method is depicted in Figure 10. A functionalized porous cellulose membrane commonly serves as a solid support for *in situ* peptide synthesis. Small droplets containing individual amino acid derivatives are dispensed onto the membrane according to a defined array pattern. Each droplet is absorbed by the membrane resulting in a circular spot, which can be treated as a confined individual chemical reactor. Being activated at their C-terminus and protected at their N-terminus, amino acid derivatives couple within their respective spots to the functional groups of the solid support. Washing steps are performed to

remove non-coupled amino acids and reaction by-products from the membrane. Thereafter, the α-amino groups of the immobilized amino acids are deprotected, and the washing step is carried out once again. By repeating the steps of amino acid deposition, coupling, washing, deprotection, and washing, a multitude of individual peptides can be synthesized in parallel in the distinct spots of the peptide microarray.

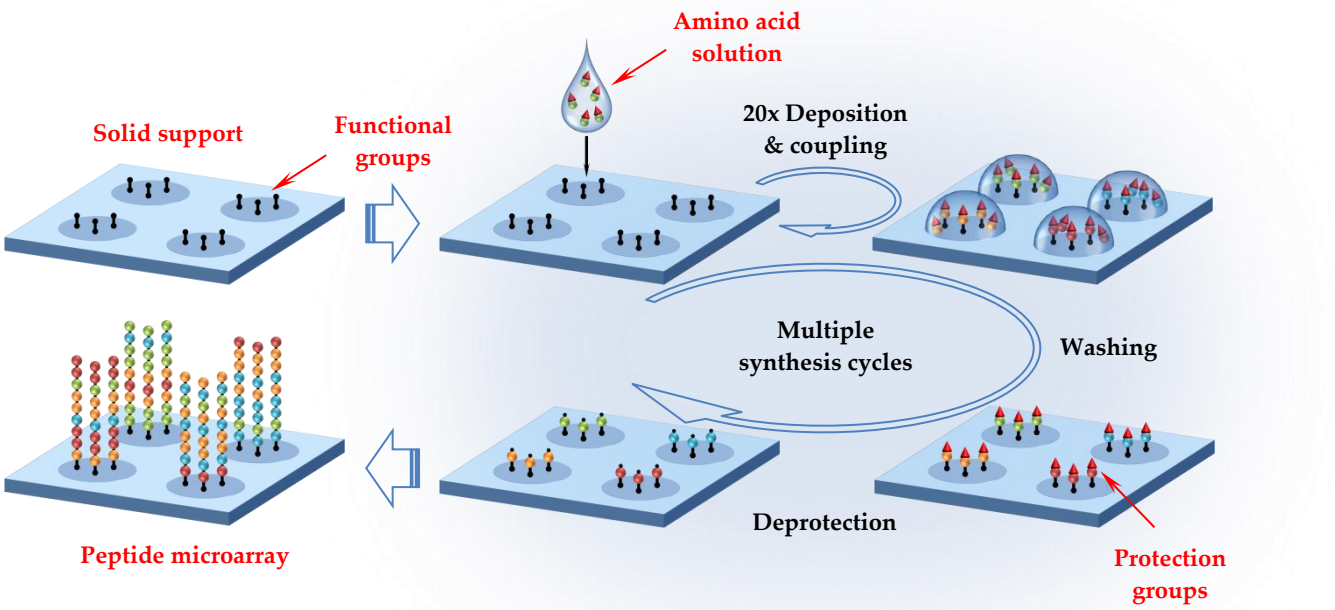

Figure 10. Schematic illustration of the SPOT-method for peptide microarray manufacturing. Peptides are synthesized *in situ* on a solid support by sequential spot-wise deposition of individual activated amino acid derivatives in dissolved form, their coupling to free functional groups, substrate washing and amino group deprotection. The synthesis cycle is performed multiple times until the desired peptide library is synthesized on the substrate.

The SPOT-technique became widespread due to flexibility and reliability of the manufacturing procedure. Using automated pipetting systems (Figure 11), a large number of different peptides can be synthesized relatively fast and in small amounts. Due to low consumption of reagents and simultaneous synthesis of the desired library, the manufacturing of a custom peptide microarray using the SPOT-method is less expensive compared to the spotting method. For commercially available peptide microarrays, the average price per spot falls within the range of €6 – €9 [16].

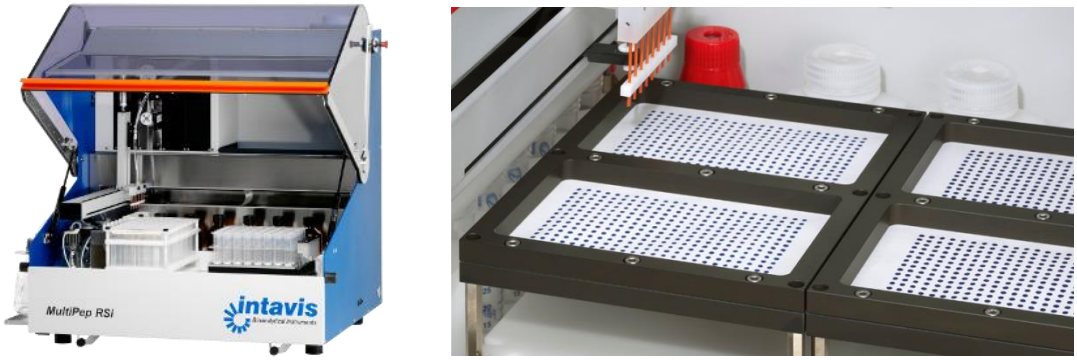

Figure 11. Automated pipetting system for *in situ* peptide synthesis on a membrane (image credit: INTAVIS Bioanalytical Instruments AG).

Besides the obvious advantages, the SPOT-technique has a number of drawbacks. Based on conventional solid-phase peptide synthesis, the SPOT-method results in peptides of quite a low purity. In the case of peptide microarrays available on the market, typical purities of >70% were reported for the peptide chains consisting of 6 to 15 amino acid residues [20]. In contrast to the peptide microarrays based on pre-synthesized and spotted libraries, the purification of *in situ* synthesized peptides is practically impossible. To partially overcome this problem, an additional capping step is generally introduced to the synthesis cycle after each coupling step. It involves acetylation of the free α-amino groups, which previously applied amino acids did not couple to. The capped sequences cannot take part in the further chain elongation. As a result, the desired peptides in each spot will be contaminated only by truncations of the target sequences. It ensures meaningful results when performing bioassays using microarrays with *in situ* synthesized peptide libraries.

The density of the microarrays manufactured using the SPOT-method is limited by the size of the spots that can be generated during dispensing of the amino acid solutions [21]. Due to natural wettability of the surface, the spot sizes are typically 1.0 mm in diameter [16]. It leads to the spot densities of approximately 25 spots/cm^2 or 400 spots per standard 75 mm x 25 mm substrate.

Xerographic method

The xerographic method, also referred to as the particle-based synthesis, is another example of an *in situ* technique for manufacturing high-density peptide microarrays [22]. The conventional solid-phase peptide synthesis is implemented to generate a peptide library in an array format on a planar surface. In contrast to the SPOT-method, the amino acid derivatives are deposited onto the substrate while being embedded into the polymer matrix of the microparticles. Spatially defined deposition of the microparticles is performed using a special laser printer (Figure 12).

Figure 12. Peptide laser printer: (left) general view; (right) amino acid printing units (image credit: PEPperPRINT GmbH).

The principle of the xerographic method is shown in Figure 13. A functionalized glass substrate is used as a solid support for peptide synthesis. Multiple types of polydisperse microparticles, each containing a specific amino acid derivative, are fabricated in advance and employed as individual toner powders for the laser printer. The toner particles are printed sequentially onto the substrate so that each type of microparticles is located in the corresponding spots of the microarray. After generating the desired pattern, the microparticles are simultaneously melted to enable the diffusion of the embedded amino acid derivatives and their coupling to the functional groups of the solid support. Coupling by-products, polymer matrix residues, and excessive amino acid derivatives are washed away. Thereafter, *N*-α-protecting groups are removed during the deprotection step, followed by the washing cycle. The steps of microparticle deposition, coupling, and deprotection along with the intermediate washing steps are performed multiple times until the desired peptide library is synthesized on the solid support.

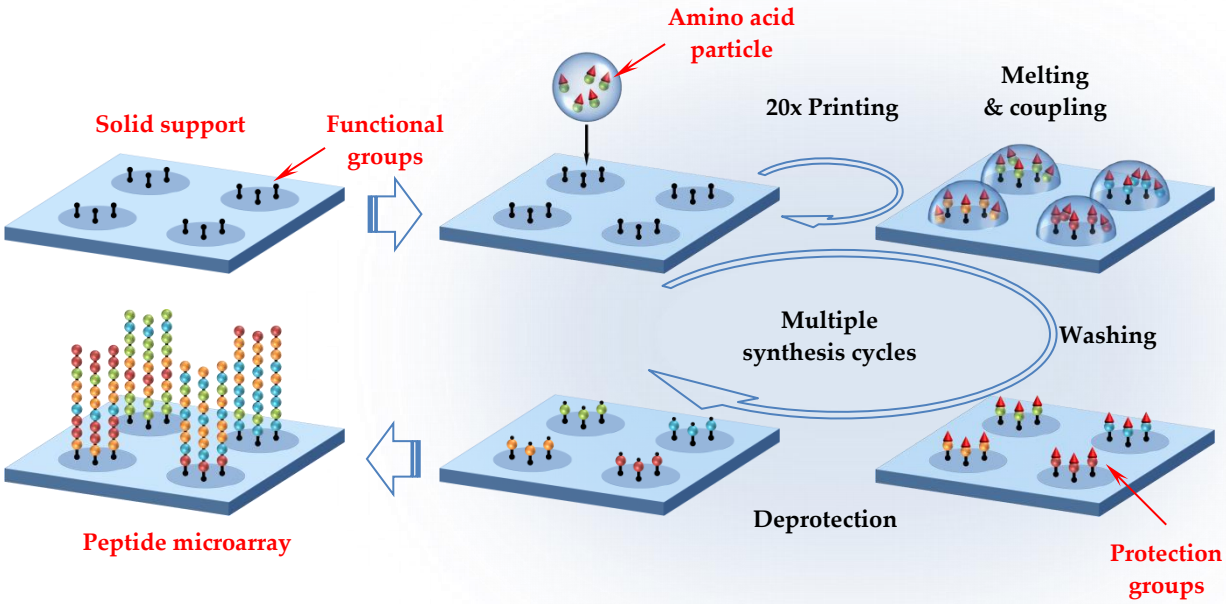

Figure 13. Schematic illustration of the xerographic method for peptide microarray manufacturing. Peptides are synthesized on a functionalized glass substrate by sequential deposition of the polymer microparticles with embedded amino acid derivatives, their melting and coupling of the monomers to the solid support. Residues of the polymer matrix and unreacted monomers are washed away, followed by amino group deprotection. The synthesis cycle is performed multiple times until the desired peptide library is synthesized.

Due to the fact that the amino acids are applied onto the substrate within the solid microparticles, the spot sizes are not affected by spreading of the monomers upon deposition. It results in the spot density of 775 spots/cm^2, which corresponds to around 10^4 spots on a standard 75 mm x 25 mm slide [23]. Another advantage of the xerographic method is the high manufacturing throughput. Using the custom-made laser printer, it is possible to print up to 275 000 spots within a minute [24]. The lower consumption of reagents in combination with the faster manufacturing procedures leads to the price per peptide of approximately €0.135 [16]. However, since this method is based on *in situ* SPPS, the purity of the synthesized peptides is relatively low. As in the case of the SPOT-method, an additional capping step has to be carried out to acetylate the free amino groups after each coupling step.

Lithographic method

The lithographic method, first reported by S. Fodor in 1991, is the second most frequently used technique for manufacturing peptide microarrays after the SPOT-method [25]. The principles of solid-phase chemistry and photolithography were

combined to carry out the light-directed spatially addressable parallel synthesis of thousands of peptides on a solid support.

The concept of the lithographic method is depicted in Figure 14. The functionalized glass substrate bears terminal amino groups, which are derivatized with special light-sensitive protecting groups. Illuminating the substrate through the first lithographic mask results in a local removal of the photolabile protecting groups according to the mask pattern. The substrate is incubated with the solution of the first amino acid, which is preliminary activated at the carboxyl group and derivatized with a photolabile *N*-α-protecting group. The coupling reaction takes place only in those regions, which were addressed by the light in a previous step. Thereafter, the substrate is illuminated again through the second photomask, which makes other regions of the substrate available for coupling of the second amino acid derivative. The steps of coupling and photo-deprotection with intermediate washing steps are carried out multiple times to obtain the desired peptide library.

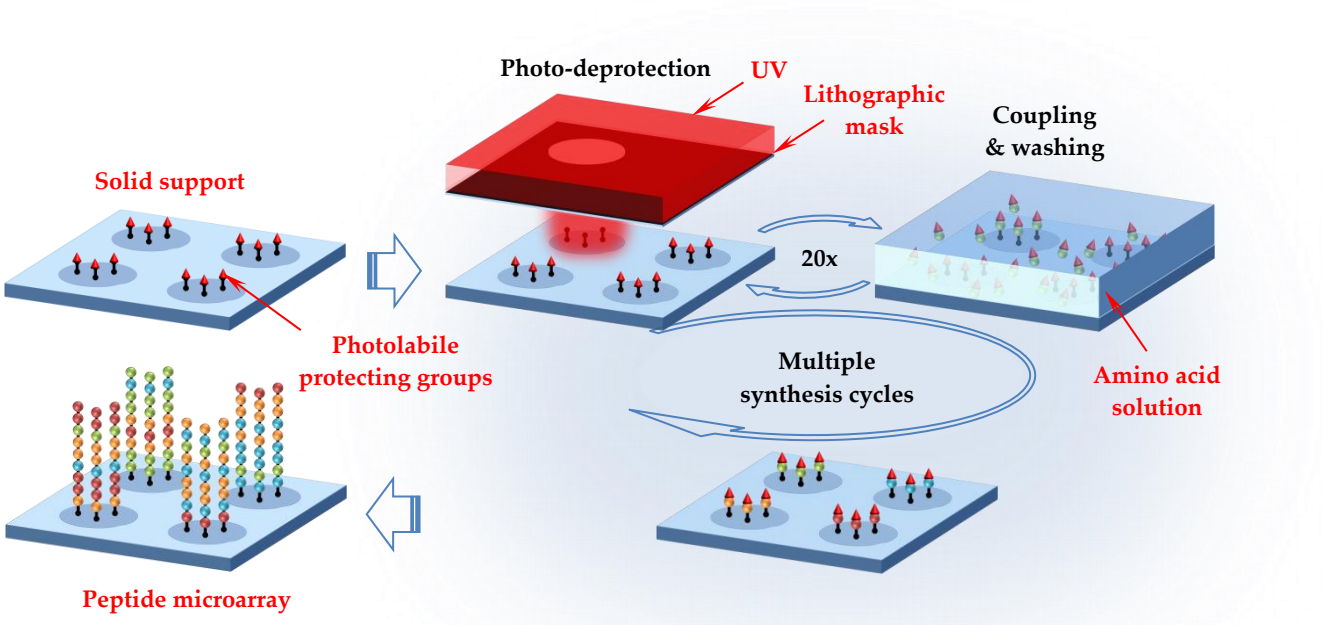

Figure 14. Schematic illustration of the lithographic method for peptide microarray manufacturing. The functionalized glass substrate bears amino groups derivatized with light-sensitive protecting groups. Illuminating the substrate through a photolithographic mask results in a local removal of the photolabile protecting groups. The amino acid derivatives couple to the free amino groups from solution. The cycles are repeated multiple times until the desired peptide library is synthesized.

The main advantage of the lithographic method is a very high spot density defined by the feature size of the photomasks. The spot size of 8 µm and the density

of $0.67 \cdot 10^6$ spots/cm^2 were reported for the peptide microarrays manufactured using the lithographic technique [26]. It results in up to 10 million spots on a standard 75 mm x 25 mm substrate.

Although promising for high-density peptide microarrays, the lithographic method has practical limitations. Manufacturing an arbitrary microarray of 15-mer peptides using 20 types of amino acids per synthesis layer requires 300 photomasks that are expensive and time-consuming to produce. This problem was solved by implementing a digital micromirror device (DMD) for light pattern projection onto the substrate, thus eliminating the need to use numerous photomasks [27]. However, the manufacturing costs remain high due to the use of expensive equipment and clean room facilities. The price of $1 150 was reported for a standard chip with 4 000 peptide spots, which corresponds to approximately $0.288 per spot [16].

Another drawback of the light-directed synthesis is a poor efficiency of the photochemistry. The cleavage of the photolabile protecting groups has a much lower yield compared to the conventional protecting groups. For instance, the coupling yield per cycle was reported to range between 85 % and 95 %, which should result in the product output of less than 50 % for the 15-mer peptides [28].

1.2 Motivation and Problem Formulation

The methods described in the previous section are widely used in commercial peptide microarray manufacturing. The characteristics of each manufacturing technique are summarized in Table 1.

Table 1. Comparison of methods for peptide microarray manufacturing.

Parameter	Peptide microarray manufacturing method			
	Spotting method	**SPOT-method**	**Xerographic method**	**Lithographic method**
Spot density, cm^{-2}	25	25	775	$< 6.7 \cdot 10^5$
Peptide quality	high	medium	low	low
Price per spot	€25	€6 – €9	€0.135	$0.288

Each of the methods considered has its advantages and disadvantages. Providing the best-quality peptide microarrays, the spotting method is not suitable for generating high-density peptide libraries. Moreover, in case of custom spotted microarrays, the price per peptide is the highest compared to the other methods. While offering a similar low spot density, the SPOT-technique possesses a higher flexibility in generating diverse peptides at a lower price than in case of the spotting method. However, the purity of the displayed peptides is worse than in case of the spotted microarrays. Using the xerographic method, the spot densities can be increased by an order of magnitude compared to the first two methods, which leads to a reduction of the price per spot, whereas the peptide quality is comparable to the SPOT-method. The lithographic technique provides the densest arrangement of the peptide spots compared to the other methods. However, the quality of the peptide microarrays is the lowest, while the price per peptide is comparable with the printer-based method.

The need to develop a novel type of peptide microarray, which would combine the advantages of currently available commercial products, has become the **prerequisite for the research project** carried out within the framework of the present dissertation.

In order to accelerate collection, analysis and interpretation of biological information, the new peptide microarray has to meet several **requirements**:

a) the spot density has to be high enough to display more than 1 million peptides on a standard 75 mm x 25 mm substrate;
b) the purity of the displayed peptides has to be acceptable to acquire meaningful results when performing biological assays;
c) the production costs have to be sufficiently low to make the peptide microarray affordable for potential users.

The non-trivial combination of the microarray's characteristics requires implementation of an innovative manufacturing approach. Therefore, development of a cost-efficient manufacturing process for high-density peptide microarrays has become the **aim of the** present **project**. The stated aim has defined the following **project objectives**:

1. Elaboration of the manufacturing concept.
The new approach has to be proposed for the manufacturing of a low-cost high-density peptide microarray. In particular, such a principle of amino acid deposition

has to be proposed, which does not require the use of expensive positioning equipment. At the same time, the new principle has to enable a time-efficient and reliable generation of the amino acid pattern in each synthesis cycle.

2. Development and optimization of the manufacturing process steps.
Implementation of the novel manufacturing principles requires development and optimization of additional tools and processes. Furthermore, the standard processes should be adapted to the new manufacturing conditions.

3. Manufacturing and testing of the microarray prototype.
In order to validate the novel manufacturing approach and the performance of the final product, a prototype microarray has to be produced and tested. A known peptide library has to be synthesized on a substrate and incubated with antibodies that demonstrate an affinity to specific peptides.

The basic principles and methods of microstructure technology, solid-phase peptide synthesis and the phenomenon of self-organization in microscale were taken as the premise for solving the stated problem. Successful project implementation resulted in a novel type of peptide microarray, which is referred in the present dissertation as a stochastic peptide microarray.

1.3 Structure of Dissertation

The present dissertation is divided into five main chapters. In Chapter 1, the basic terms and concepts related to the field of studies were reviewed. In particular, the idea of a peptide microarray as a screening tool for assessment of protein-protein interactions was introduced. To understand the origin of the peptide microarrays' diversity, the state-of-the-art manufacturing methods were described in details. By comparing strengths and weaknesses of these methods, the conclusion was made that none of the existing techniques enables low-cost manufacturing of high-density peptide microarrays with sufficient purity of the displayed peptides. This enabled us to formulate the aim of the project and the related project objectives.

Chapter 2 describes the concept of manufacturing stochastic peptide microarrays. After presenting basic principles of the microarray manufacturing, each process step is considered in details in terms of the imposed requirements and its possible

implementation. Additionally, the basic theoretical aspects related to the established procedures are considered. In general, Chapter 2 gives an idea on the evolution of the manufacturing process and the constraints faced with.

Chapter 3 provides information on materials and methods used within the scope of experimental work. In particular, the methods and procedures developed and optimized for manufacturing of amino acid carrying microbeads, their deposition into the microwells of a microstructured substrate, imaging of their random deposition pattern, as well as extraction and coupling of the amino acid derivatives are explained in details. Besides that, an unsupervised machine learning algorithm developed for the automated decoding of the amino acid allocation pattern is reviewed. Eventually, the framework for the manufacturing of the prototype microarray is described.

Chapter 4 presents the main results of the experimental work and their discussion. Particularly, the optimal parameters of the microstructured substrate, the rational composition and structure of the microbeads, as well as favorable conditions for amino acid extraction and coupling are derived from the outcome of several series of experiments. Additionally, the problems of microbead deposition and removal are considered and explained. Finally, the results on manufacturing the prototype of a stochastic peptide microarray are presented.

Chapter 5 draws the conclusions on the research project carried out. The outcome of the proposed strategy for manufacturing stochastic peptide microarrays is summarized and evaluated in terms of meeting the initial requirements. Besides that, the outlook on further development related to the expansion of the production line and enhancing the spectrum of biological applications is provided.

2 Stochastic Peptide Microarrays

A stochastic peptide microarray is a novel type of peptide microchip developed within the scope of the present work. It comprises a unique set of characteristics resulted from an innovative approach in microarray manufacturing. In general, one stochastic microarray contains approximately 3 million peptides displayed on a 75 mm x 25 mm glass substrate (Figure 15). In contrast to conventional peptide microarrays, the glass substrate is microstructured. It represents a multitude of microwells arranged in an array format. Individual peptides are confined within the microwells so that the microwell pattern of the substrate represents the mutual arrangement of the peptide spots. Another characteristic feature of the stochastic microarray is that the peptide library is not defined in advance but is derived upon the manufacturing process is completed. Therefore, the resulting peptide library displayed on the microarray is random.

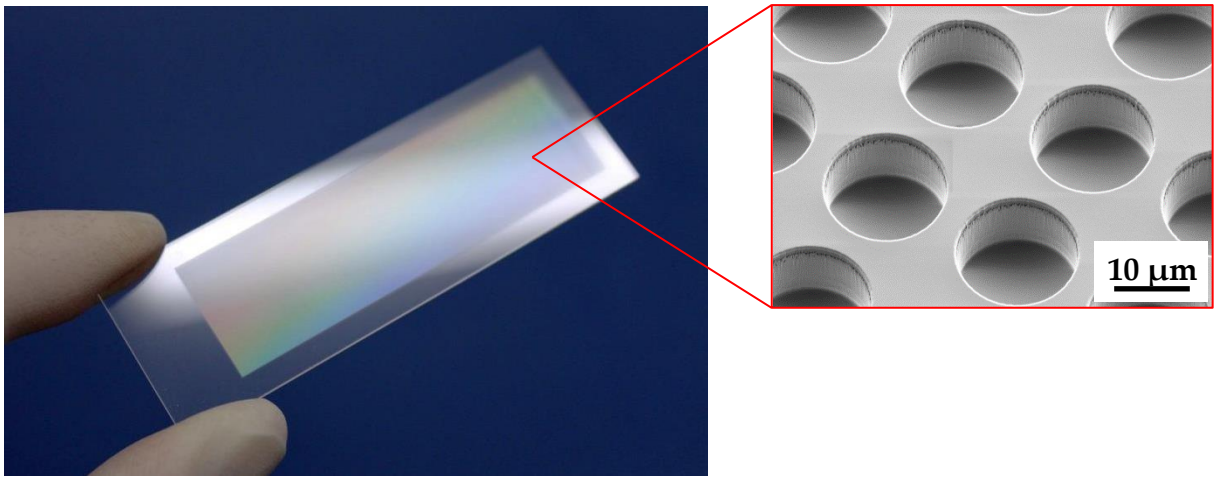

Figure 15. Stochastic peptide microarray. Individual peptides are synthesized in each of approximately 3 million microwells of the microstructured functionalized glass substrate (75 mm x 25 mm).

In order to understand the origin and the nature of the stochastic peptide microarray features, the principles underlying the manufacturing process are considered in the present chapter. In Section 2.1, the concept for manufacturing stochastic peptide microarrays is described in details. The process steps and the fundamental requirements are further discussed in Section 2.2. Finally, theoretical foundations of the underlying processes are briefly reviewed in Section 2.3.

2.1 Manufacturing Concept

Stochastic peptide microarrays are manufactured using the chemical principles of *in situ* solid-phase peptide synthesis. A multitude of peptides is generated directly on the solid support by sequential coupling of the amino acid derivatives to the terminal groups of the growing peptide chains. The elongation of the synthetic peptides takes place from C-terminus to N-terminus and requires the amino acid derivatives to be OPfp-activated at their carboxyl group and Fmoc-protected at their amino group (Figure 16). SPPS technique implies the repetitive steps of Fmoc-deprotection, amino acid deposition, coupling and blocking to be performed until the oligopeptides of the desired length are synthesized. Since 3 million different peptides are generated simultaneously in a high-throughput parallel synthesis, the targeted addressing of each reaction site by an individual amino acid derivative becomes crucial.

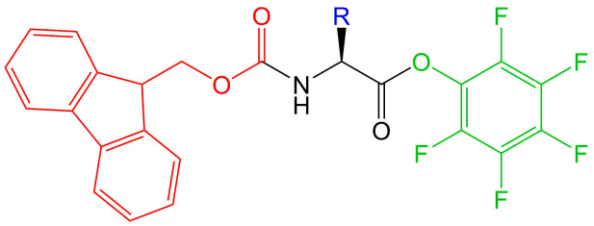

Figure 16. Chemical structure of an amino acid derivative protected by Fmoc-group at N-terminus (red) and activated by OPfp-group at C-terminus (green). The side chain R (blue) varies for different amino acid derivatives.

Prior to each step of peptide chain elongation, the amino acid derivatives are transferred onto the substrate by special polymer microbeads, wherein each microbead contains an individual type of the monomer. The accuracy and repeatability of the amino acid deposition to the specific reaction sites, representing individual peptide spots, is ensured by the phenomenon of self-organization of the microbeads in the microwells of the microstructured substrate (Figure 17). The size and shape of the microbeads and the microwells are selected in such a way so that only one microbead can fit into the respective microwell. Such a geometric constraint does not allow more than one type of amino acid derivative to be present in each microwell during the coupling step. As a result, the microarray spots are expected to contain predominantly individual kinds of the amino acid sequences after the peptide synthesis is completed.

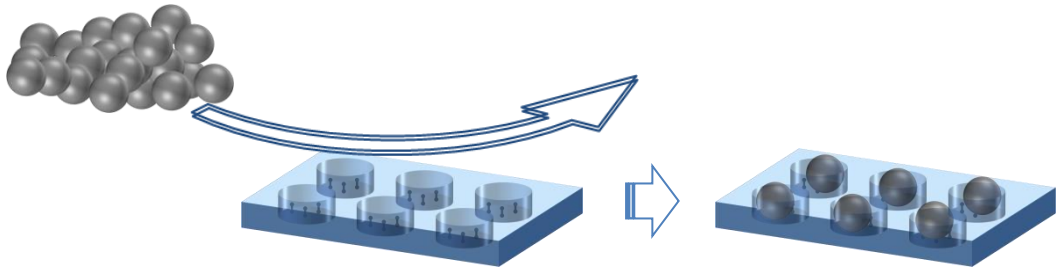

Figure 17. Stochastic microbead deposition. A mixture of amino acid carrying microbeads is stochastically deposited into the microwells of a microstructured substrate. The size and shape of the microbeads and the microwells allow fitting of not more than one microbead into one microwell.

The generation of the amino acid deposition pattern takes place in a single step by mechanically applying a mixture of different microbeads into the microwells of the microstructured substrate. Since the deposition of the microbeads is performed in a random, or stochastic, process, it is not known in advance which type of microbead will be located in each microwell. Therefore, after introducing the microbeads into the microwells, the amino acid deposition pattern has to be derived in an additional step. To differentiate between the microbeads carrying different amino acid derivatives, specific fluorescent labels are preliminary introduced into the microbeads. Fluorescence imaging and subsequent data analysis enable decoding of the amino acid deposition pattern (Figure 18).

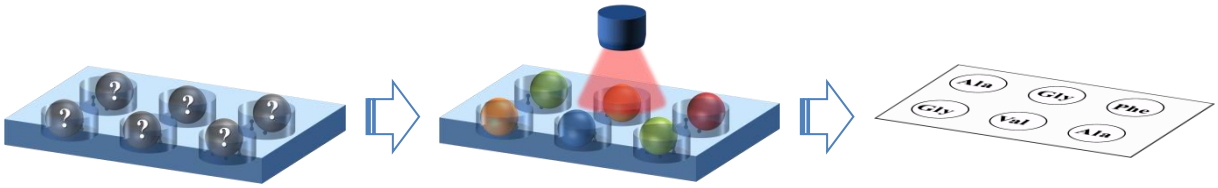

Figure 18. Decoding of an amino acid deposition pattern. The microbead deposition pattern derived upon fluorescence imaging is further translated into the amino acid deposition pattern.

The fact that the amino acid derivatives are transferred onto the substrate being embedded into the solid microbeads hinders their interchange and prevents their immediate reaction with the functional groups on the solid support. Under certain conditions, the amino acid derivatives are released from the microbeads to enable their diffusion to the functional layer and further coupling to the terminal free amino groups (Figure 19). After the coupling step is completed, the excess of amino acid derivatives and the process by-products are washed away, whereas the microbeads are mechanically removed from the microwells.

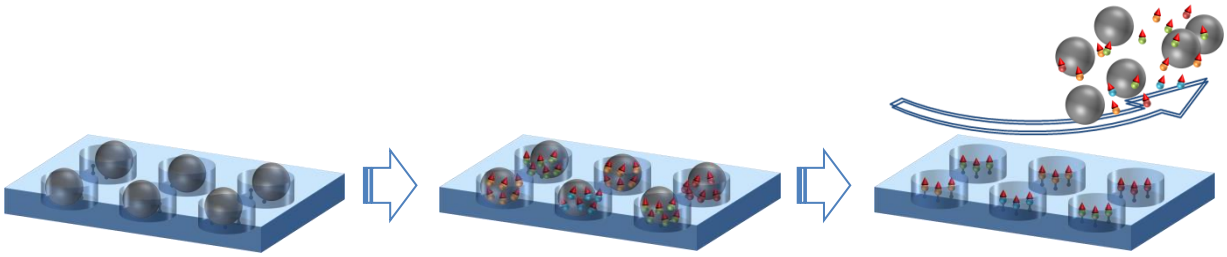

Figure 19. Extraction and coupling of amino acid derivatives. Exposed to certain conditions, the microbeads release the amino acid derivatives, which diffuse and couple to the functional groups of the substrate. Thereafter, the excessive monomers and process by-products are washed away, whereas the microbeads are removed from the microwells.

The process of manufacturing stochastic peptide microarrays is schematically shown in Figure 20. Prior to peptide microarray synthesis, 20 different types of microbeads are fabricated. Each microbead is loaded with a certain type of amino acid derivative and accordingly labelled with a specific fluorescent marker. The solid support for the peptide synthesis undergoes preliminary microstructuring, followed by chemical functionalization of its surface. The synthesis of the peptide library begins with the deprotection of the amino groups borne by the functional layer of the solid support. Thereafter, a mixture of microbeads is applied into the microwells of the substrate. The amino acid deposition pattern is derived upon optical imaging of the microbeads, followed by their label decoding. During the next steps, the amino acid derivatives are extracted from the microbeads and coupled to the amino groups on the substrate. After the coupling step, the microbeads are removed from the microwells, whereas the amino acid residues and the process by-products are washed away. The blocking of non-reacted amino groups is performed to avoid generation of undesired peptide sequences. Thereafter, the steps of amino group deprotection, particle deposition, fluorescence scanning, label decoding, amino acid extraction and coupling, microbead removal and blocking are performed multiple times depending on the desired length of the peptide to be synthesized. The resulting peptide microarray is complemented with a file, which contains information on the amino acid sequences randomly generated in each microwell of the substrate.

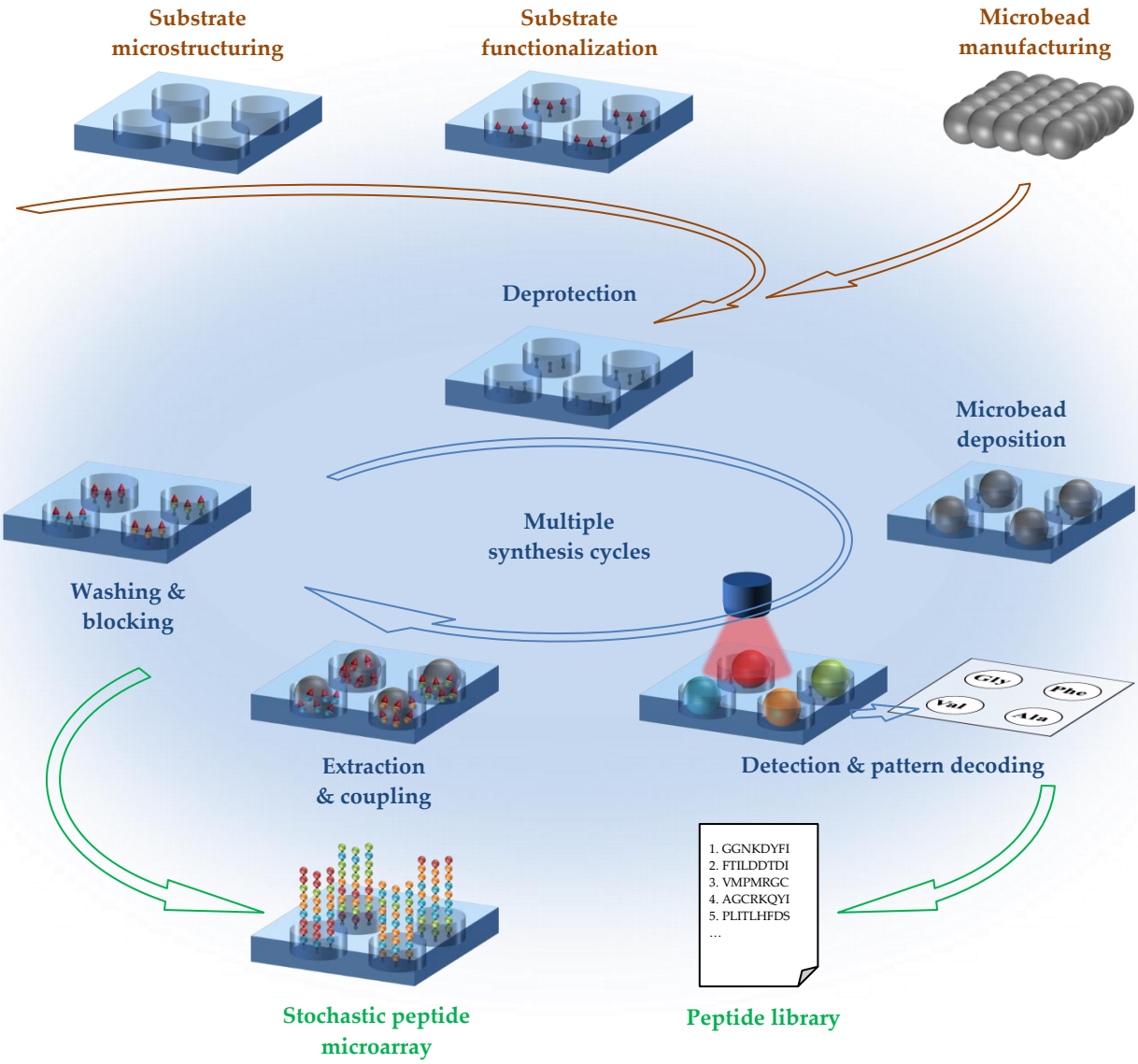

Figure 20. Schematic illustration of the stochastic peptide microarray manufacturing. Random peptides are synthesized in the microwells of a microstructured substrate by stochastic deposition of a mixture of microbeads, decoding of their deposition pattern, followed by extraction and coupling of the amino acid derivatives, removal of the microbeads, blocking remaining free amino groups and deprotection of the terminal groups for the next synthesis cycle. The process steps are repeated multiple times until the peptides of a desired length are synthesized.

After the terminal and the side chain groups of the peptides are deprotected, the stochastic peptide microarray can be incubated with a biological analyte.

2.2 Process Steps: Requirements and Implementation

In this section, the manufacturing process steps are discussed in details in terms of the imposed requirements and their possible implementation.

2.2.1 Substrate Manufacturing

Requirements

The function of the substrate for the stochastic peptide microarray is to enable the synthesis, representation and implementation of a high-density peptide library in a most reliable and convenient way. Particularly, the substrate has to allow for chemical immobilization of the amino acid derivatives on its surface. At the same time, it has to be resistant to the chemical and physical conditions during SPPS. The format of the slide has to be compatible with the standard tools and equipment used in peptide microarray manufacturing and biological applications. Finally, the substrate has to ensure the self-organization of the microbeads on its surface so that individual types of amino acid residues are deposited to the synthesis spots prior to each step of peptide chain elongation. The stated requirements impose a number of restrictions on the architecture of the substrate for the stochastic peptide microarray.

Implementation

From an end-user perspective, the format of a standard 75 mm x 25 mm x 1 mm microscope slide is the most preferred for the substrate of the stochastic peptide microarray. This format makes the peptide chip compatible with conventional microarray incubation chambers, as well as with modern fluorescence scanners used for readout of the incubation results. The substrates with smaller dimensions are also applicable if special adaptors are provided. However, the peptide library would be limited in this case by the smaller size of the substrate.

The substrate can be made of fused silica, quartz, silicon, plastics, metals, or composites. On the one hand side, the material has to be rigid, inert to the chemicals used in SPPS, and stable at temperatures up to 100 °C. On the other hand side, it has to be able to undergo microstructuring, as well as chemical modification by the functional layer. Fused silica, quartz, and silicon are the most frequently used materials for the substrates of high-density microarrays.

The surface of the substrate has to be microstructured to facilitate the deposition of the microbeads into the peptide synthesis spots. The most reasonable microstructure pattern comprises a multitude of cylindrical microwells arranged in a rectangular or hexagonal grid format (Figure 21). Besides its geometric layout, the array grid is defined by the pitch size, as well as by the number of rows and columns of the microwells fitting on a given surface area of the substrate. A higher spot density can be achieved by implementing hexagonal grid with a smaller pitch size.

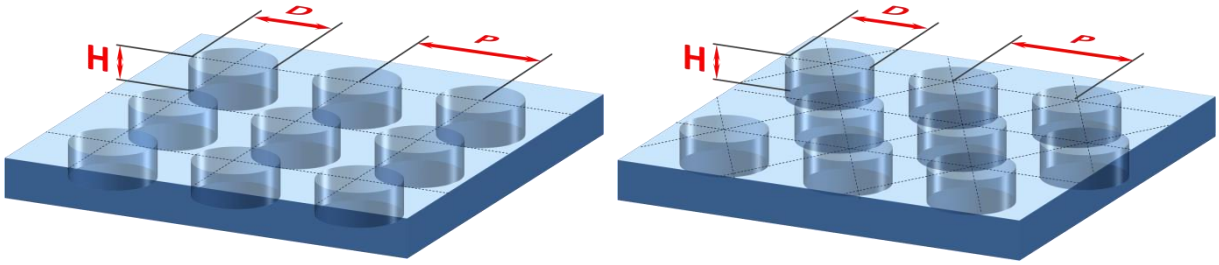

Figure 21. Microstructure patterns: (left) rectangular; (right) hexagonal. Microstructures are characterized by the pitch size (P), microwell diameter (D), and microwell depth (H).

The microwells are characterized by their diameter and depth. The aspect ratio, defined as a proportional relationship between the diameter and the depth of the microwell, has to enable a reliable deposition and removal of a single microbead from the microwell. The spacing between the two closest neighboring microwells, calculated as a difference between the pitch size and the microwell diameter, has to be sufficient to ensure differentiation of their fluorescence signals and mechanical stability of the microstructures.

The microstructuring of the substrate surface can be performed using different techniques depending on the material to be processed and the requirements set for the accuracy and geometry of the microstructures. For the substrates made of fused silica and quartz, the most accurate, reproducible and homogeneous results in generating the microwells with the depth of up to 10 µm can be achieved by combining photolithographic patterning and reactive ion etching (RIE) techniques.

After microstructuring, the surface of the substrate rarely bears functional groups for anchoring of the amino acid derivatives. Therefore, the substrate has to be additionally modified by a special functional layer containing free amino groups that the monomer molecules can bind to. Within the framework of the present project, the substrate was functionalized by a thin copolymer layer of poly(ethylene glycol)

methacrylate (PEGMA) and methyl methacrylate (MMA) with mole fractions of 10 % and 90 %, respectively (10:90-poly(PEGMA-co-MMA)). This functional layer is covalently immobilized on the solid support which ensures its spatial integrity throughout the entire peptide synthesis process. At the same time, the surface coating is compatible with the solid-phase peptide chemistry and demonstrates resistance to various organic solvents, strong organic acids and bases. Moreover, the implemented functional layer is suitable for biological assays by eliminating non-specific binding or repulsion of the analyte proteins [29].

2.2.2 Microbead Manufacturing

Requirements

In the stochastic peptide microarray fabrication, the microbeads serve as a transportation entity for the amino acid derivatives. Each microbead contains an individual type of monomer and ensures its transfer into an arbitrary microwell on the substrate. Generally, the microbeads carrying different amino acid derivatives are applied over the substrate as a dry mixture being exposed to a mechanical action. Under mechanical stress, the rigid carriers are subject to fracture, whereas too soft materials can stretch out, lose their shape and spread over the surface. Hence, the microbeads have to be mechanically stable to eliminate the risk of their fragmentation. Moreover, the microbead architecture should prevent the monomer exchange between different carriers, as well as surface contamination by the monomers during their deposition. It requires the amino acid derivatives to be embedded into the body of the carriers to avoid their direct contact with external surfaces. At the same time, the microbead composition should enable extraction of the amino acid derivatives under certain conditions, so that they can take part in the peptide chain elongation process.

The microbeads should meet the requirement of depositing not more than one type of amino acid derivative per microwell in each coupling step to prevent generation of different amino acid sequences within a single spot of the microarray. It requires the shape and size of the microbeads to correspond to the dimensions and geometry of the microwells so that only one carrier can fit into a given microwell. The spherical shape of the microbeads is preferable since it facilitates their deposition into the cylindrical microwells, as well as their removal from the top surface of the substrate.

The ratio between the microwell diameter and the microbead diameter, as well as the ratio between the microwell depth and the microbead diameter, determine the maximum number of spherical microbeads fitting into a microwell. Since the range of acceptable ratios is quite narrow, the microbeads have to be quasi-monodisperse.

The microbeads are applied into the microwells stochastically, which means that it is not known in advance which type of amino acid derivative will be deposited in each microwell. Therefore, there should be a certain principle behind the microbead deposition, which would enable decoding of their allocation pattern on the substrate.

Implementation

The architecture and composition of the microbeads have to comply with all the requirements mentioned above. Two conceptually different approaches to design the microbeads were considered during preliminary studies.

The first approach implies that the microbead is composed of a soluble polymer matrix with amino acid derivatives embedded inside (Figure 22, left). After deposition of the microbeads into the microwells, the polymer matrix undergoes melting while being exposed to elevated temperatures so that the embedded monomers can diffuse to the surface of the substrate and couple to its functional groups. Using the styrene-acrylic-copolymer resin as a matrix material has several advantages compared to alternative substances. The glass transition temperature of the copolymer resin is low enough to enable melting of the microbeads at 90 °C.

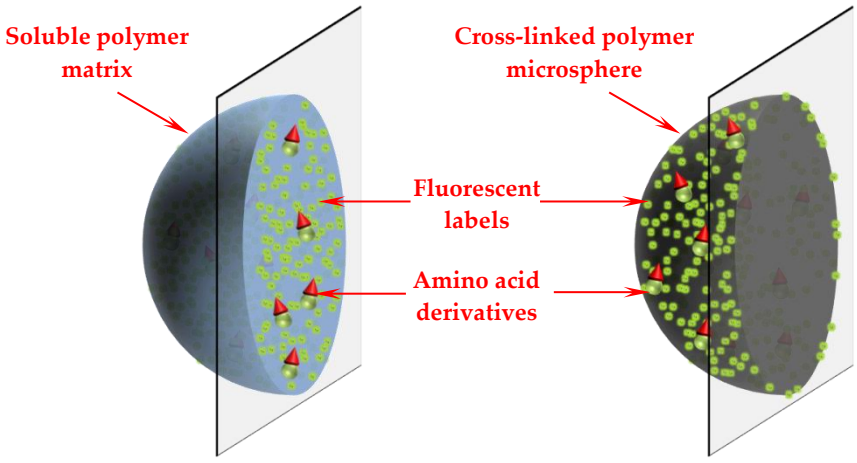

Figure 22. Microbead architecture: (left) soluble polymer microbeads with amino acid derivatives and fluorescent labels embedded inside; (right) cross-linked polymer microsphere with amino acid derivatives and fluorescent labels incorporated into a thin outer surface layer.

Moreover, the styrene-acrylic-copolymer resin is soluble in standard organic solvents, such as acetone or dichloromethane (DCM), which makes the removal of the polymer residues after the amino acid coupling easy and straightforward.

The microbeads based on the soluble polymer matrix can be manufactured using a spray drying technique [30]. This method is suitable for generating microbeads of a quasi-spherical shape with an output of up to 100 gram per process run. However, the resulting microbeads are polydisperse, which requires an additional step of fine separation using sieving instrumentation (Figure 23).

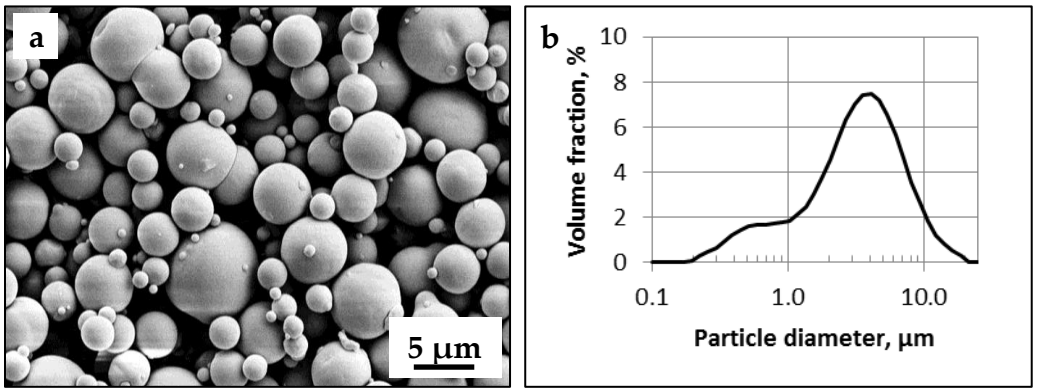

Figure 23. Styrene acrylic copolymer microbeads manufactured with a spray drying technique: (a) SEM image of the microbeads with embedded amino acid derivatives; (b) microbead size distribution **[30]**.

An alternative microbead architecture was suggested and implemented within the scope of the present research project. Special polymer-based microspheres are used as solid carriers of the amino acid derivatives (Figure 22, right). They are pre-synthesized by emulsification polymerization with subsequent cross-linking, which makes them mechanically stable and not soluble in organic solvents. The polymerization process results in the microspheres with an extremely narrow size distribution, whereas the degree of cross-linking defines their mechanical stability and swelling limits in organic solvents. Under certain conditions, the polymer undergoes swelling, which enables the diffusion of the amino acid derivatives into the outer surface layer of the microspheres. During the subsequent shrinkage of the cross-linked polymer, the introduced substances are immobilized within the microspheres making them suitable for peptide microarray manufacturing.

The aspects related to the decoding of the microbead deposition pattern require a separate consideration. A straightforward approach to derive information on the

microbead allocation is to sequentially deposit different types of microbeads with intermediate optical detection of the substrate's filling pattern (Figure 24). Initially, the microbeads carrying the first type of amino acid derivative are randomly distributed between the microwells of the substrate. The deposition pattern is derived upon image acquisition of the structured surface, followed by image analysis and data processing. Prior to deposition of the second type of microbeads, the recently deposited carriers have to be fixed within the cavities to prevent their removal or exchange with the carriers of the second type. The process of microbead deposition, imaging and fixation is performed until all the microwells are filled with the microbeads of various types.

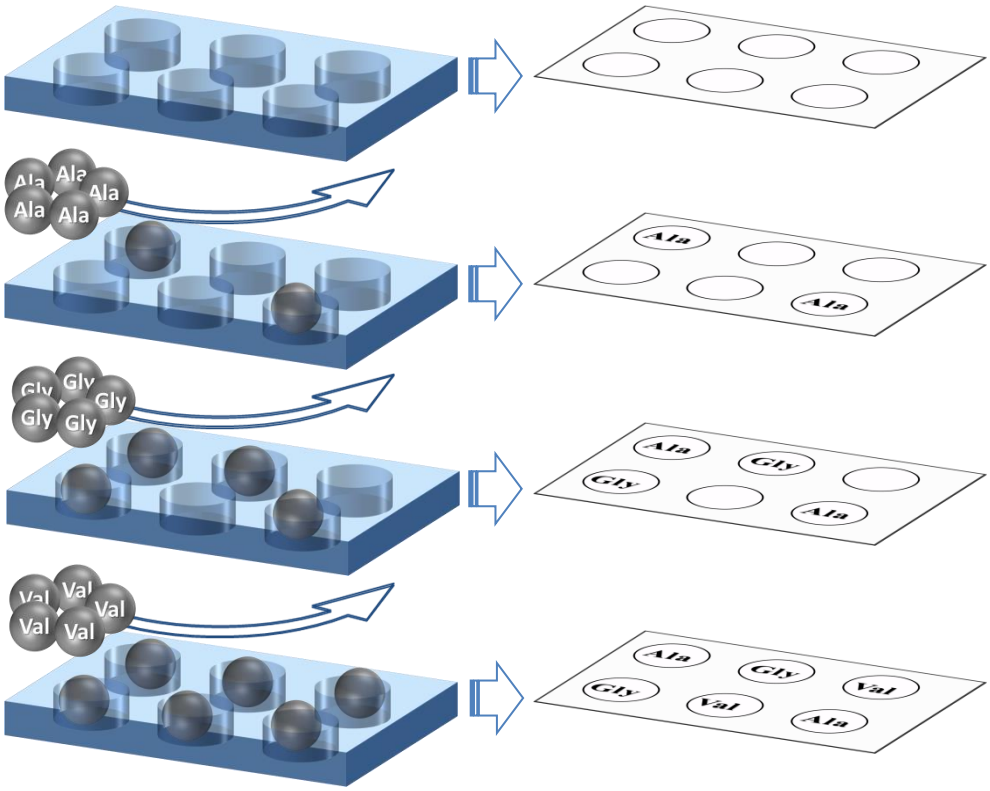

Figure 24. Schematic illustration of an amino acid pattern decoding based on sequential deposition of the microbeads, carrying individual monomers, and their intermediate optical imaging. This approach implies that within a single synthesis cycle the microbead deposition and optical imaging have to be done up to 20 times to fill the microwells with 20 different amino acid derivatives.

The main disadvantage of this approach is that it is labor-intensive and time-consuming. Moreover, the risk of microbeads' removal and exchange is significant due to the fact that the subsequent carriers are mechanically applied over previously

deposited ones. Furthermore, the filling rate of the microstructures by each type of microbeads is not homogenous and mainly depends on the deposition procedure.

An alternative approach in deriving the amino acid deposition pattern involves preliminary labelling of the microbeads with special fluorescent markers that can be detected by using modern readout instrumentation (Figure 18). The fluorescent labels have to be unique in terms of their emission spectrum to enable decoding of 20 different types of microbeads. Organic fluorophores are not suitable for this purpose since their emission spectra are too broad to encode multiple types of microcarriers (Figure 25a). Furthermore, they are not convenient to utilize due to having different excitation wavelengths and a low photostability. To overcome the limitations of the fluorescent organic dyes, it was proposed to use quantum dots (QD) for labelling of the microbeads. These nanoscale semiconductor particles emit light in a narrow range of frequencies, which makes it possible to differentiate between multiple types of QDs (Figure 25b). At the same time, the excitation of QDs can be performed at any wavelength lower than their emission. Compared to organic fluorophores, QD based labels are 20 times brighter and 100 times more stable [31].

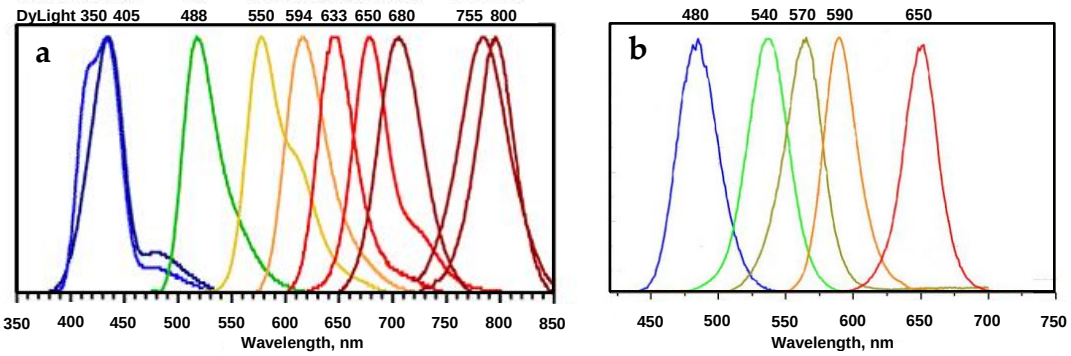

Figure 25. Emission spectra of organic fluorophores in comparison with QDs: (a) emission spectra of different DyLight dyes; (b) emission spectra of CdSe/ZnS quantum dots (image credit: Thermo Fischer Scientific and PlasmaChem GmbH).

Despite the fact the emission spectra of the fluorescent semiconductor nanoparticles are relatively narrow, it is practically impossible to choose 20 different types of QDs that can be reliably differentiated from each other. However, using multiplexed optical encoding, the number of fluorescent labels can be increased significantly [32, 33]. Implementing five types of spectrally resolved QDs and combining up to three types of QDs per microbead enables encoding of 25 types of microbeads (Figure 26).

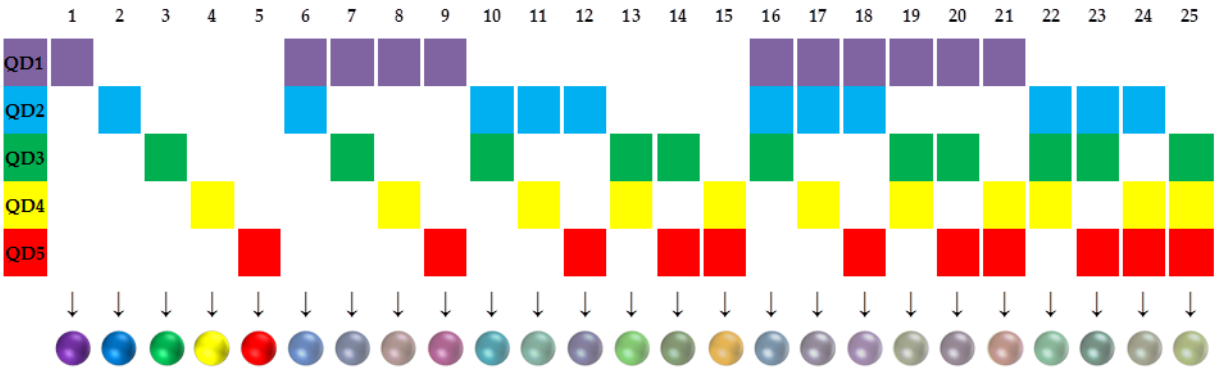

Figure 26. Schematic illustration of a multiplexed encoding of microbeads by various combinations of QDs. Selecting five types of spectrally resolved QDs and combining up to three types of QDs per microsphere enables encoding of up to 25 types of microbeads.

Due to their nanoscale size, the QDs can be implemented as fluorescent labels within the microbeads based on both architectures. In case the microbeads are made of the soluble polymer resin, the QDs are immobilized inside along with the amino acid derivatives. In case the microbeads are based on the solid-carrier architecture, the QDs are incorporated into the outer surface layer of the microspheres. In both cases, the matrix material should serve as a good solvent for the QDs to prevent their aggregation and mutual quantum influence. At the same time, the microbeads have to be transparent for the excitation and emission of the embedded QDs.

During preliminary trials, the microbeads based on the soluble styrene-acrylic-copolymer resin demonstrated low mechanical stability. Moreover, the solubility of QDs in the polymer matrix was not sufficient to enable appropriate labelling of the microbeads. Due to these reasons, the decision was made to proceed further with the microbeads based on the solid-carrier architecture.

2.2.3 Microbead Deposition

Requirements

The microbead deposition into the microwells of the substrate takes place prior to each step of peptide chain elongation. The microwells, which unintentionally remain unfilled, contain no amino acid derivatives that could couple to the free amino groups of the functional layer. During the subsequent capping step, the terminal free amino groups are acetylated, which results in termination of the peptide synthesis

process. In order to minimize the risk of generating truncated amino acid sequences, the microwell filling rate has to be as close to 100 % as possible.

The microbeads are applied over the substrate in a substantial excess compared to the number of the microwells to be filled. The microbeads, which are left on the top surface of the microstructured substrate, can cause problems during the amino acid extraction and coupling steps. The amino acid derivatives from the microbeads left on the top surface can diffuse into the neighboring microwells containing the amino acid derivatives of a different type. It results in a contamination of a given peptide spot by peptide chains with randomly substituted unknown monomers, which, in turn, can induce false positive signals when performing a bioassay. Therefore, it is crucial to prevent any microbead residues of the on the top surface of the substrate.

The microbeads are exposed to certain forces during their deposition and removal. These forces have to be sufficient to overcome an adhesion of the microbeads to each other, as well as to the functional layer of the substrate. At the same time, the method of microbead deposition and removal has to be gentle enough not to induce their mashing or destruction when hitting the edges of the microwells. The debris from the destroyed microbeads can lead to the contamination of the microwells with arbitrary amino acid derivatives.

Implementation

The methods of microbead deposition can be split in two groups: suspension-based methods and powder-based methods. Suspension-based methods imply that the microbeads are applied over the microstructured substrate being dispersed in a continuous liquid phase. The main advantage of using liquid medium is a significant reduction of adhesion forces between the microbeads and the surface, which enables subtle movement of the microbeads with minimal forces applied. However, the liquid medium has to be carefully selected not to affect the physical or chemical stability of the microbeads.

Provided that the density of the liquid phase is lower than the density of the microbeads, the latter can sediment onto the microstructured substrate immersed in the suspension [34]. After a multilayer of microbeads is generated over the substrate, minor lateral movements of the medium can be induced by placing the vessel with the suspension onto a rotary shaker (Figure 27). The movement of the microbeads

introduced into the microwells is restricted by the walls of the microwells, whereas the microbeads on the top surface undergo lateral displacement being stochastically guided into the vacant microwells. After repeating the steps of sedimentation and lateral shaking several times, the microwells are considered to be filled, while the microbeads from the top surface are washed away.

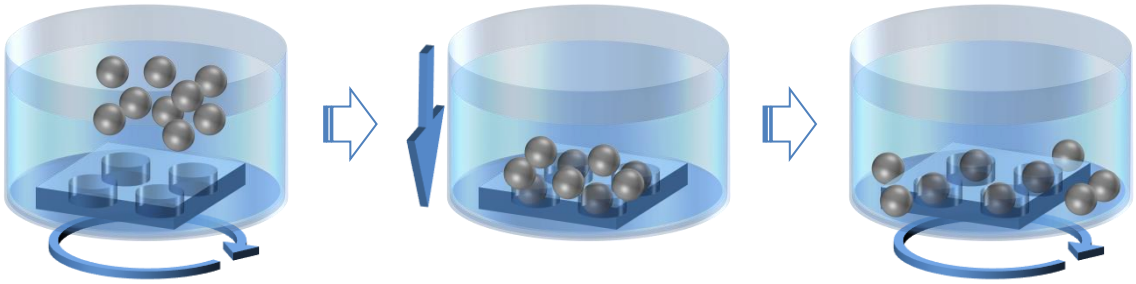

Figure 27. Microbead deposition by sedimentation from a suspension. A suspension of microbeads is applied over the microstructured substrate (left). Upon sedimentation, the microbeads fill the microwells and cover the top surface of the substrate (middle). After slight lateral movements of the liquid phase, the microbeads from the top surface are moved away, whereas the movement of the microbeads in the microwells is geometrically restricted (right). The steps of sedimentation and lateral shaking can be performed several times to achieve higher filling rates.

Another suspension-based method employs a microfluidic channel with the microstructured substrate placed inside (Figure 28) [35]. The suspension of the microbeads is slowly pumped through the channel with the front meniscus and the rear meniscus moving along the surface of the substrate. The microbeads are pushed by the capillary force of the rear meniscus into the vacant microwells. The excessive microbeads are taken away by the flow of the continuous liquid phase.

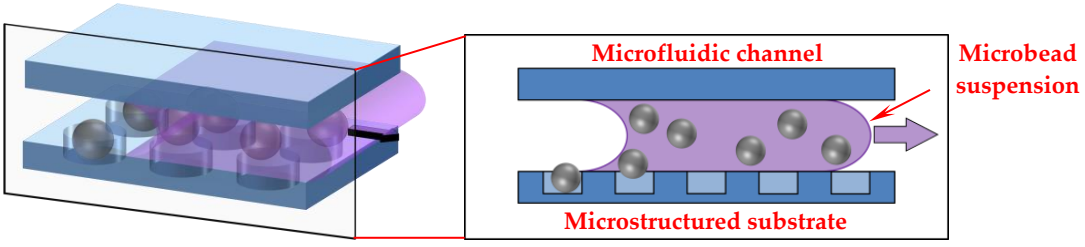

Figure 28. Microbead deposition using a microfluidic channel. A microbead suspension is pumped through the microfluidic channel so that the rear meniscus pushes the microbeads into the vacant microwells and pulls the excessive microbeads along the surface of the substrate.

During preliminary trials, the suspension-based methods demonstrated promising results in terms of the filling rates. However, a deeper analysis revealed a conceptual problem: The continuous liquid phase acts as an extraction and diffusion medium for the amino acid derivatives. This results in a massive contamination of the microwells with various types of monomers during the microbead deposition step. Therefore, the decision was made to avoid using the liquid phase and apply the microbeads into the microwells in a powder form (Figure 29).

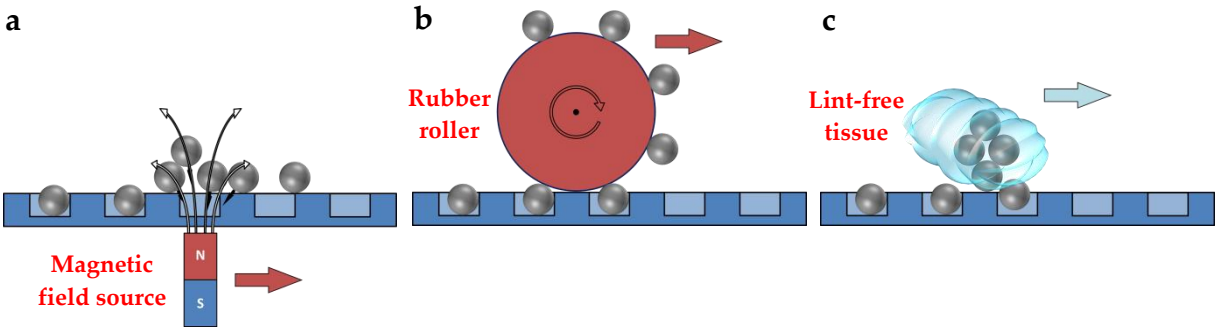

Figure 29. Dry microbead deposition methods: (a) a dynamic magnetic field guiding the microbeads doped with paramagnetic nanoparticles; (b) a rubber-based roller orthogonally introduces the microbeads into the microwells; (c) a lint-free tissue spreads the microbeads over the surface depositing them into the vacant microwells.

The powder-based deposition implies that the mixture of dry microbeads is applied over the substrate. Perhaps the most sophisticated method is using the microbeads doped with paramagnetic nanoparticles so that the microbead mixture can be stochastically guided by a dynamic magnetic field [36, 37] (Figure 29a). A much easier approach is to implement a special rubber-based roller, similar to those used in laser printers, to orthogonally deposit the microbeads into the microwells, while removing the excessive microbeads from the top surface (Figure 29b) [38]. An alternative method utilizes a soft lint-free tissue for rubbing the microbeads into the microwells, whereas the microbead residues are removed from the top surface by an air flow applied laterally along the surface of the substrate (Figure 29c) [38].

2.2.4 Image Acquisition

Requirements

The principle of the stochastic peptide microarray manufacturing implies that the microbead deposition is performed in a random way. It is not defined in advance, which microbead will be deposited in each microwell of the substrate. The actual amino acid deposition pattern has to be derived prior to each coupling step to enable generation of the peptide library file.

The microbeads developed within the scope of the present research project are labelled with a combination of different QDs corresponding to the amino acid derivatives embedded inside the microbeads. By acquiring images of the substrate in various fluorescent channels, the QDs emitting at the respective wavelengths can be visualized and further differentiated (Figure 30). In order to enable excitation of the fluorescent labels and readout of their emission signals, a special optical system, equipped with an appropriate excitation source and a set of matching narrow-band fluorescence filters, has to be implemented.

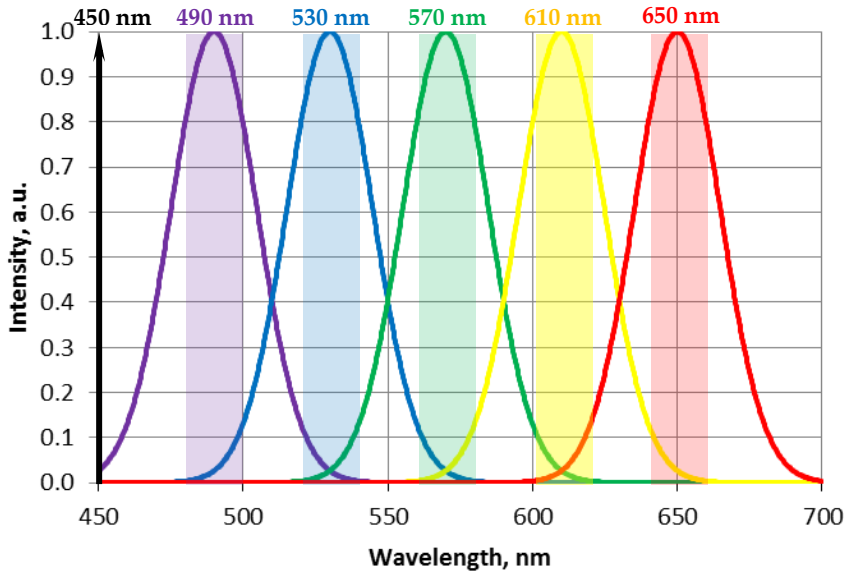

Figure 30. Schematic illustration of the QD readout principle. Five types of spectrally resolved QDs are simultaneously excited at 450 nm. Emission signals of the QDs are registered in the corresponding fluorescence channels equipped with narrow-band fluorescence filters with central transmission wavelengths matching the maximum emission wavelengths of the QDs.

The size of the microbeads imposes a restriction on the spatial resolution of the digital images acquired by the optical system. To enable an accurate calculation of the photometric data for each microbead, the image resolution has to be at least 2 µm/pixel. At the same time, the data acquisition has to be fast enough to obtain a full set of images in each fluorescent channel within 2 hours.

Implementation

Two optical systems were considered to address the task of image acquisition of the microbead deposition pattern. The first system was developed in the Peptide Array group at the Institute of Microstructure Technology (IMT), a part of the Karlsruhe Institute of Technology (KIT) [39]. It employs the principles of digital macro-photography and fluorescence imaging. The optical setup comprises of a DSLR camera with a 36 mm x 24 mm CMOS chip, an objective lens, an LED-based excitation source, an XY-translation stage, and two motorized filter wheels with a set of fluorescent filters (Figure 31). The optical setup is mounted on an optical table and enclosed by light curtains. The fact that the objective lens is placed approximately 35 cm from the CMOS sensor results in the maximum theoretical image resolution of 1.4 µm/pixel. The size of the CMOS chip enables imaging of a 10 mm x 7 mm area, which requires taking multiple pictures of the substrate followed by their stitching.

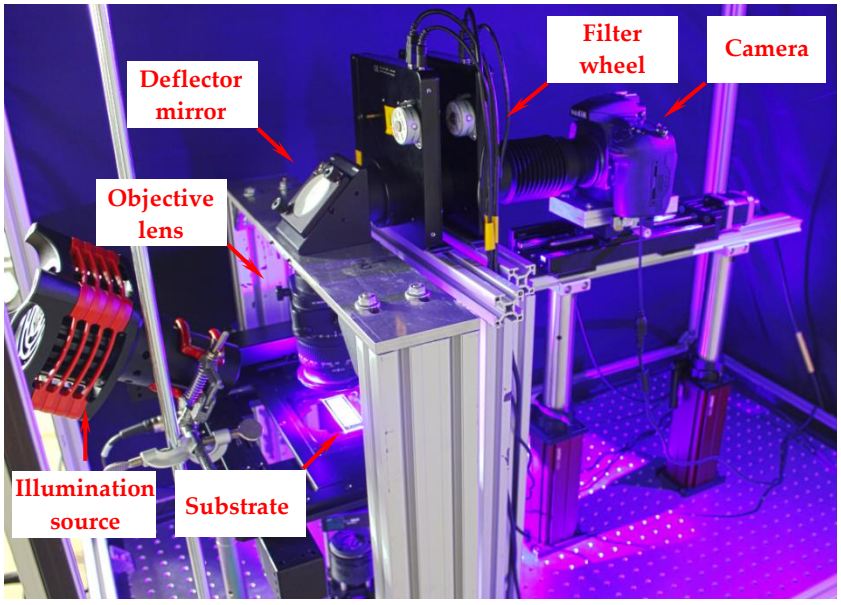

Figure 31. Optical system based on the principles of digital macro-photography and fluorescence imaging **[39]**. The illumination source excites the QD labels of the microbeads deposited into the microwells of the substrate. Fluorescence emission from the sample is collected by the objective lens and guided by the deflector mirror through the filter wheel to the CMOS sensor of the camera.

The optical setup developed at the IMT is a flexible system: It enables the exchange of the excitation source and the fluorescent filters, adjustment of the image resolution and the imaging procedure. However, the inherent drawback of the camera-based system is optical aberrations. To compensate chromatic aberrations, the position of the camera has to be adjusted for each fluorescence channel to ensure that the focal plane matches the substrate surface. Moreover, the need to combine up to 32 partially overlapping pictures into one image comes across the limitations of the stitching algorithm: In some cases, the image stitching process results in critical errors.

An alternative approach to image acquisition is using a fluorescence scanning technique. It enables point-by-point excitation of the sample with different laser sources and readout of the fluorescence emission in several optical channels (Figure 32). The principle of confocal fluorescence scanning enables aberration-free image acquisition of the whole substrate in a single run. A spatial resolution of up to 0.5 µm/pixel can be provided by the fluorescence scanners available on the market.

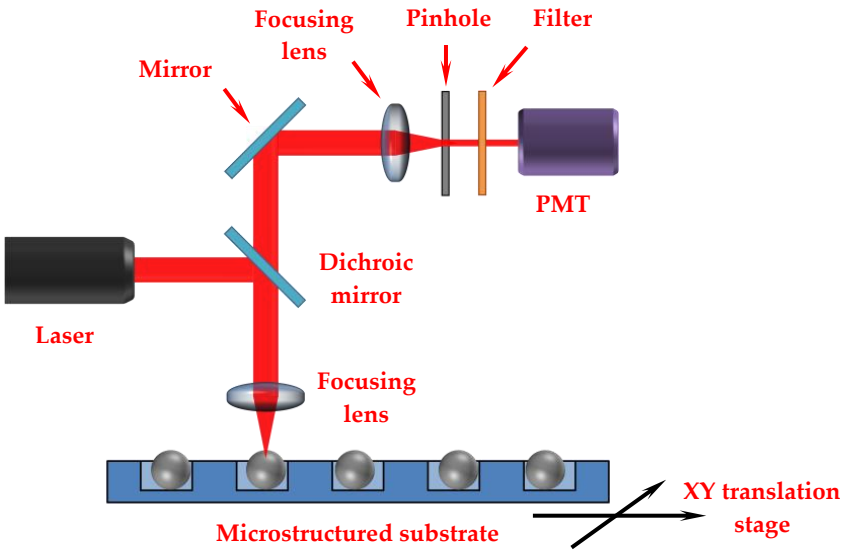

Figure 32. Schematic illustration of the optical setup of a confocal laser scanner.

Based on comparative studies of the camera-based optical setup and the fluorescence scanner available at IMT, the decision was made to proceed with the confocal scanning technique for image acquisition.

2.2.5 QD Label Decoding

Requirements

The images of the microstructured substrate are used to acquire information on the QD fluorescence signals of approximately 3 million microbeads. These signals have to be further analyzed and interpreted with an aim to derive the amino acid deposition pattern in the microwells of the substrate.

In the first step, the QD signals originating from each microwell have to be quantified for different fluorescence channels. Thereafter, the microwells containing the microbeads of the same type have to be grouped into clusters. In the final step, a certain type of amino acid derivative has to be assigned to each cluster, thereby resulting in the amino acid deposition pattern on the substrate.

Implementation

The first step of image analysis with an aim to derive photometric data for each microwell can be performed using the software supplied by the manufacturer of the fluorescence scanner. For this purpose, a virtual grid is applied over the microstructured area in the image so that each microwell is treated as an individual grid element. The pixels of each grid element are automatically processed resulting in a numeric data array of the spot signal values.

The second step of grouping the microwells into clusters can be performed using two conceptually different approaches. The first approach is based on supervised machine learning. It implies that prior to peptide microarray manufacturing a set of training data is individually obtained for a statistically relevant number of microbeads of each type. This data is further processed to derive characteristic signal ranges for all 20 types of microbeads. These characteristic signals are used later on for the classification of the microbeads stochastically deposited into the microwells.

The methods based on supervised learning are relatively easy and straightforward to implement. However, they possess several drawbacks in context of the microbead-based stochastic peptide microarray manufacturing. Every time a new batch of microbeads is fabricated, their fluorescence signals are slightly different from those of a previous batch. It means that the tedious training of the algorithm has to be performed for each batch of the microbeads. Moreover, the classification criteria

become obsolete due to the aging of the QDs during long-term storage of the microbeads and emission spectrum shifts in different environmental conditions.

An alternative approach to microbead differentiation is based on unsupervised learning. It implies that the objects to be classified possess a hidden structure, which can be derived from their analysis. Unsupervised learning algorithms do not require any preliminary information on the statistical distribution of the microbead signals. They are mainly based on the assumption that the microbeads of a similar type will be described by similar sets of fluorescence signals obtained in different optical channels.

Three methods of unsupervised learning were considered to address the task of microbead classification: *k*-means clustering, expectation-maximization (EM) clustering, and density-based spatial clustering of applications with noise (DBSCAN). The method of *k*-means does not demonstrate sufficiently good results due to the fact that the clusters of various types significantly differ from each other in size and object density. The EM method shows poor performance in high-dimensional cases and therefore is not suitable when working with multiple fluorescence channels. The best results during preliminary tests were obtained using the DBSCAN method. It employs the principle of density-based clustering: The objects closely packed in a given space are grouped together into a cluster, whereas the objects which are located in low-density regions are considered to be outliers. This method is described in details in Section 2.3.3.

2.2.6 Amino Acid Extraction and Coupling

Requirements

The amino acid derivatives are transferred into the microwells of the substrate being embedded into the polymer microspheres. It ensures that the monomers are not exchanged between the microbeads carrying different amino acids. However, the microbeads should be capable to release the embedded monomers under certain conditions so that they can take part in peptide chain elongation. Therefore, a special procedure had to be developed to enable extraction of the amino acid derivatives from the microbeads, their diffusion to the functional layer and coupling to the terminal amino groups of the growing peptide chains.

In stochastic microbead-assisted peptide synthesis, the amount of monomers available for coupling depends on the carrying capacity of the microbeads and the efficiency of the extraction process. An insufficient amount of monomers in the functional layer imposes the risk that the output of the full-length synthetic peptides will be very low. Therefore, the primal requirement for the amino acid extraction and coupling procedure is the maximization of the coupling yield in each synthesis cycle.

The coupling of the amino acid derivatives requires a certain medium to be present in each microwell that enables their diffusion to the functional groups of the substrate. If the amount of this medium exceeds a certain limit, it can form a continuous layer over the surface, whereby the amino acid derivatives can diffuse into the neighboring microwells. Therefore, the extraction and coupling have to be performed in such a way so that the diffusion of the monomers is prevented.

Implementation

Two approaches of the amino acid extraction and coupling were considered. The first approach is to expose the microbeads to elevated temperatures, whereby the polymer matrix undergoes melting [22]. The amino acid derivatives gain mobility and can diffuse to the functional layer of the substrate through the molten matrix material (Figure 33). This approach is suitable for the microbeads made of a soluble polymer resin with low glass transition temperature and not applicable in case the microbeads are based on the cross-linked polymer microspheres.

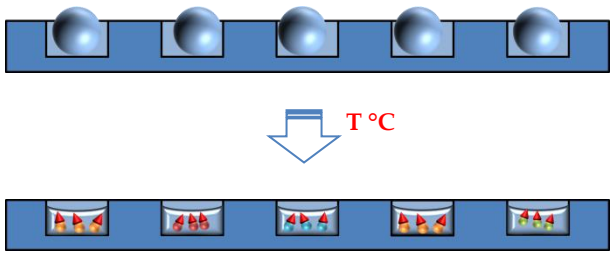

Figure 33. Amino acid extraction at elevated temperatures. Polymer microbeads undergo melting at elevated temperatures, whereby the embedded amino acids gain mobility so that they can diffuse and couple to the functional groups of the substrate.

Within the scope of the present project, an alternative approach to amino acid extraction and coupling was proposed and implemented. The amino acid derivatives are extracted from the microbeads by an appropriate organic solvent that additionally serves as a diffusion medium. The liquid medium has to facilitate

swelling of the cross-linked polymer and dissolving of the embedded amino acid derivatives. Moreover, it has to be confined to each microwell to prevent diffusion of the monomers over the substrate. The challenge is to apply tiny amounts of the liquid medium simultaneously into all microwells, while the top surface of the substrate remains dry. To address this problem, it was proposed to employ the principle of capillary condensation of an organic solvent from a saturated gas atmosphere into the microwells of the microstructured substrate (Figure 34).

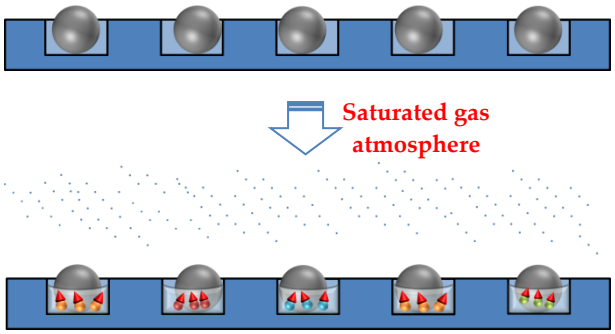

Figure 34. Amino acid extraction in a saturated atmosphere. A saturated gas of an organic solvent is subjected to capillary condensation in the microwells of the microstructured substrate, whereby the cross-linked polymer microspheres undergo swelling and release the amino acid residues.

The organic solvent in a liquid state is placed into a special chamber closed thereafter by a lid. While the solvent evaporates, its concentration in the gas phase gradually increases until the adsorption-desorption equilibrium is achieved. The steady-state concentration of the solvent vapor corresponds to a saturated gas at given ambient conditions. Thereafter, the substrate with deposited microbeads is placed into the chamber. Due to the fact the saturated vapor pressure in the microwells is lower than the saturated vapor pressure over the flat surface, the organic solvent starts to condensate in the microstructures. By controlling the process duration, the amount of the condensate can be fine-tuned. After the substrate is taken out of the chamber, the organic solvent undergoes evaporation from the microwells leaving the extracted amino acid derivatives in the functional layer.

The coupling of the extracted amino acid derivatives takes place in an additional process step. The substrate is placed in the oven in a special chamber filled by an inert gas. At elevated temperatures, the amino acid derivatives react with the functional groups of the substrate much faster resulting in high coupling yields.

2.2.7 Microbead Removal

Requirements

After the extraction and coupling steps are performed, the main function of the microbeads as carriers of the amino acid derivatives is considered to be fulfilled. They have to be removed from the microwells of the substrate to enable deposition of fresh microbeads for the next coupling iteration. However, being exposed to the organic solvent and elevated temperatures, the microbeads based on a cross-linked polymer are firmly attached to the functional layer of the substrate. In order to prevent the permanent blocking of the microwells, a special procedure has to be implemented for the complete removal of the microbeads from the microstructures.

The amino acid derivatives are embedded into the microbeads in a certain excess. During removal of the microbeads, the residues of the activated amino acids can lead to contamination of the microwells. Therefore, the removal of the microbeads has to be performed in such a way so that the risk of the cross-contamination is eliminated.

Implementation

Several techniques can be implemented to ensure removal of the microbeads from the substrate. The microbeads based on the polymer resin can be easily removed by washing the substrate in a suitable organic solvent (Figure 35). The polymer matrix, QD labels and the residues of the amino acid derivatives dissolve well in chlorinated organic solvents. Repeating the washing cycle several times ensures that the microwells are devoid of any residues. Since the washing takes place in a liquid state, a special agent is added to the solvent, which passivates the amino acid residues. It prevents contamination of the microwells by a mixture of different monomers. Although this method is simple and straightforward, it is not suitable for the microbeads based on the cross-linked polymer microspheres.

Figure 35. Removal of the polymer matrix and the excessive amino acid derivatives by dissolving them in an appropriate organic solvent. Special additives are implemented to passivate the residual monomers (the coupled amino acids are not shown for simplicity).

An alternative approach employs an adhesive tape to collect the microbeads from the microwells of the substrate (Figure 36). An adhesive tape is applied over the substrate, whereby all the microbeads get attached to the adhesive layer. In case the adhesion of the microbeads to the adhesive layer is stronger than to the functional layer of the substrate, they are removed from the microwells by detaching the tape from the substrate. This method does not impose any risk of amino acid cross-contamination. However, its reproducibility depends on the homogeneity of the adhesive layer and the uniformity of applying the tape over the substrate.

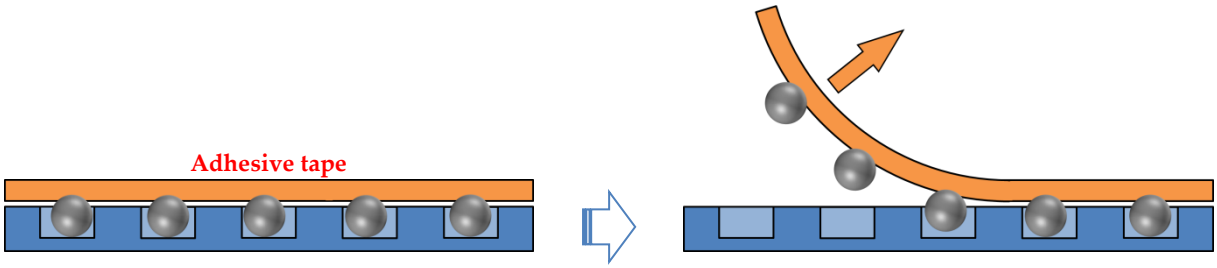

Figure 36. Microbead removal using an adhesive tape.

The microbeads can be removed from the microwells by immersing the substrate in an appropriate solvent and exposing it to the acoustic vibrations generated in an ultrasonic bath (Figure 37). The microbeads swell in the solvent, which facilitates their detachment from the surface of the substrate. A special agent, preliminary added to the solvent, passivates the monomer residues. The acoustic waves, transmitted through the liquid medium, induce the removal of the microbeads from the microwells. Exchanging the liquid medium and repeating the process several times ensures a complete removal of the microbeads from the microstructures.

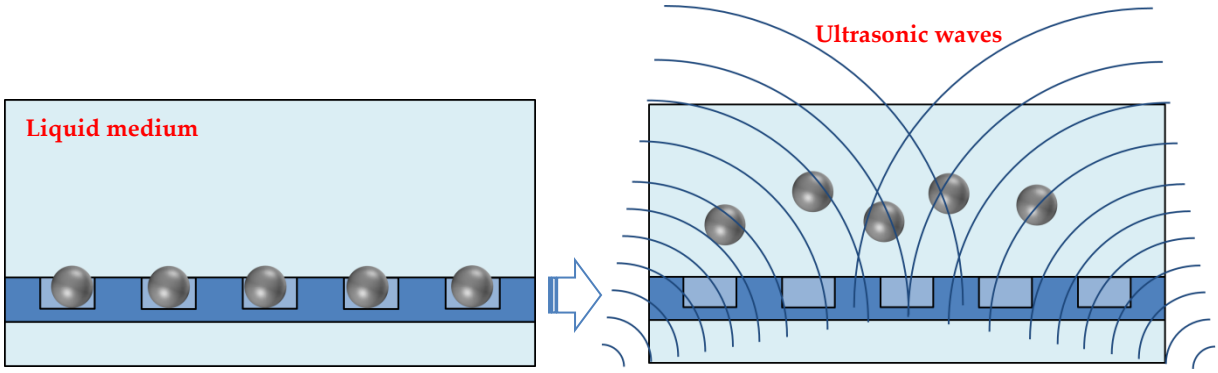

Figure 37. Microbead removal using ultrasonic waves. The microstructured substrate is immersed into an appropriate liquid medium and exposed to the acoustic vibrations generated in an ultrasonic bath, whereby the microbeads are removed from the microwells.

2.3 Theoretical Foundations

In this section, the theoretical foundations of the processes underlying the stochastic peptide microarray manufacturing are briefly reviewed.

2.3.1 Adhesion of Microbeads

The principle of microbead deposition is based on the geometric constraints the microwells impose on the microbeads. Applying a sufficient tangential force enables removal of the excessive microbeads from the top surface without affecting the microbeads inside the microstructures.

The adhesion of microbeads to a solid surface in a gas medium can be caused by the van der Waals force (F_{vW}), the electrostatic force (F_{el}), and the capillary force (F_c):

$$F_{ad} = F_{vW} + F_{el} + F_c \tag{1}$$

For absolutely smooth and undeformable bodies, the force of the van der Waals interaction between a spherical particle and a plane is defined as [40]:

$$F_{vW} = \frac{Ar}{6H^2} \tag{2}$$

where A is the material-dependent Hamaker constant of the molecular interaction of the condensed bodies, r is the radius of the particle, and H is the gap width determined by the Born repulsion and is usually taken as 0.4 nm in air.

When rubbing a mixture of microbeads with a lint-free tissue over the substrate, the microbeads may become electrically charged due to the triboelectric effect. Assuming that the charged microbeads induce an equal and opposite charge on the surface, the resulting electrostatic force can be approximated by the formula [40]:

$$F_{el} = \frac{1}{4\pi\varepsilon_0}\frac{q^2}{(2r)^2} \tag{3}$$

where q is the particle charge, and ε_0 is the vacuum permittivity.

When the relative humidity exceeds 65 %, condensation of water vapor takes place at the contact point between the microbead and the surface, which leads to a liquid bridge formation. The arising capillary force contributes to the adhesion of the microbead to the substrate according to the formula [40]:

$$F_c = 4\pi\gamma r\cos\theta \tag{4}$$

where γ is the surface tension of the liquid, and θ is the contact angle between the liquid and the surface.

For the microbeads with a diameter of 10 μm, the capillary force is the dominating component of the microbead adhesion to the substrate, as long as the liquid bridge is formed [41]. The second largest component is the van der Waal force, which is lower by an order of magnitude than the capillary force. Even in the case the model microbeads have the maximum surface charge density (defined by the electric field limit for discharging), the contribution of the electrostatic force to the adhesion is lower by one order of magnitude than the van der Waals force.

When removing the excessive microbeads from the top surface of the substrate with a compressed air flow, the microbeads are subjected to the adhesion force (F_{ad}), the microbead weight (F_g), the drag force (F_{dr}), and the lift force (F_{lif}). The condition for the detachment of a microbead can be expressed by inequality [40]:

$$F_{dr} \geq \mu\left(F_{ad} + F_g + F_{lif}\right) \tag{5}$$

where μ is the coefficient of friction.

For 10 μm microbeads, $F_{ad} >> F_g$ and $F_{dr} >> F_{lif}$ so that the criterion for their detachment can be defined as follows:

$$F_{dr} \geq \mu F_{ad} \tag{6}$$

Assuming the microbeads on the top surface of the substrate are completely submerged into the laminar boundary layer, the drag force arising from the air flow around the microbead can be calculated from the formula [40]:

$$F_{dr} = 6\pi\eta v_p r \tag{7}$$

where η is the dynamic viscosity of the air stream, and v_p is the air flow velocity at the level of the particle center.

Neglecting the electrostatic interactions and the liquid bridge formation (at the relative humidity < 65 %), the air flow velocity needed to remove the microbeads from the top surface can be estimated by combining Eq. (1), Eq. (2), Eq. (6) and Eq. (7):

$$v_p \geq \frac{\mu A}{36\pi\eta H^2} \tag{8}$$

The critical air flow velocity was estimated to be around 175 $m \cdot s^{-1}$, which is one order of magnitude greater than the actual airflow needed to remove the microbeads from the top surface of the substrate. We assume that the microbeads were partially submerged into the turbulent boundary layer during their removal with a compressed air flow. For a given free-stream velocity, the drag force under turbulent flow conditions is approximately two orders of magnitude greater than the drag in a laminar boundary layer [40]. It means that the microbeads could be removed from the top surface by far lower stream velocities than estimated by Eq. (8) in case their detachment took place under the turbulent boundary conditions.

2.3.2 Excitation and Emission of Quantum Dots

QDs are semiconductor particles with a diameter of several nanometers. Due to their extremely small size, QDs behave similarly to three-dimensional quantum wells. The energy states allowed in a quantum well correspond to the energy levels that cause the de Broglie wavelength to form a standing wave. The de Broglie wavelength λ_{dB} of a charge carrier with the mass m and energy E is defined as:

$$\lambda_{dB} = \sqrt{\frac{h^2}{2mE}} \tag{9}$$

where h is the Planck constant. The condition for a standing wave is given by:

$$n\lambda_{dB} = 2d \tag{10}$$

where d is the quantum well width, and n is an integer.

Combining Eq. (9) and Eq. (10) results in the discrete-energy levels of a confined electron in the quantum well as a function of the integer n:

$$E_n^{conf} = \frac{h^2 n^2}{8md^2} \tag{11}$$

Under exposure to an electrical charge or a light source, an electron in the QD can be excited into the conduction band, leaving a hole in the valence band. Both the excited electron and the hole exist in one of the n energy states of the respective bands. Emission of a photon can take place when the electron from the $n = 1$ energy state in the conduction band undergoes relaxation to the $n' = 1$ energy state in the valence band. The energy of the emitted photon E_{photon} can be approximated as the sum of the

bulk band gap energy E_{BG} and the confinement energies of the hole and the excited electron (the term describing the bound energy of the exciton is neglected) [42, 43]:

$$E_{photon} = E_{BG} + \frac{h^2}{8m_e^* d^2} + \frac{h^2}{8m_h^* d^2} \tag{12}$$

where m^*_e and m^*_h are the effective masses of the electron and the hole.

The photon energy is defined by its wavelength λ_{ex} as:

$$E_{photon} = \frac{hc}{\lambda_{ex}} \tag{13}$$

where c is the speed of light in vacuum.

Assuming that the QD diameter can be approximated by d, the relation between the emission wavelength and the QD size is derived in the form:

$$\frac{1}{\lambda_{ex}} = \frac{E_{BG}}{hc} + \frac{h}{8c}\left(\frac{1}{m_e^*} + \frac{1}{m_h^*}\right)\frac{1}{d^2} \tag{14}$$

As follows from Eq. (14), the emission wavelength of QDs can be tuned by changing their size, shape and composition. In particular, the QDs with larger diameters emit longer wavelength (Figure 38). For instance, the CdSe QDs with a diameter of 6 nm emit in the red region of the spectrum, whereas the CdSe QDs with a diameter of 2 nm emit in the blue region of the spectrum [44].

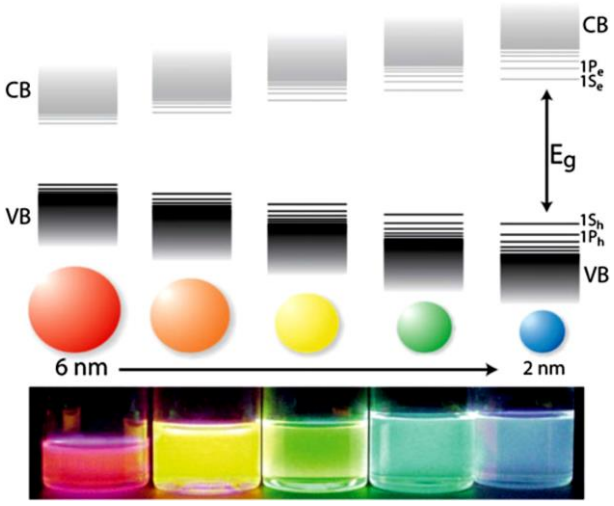

Figure 38. Schematic illustration of the quantum confinement effect. The bandgap of the semiconductor material increases with the decreasing size of the QDs, resulting in shorter emission wavelengths. Reproduced from **[44]** with permission of The Royal Society of Chemistry (http://dx.doi.org/10.1039/C0CS00055H).

The emission spectrum of a single QD is described by a Lorentzian function due to homogeneous spectral line broadening. In case of an ensemble of QDs, having a statistical size distribution, their emission spectrum is described by a Gaussian function due to the superposition of the spectral Lorentzian functions.

2.3.3 DBSCAN Clustering

The DBSCAN algorithm, proposed in 1996, is nowadays one of the most common data clustering methods [45]. Its principle is based on grouping together closely packed data points, whereas the data points in low-density regions are marked as outliers.

Two parameters are required for DBSCAN, which are the neighborhood radius (ε_c) and the minimum number of neighbors (N_{min}). For a certain set of points to be clustered, each element is classified either as a core point (if at least N_{min} points are within its ε_c-neighborhood including the core point itself), a border point (if less than N_{min} points are within its ε_c-neighborhood and at least one of them is a core point), or a noise point (not a core point nor a border point). A given core point forms a cluster together with all the core and border points reachable from it (Figure 39).

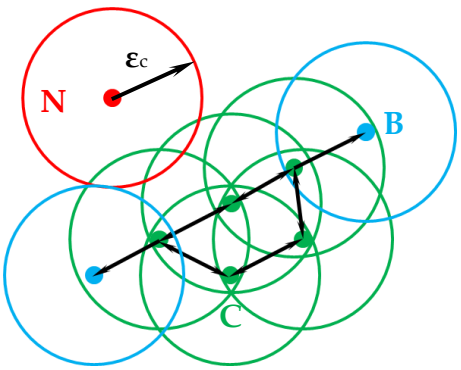

Figure 39. Schematic illustration of DBSCAN clustering. Point C and other green points are assigned as core points since each of them has at least three neighbor points ($N_{min} = 3$) reachable within ε. Since each of the core points is reachable from one another, they build up a cluster. Point B and another blue point are border points. They belong to the cluster, being reachable from the core points. Point N is a noise point. It is not reachable from any of the core points; therefore it does not belong to the cluster.

An abstract DBSCAN algorithm is performed in three steps. First, the number of neighbors within the ε_c-neighborhood is defined for each point. The core points are identified with at least N_{min} neighbors (including the point itself). Second, the core points reachable from each other are grouped into individual clusters. Third, the

non-core points, reachable from at least one core point, are assigned to the respective cluster as border points. The remaining points are assigned as noise. The run time complexity of such an algorithm is $O(n^2)$ [46]. In case a query-based algorithm is implemented, an overall run time complexity is reduced to $O(n \log n)$.

With respect to the problem of decoding the microbeads of various types, the DBSCAN algorithm has several advantages compared to other methods. It enables classification of arbitrarily distributed data into clusters of any shape. The algorithm makes it possible to identify noise points, whereas its overall performance is not affected by the outliers. The DBSCAN method requires just two parameters that can be pre-set for a well-understood data. The main drawback of DBSCAN is that it cannot properly handle data sets with highly different densities.

2.3.4 Capillary Condensation

The amino acid derivatives are extracted from the microbeads using an appropriate organic solvent in a liquid state. To avoid diffusion of the monomers to the neighboring microwells, the liquid medium has to be confined to the microstructures without forming a continuous layer over the top surface of the substrate. The problem of simultaneous and precise deposition of the extraction medium into the microwells was solved by its capillary condensation from a saturated gas.

When placed into a closed extraction chamber, the organic solvent in the liquid state undergoes evaporation, thereby increasing the concentration of its molecules in the gas state. In a closed system, the pressure of the vapor in thermodynamic equilibrium with its condensed phase defines the equilibrium vapor pressure at a given temperature. It can be approximated by the semi-empirical Antoine equation in the basic form:

$$\log_{10} P = A - \frac{B}{C + T} \tag{15}$$

where P is the vapor pressure, T is the temperature and A, B and C are substance-specific constants.

The state of thermodynamic equilibrium between the vapor and the liquid medium depends on the curvature of the interface between the two phases. In case of a spherical meniscus the liquid medium forms in a microwell, the equilibrium vapor pressure is described by the Kelvin equation [47]:

$$P(r) = P(\infty)\exp\left(-\frac{2\gamma V_m}{RTr}\right) \quad (16)$$

where $P(\infty)$ is the saturating vapor pressure when the surface of the liquid is flat, γ is the surface tension of the liquid, V_m is the molar volume of the liquid, R is the universal gas constant, and r is the radius of the spherical meniscus.

The radius of the spherical meniscus depends on the radius of the microwell r_c and the contact angle θ between the liquid and the surface and can be derived as [47]:

$$r = \frac{r_c}{\cos\theta} \quad (17)$$

In view of Kelvin equation, the saturating pressure of the organic solvent in the microwell is less than the saturating vapor pressure in the extraction chamber. This may result in condensation of the organic solvent in the microwells at the vapor pressures lower than the normal saturating vapor pressure when the surface of the liquid is flat. In the following, three different scenarios are considered for a cylindrical microwell with radius r_c, exposed to the vapor pressure P_v.

If the actual vapor pressure is lower than the saturating vapor pressure in the microwell $P_v < P(r)$, the condensation does not take place. If the vapor pressure is equal to the saturating vapor pressure in the microwell $P_v = P(r)$, the organic solvent condensates in the microwell and fills it until the meniscus with radius r reaches the edge of the microwell. If the vapor pressure is between the saturating vapor pressure in the microwell and the saturating vapor pressure when the surface of the liquid is flat $P(r) < P_v \leq P(\infty)$, the organic solvent condensates in the microwell and fills it until the meniscus with infinite radius is formed at the edge of the microwell.

In case the microwells are filled with microbeads, the radius of the meniscus is expected to be much smaller than that in the empty microwell. It should result in a lower saturating vapor pressure in the filled microwell and enhanced condensation of the organic solvent in the microwell from its saturated vapor.

2.3.5 Diffusion of Amino Acid Derivatives

During their extraction from the microbeads, the amino acid derivatives diffuse over the functional layer wetted by the organic solvent. The diffusion of the monomers should be sufficient to cover the bottom of the microwell and at the same time it

should be limited by the microwell surface area to prevent contamination of the neighboring microwells.

To simplify the problem, assume a microbead is deposited onto a flat functionalized substrate. The contact point between the microbead and the substrate can be considered as a point source of the extracted amino acid derivatives with the initial amount of n_0. In this case, the time-dependent concentration profile of the amino acid derivatives over the surface can be described by the formula [48]:

$$c(r,t) = \frac{n_0}{4\pi Dt} \exp\left(-\frac{r^2}{4Dt}\right) \tag{18}$$

where D is the diffusion constant and r is the distance in two-dimensional space:

Assuming the amino acid derivatives behave as spherical nanoparticles, the diffusion constant can be estimated from the Stokes-Einstein law [48]:

$$D = \frac{kT}{6\pi\eta a} \tag{19}$$

where k is the Boltzmann constant, T is the absolute temperature, η is the viscosity of the diffusion medium, and a is the radius of the sphere approximating the amino acid derivative.

At each time point, the diffusion profile of the amino acid derivatives is described by a two-dimensional Gaussian function with a time-dependent height and width of the bell curve's peak. In reality, the amount of the amino acid derivatives at the source point depends on the extraction dynamics and varies over time. Moreover, the diffusion medium itself originates at the contact point between the microbead and the substrate and tends to spread over the surface over time. Both factors make the problem complicated to be solved analytically and therefore are not considered here.

3 Materials and Methods

In this chapter, the materials and methods implemented within the scope of the present work are described in details. Different types of functionalized substrates are introduced in Section 3.1. The architecture and composition of the microbeads, as well as their manufacturing procedure, are discussed in Section 3.2. Section 3.3 reviews the microbead deposition methods, whereas the imaging technique and the algorithm for decoding of the amino acid allocation pattern are described in Chapter 3.4 and Chapter 3.5, respectively. The extraction and coupling of the amino acid derivatives are considered in Section 3.6, followed by the description of the microbead removal in Section 3.7. Section 3.8 introduces general chemical procedures implemented in series of experiments. Finally, the framework for the prototype manufacturing is described in Section 3.9.

3.1 Functionalized Substrates

Two different types of functionalized substrates were used in experiments, which are microstructured and flat substrates. The purpose and characteristics of each type of substrate are described below.

3.1.1 Microstructured Substrates

Microstructured functionalized substrates are essential in stochastic peptide microarray manufacturing. They were used in several series of experiments with the aim to identify appropriate parameters of the microstructures, elaborate the microbead deposition and removal techniques, as well as optimize the extraction and coupling conditions for the amino acid derivatives.

Initially, the microstructured slides with various layouts of microwells were thought over and later on manufactured in the clean room facilities at the IMT (Figure 40). The substrates were made of fused silica and had dimensions of 20 mm x 20 mm x 0.5 mm. Each slide had nine separate fields representing microstructured sub-arrays with individual pitch size (P, in μm) and microwell

diameter (D, in μm): P40 D35, P30 D25, P20 D15, P15 D13, P15 D12, P15 D11, P10 D8, P10 D7, and P10 D6. The microstructures had the depth of either 9 μm or 10 μm.

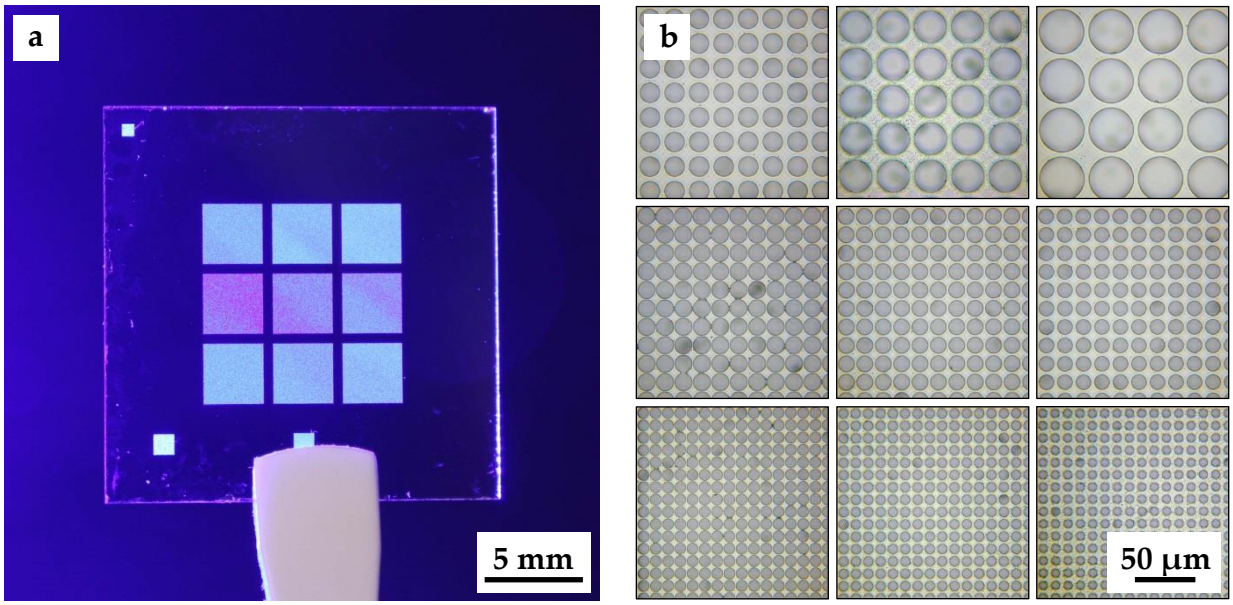

Figure 40. Microstructured substrate (20 mm x 20 mm x 0.5 mm): (a) general view; (b) optical images of the microstructures with various pitch size (P, in μm) and microwell diameter (D, in μm) (from top to bottom row-wise): P20 D15, P30 D25, P40 D35, P15 D13, P15 D12, P15 D11, P10 D8, P10 D7, and P10 D6.

The microstructuring process was performed according to the protocols devised in the Peptide Array group at the IMT [38]. The procedure is schematically depicted in Figure 41. A 4-inch fused silica wafer (SIEGERT WAFER GmbH) undergoes preliminary wet chemical treatment to remove any organic or inorganic contamination from its surface. A sub-micrometer layer of chromium is coated on the wafer by either thermal evaporation or by sputtering. A photoresist is applied over the chromium layer by spin coating. After prebaking of the photoresist, it undergoes exposure to the UV-light pattern generated by a chromium photo-mask aligned between the wafer and the UV-light source. Under exposure to the UV light, the positive photoresist decomposes, so that it can be selectively removed by a special solution during a subsequent developing process, followed by a post-baking step. As a result, the photomask pattern is translated into the photoresist pattern on the wafer. On the next step, the chromium layer, unprotected by the photoresist, is selectively removed by reactive ion etching (RIE) in a mixture of Cl_2, O_2, and He. Thereby, the photoresist pattern is translated into the chromium pattern. After the photoresist residues are removed in a stripping step, the wafer undergoes RIE in

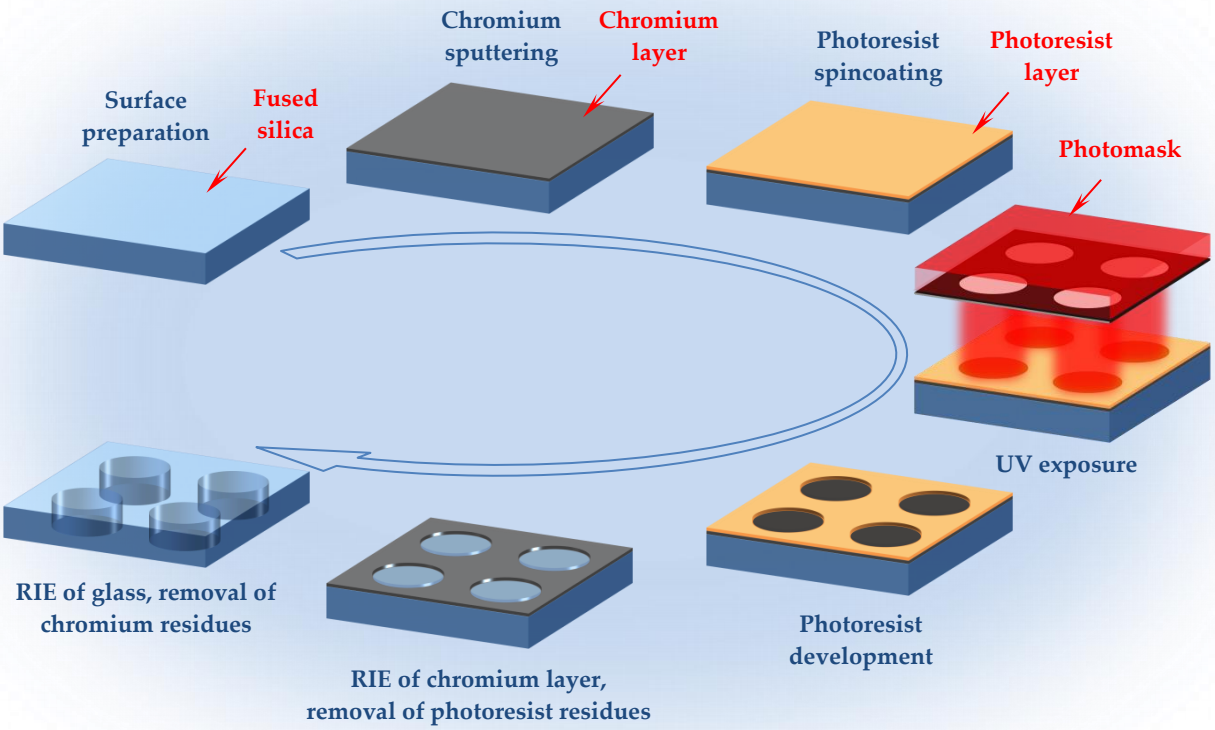

Figure 41. Simplified illustration of the microstructuring process using photolithography and RIE. A thin chromium layer is sputtered onto a fused silica wafer. A photoresist is applied over the chromium layer by spin coating, followed by its pre-baking. The positive photoresist is exposed to the UV light resulting in its selective decomposition and further removal. In the next step, the chromium layer not protected by the photoresist undergoes RIE, followed by removal of the photoresist residues. Finally, the fused silica wafer undergoes selective RIE with subsequent chromium removal.

CHF_3 plasma, resulting in the selective removal of SiO_2 from the surface unprotected by the chromium mask. The RIE parameters and the thickness of the chromium layer define the depth of the microstructures. During the next step, the chromium residues are removed from the surface. Finally, the wafer is cut into pieces having the format of a substrate slide.

After the optimum parameters of the microstructures were identified in a series of experiments, the full-size microstructured substrates were ordered from the company AMO GmbH. The substrates were made of fused silica and had dimensions of a standard microscopic slide (75 mm x 25 mm x 1 mm). The manufacturing of the substrates was performed using photolithography and RIE according to internal protocols of the company.

Regardless of the format of the microstructured slides, they were functionalized by a thin copolymer layer of poly(ethylene glycol) methacrylate (PEGMA) and methyl methacrylate (MMA) with mole fractions of 10 % and 90 %, respectively. The thickness of the functional layer ranged between 10 nm and 15 nm, whereas the surface density of the amino groups ranged between 1.5 nmol/cm² and 2.5 nmol/cm² [49]. The functionalization of the substrates was performed according to the procedures developed and optimized in the Peptide Array group at the IMT. The process is schematically depicted in Figure 42.

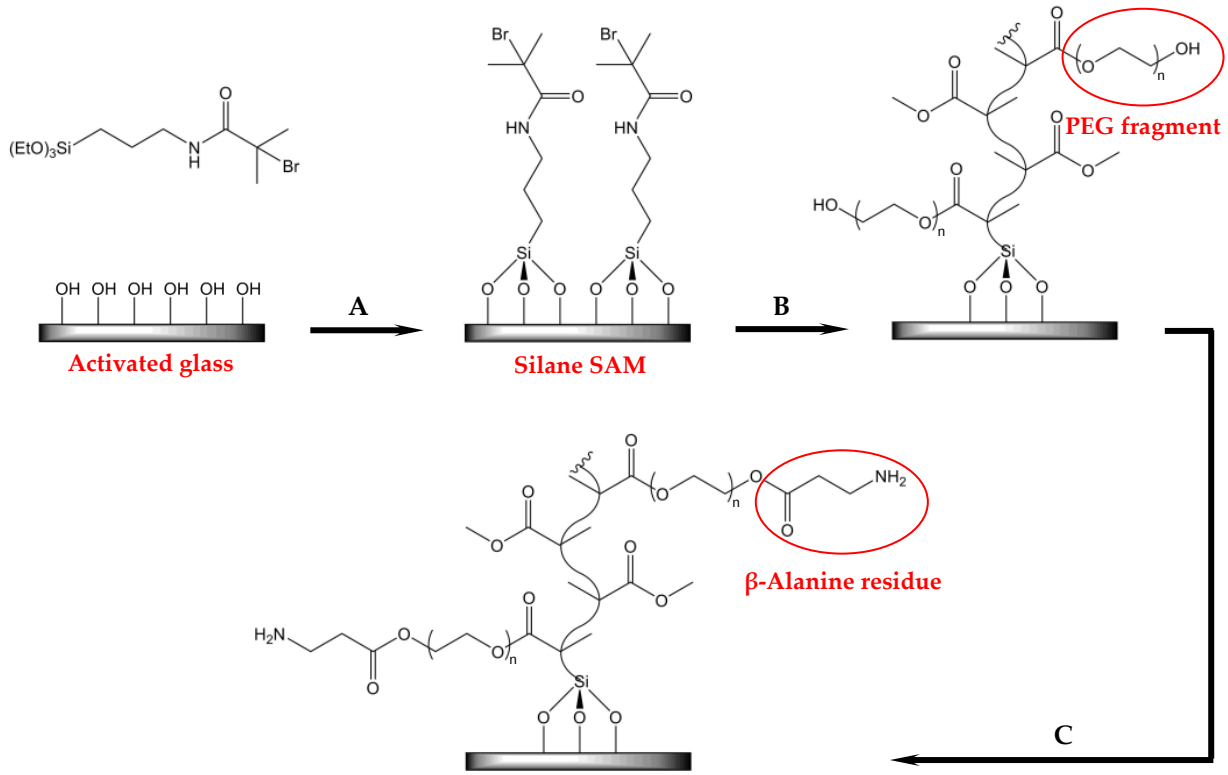

Figure 42. Schematic illustration of the surface functionalization process: (A) an activated glass surface bearing hydroxyl groups undergoes silanization with bromine silane; (B) the resulting silane SAM serves as a surface-bound initiator for radical polymerization with the monomers of PEGMA and MMA. The polymethacrylate backbone chain is shown schematically; (C) the hydroxyl groups of PEG fragments are modified with Fmoc-β-alanine to yield amino groups.

Prior to generating the polymer film, the substrate undergoes wet chemical treatment in KOH to remove any organic or inorganic contamination, as well as to activate the surface to yield hydroxyl groups. Thereafter, the surface undergoes salinization with 2-bromo-*N*-(3-triethoxysilylpropyl) isobutyramide (bromine silane) resulting in the formation of a thin self-assembled monolayer (SAM). The main step of generating

poly(PEGMA-co-MMA) copolymer layer anchored to the silane SAM is performed by using surface-initiated atom transfer radical polymerization (siATRP) with the monomers of PEGMA and MMA mixed in a molar ratio of 10 to 90. Finally, the hydroxyl groups of the poly(ethylene glycol) (PEG) side chains are modified with Fmoc-β-alanine to introduce the amino groups to the functional layer. Since the amino groups of the polymer coating are Fmoc-protected, the substrate can be stored under argon at temperatures between 2 °C and 8 °C.

3.1.2 Flat Substrates

Flat functionalized substrates were used in a series of experiments related to optimization of the microbead architecture and composition, as well as in preliminary studies of the amino acid extraction and coupling. In contrast to the microstructured substrates, the flat substrates enable analysis of the amino acid diffusion profiles. At the same time, they are much cheaper and faster to produce.

Flat functionalized substrates with dimensions of 75 mm x 25 mm x 1 mm were provided by PEPperPRINT GmbH (Figure 43). The substrates were made of glass and were functionalized by a layer of 10:90-poly(PEGMA-co-MMA) according to the internal protocols of the company similar to those used in the Peptide Array group. The declared thickness of the polymer film ranged between 10 nm and 15 nm.

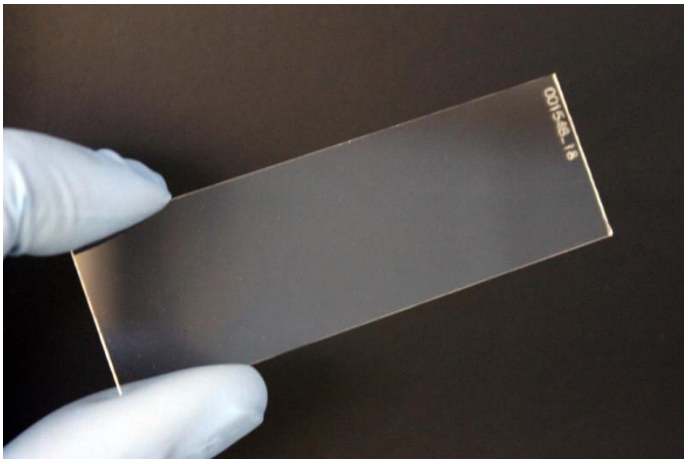

Figure 43. Flat functionalized substrate (75 mm x 25 mm x 1 mm).

3.1.3 Quality Control

The quality of the microstructured substrates was systematically monitored in terms of two criteria. First, the parameters of the microstructures had to comply with the declared specifications. Therefore, the pitch size of the microstructures, as well as the diameter and the depth of the microwells were controlled using white light interferometry (Contour GT, Bruker). Second, the functional layer of the substrates had to be homogeneous enough in terms of the surface concentration of the amino groups available for peptide synthesis. The quality control of the functional layer was performed for a single slide out of each batch of the functionalized substrates. The functional amino groups were Fmoc-deprotected and labelled by N-terminal 5(6)-carboxytetramethyl rhodamine (TAMRA) fluorescent dye. The fluorescence signal was assumed to be proportional to the surface concentration of the functional amino groups and was used for the quantitative analysis of the surface homogeneity.

3.2 Microbeads

Several approaches in microbead manufacturing were tested during the initial phase of the project. Most of them turned out to be not viable in terms of the compliance of the resulting microbeads to the imposed requirements. Within the scope of the present dissertation, the microbeads that met the initial requirements are considered.

3.2.1 Architecture and Composition

The microbeads developed within the framework of the present project are based on the solid-carrier architecture. Special polymer-based microspheres were used as microcarriers of the amino acid derivatives and QDs.

Solid carriers

The cross-linked PMMA microspheres (Spheromers® CA10, Microbeads AS) were selected as solid carriers of the amino acid derivatives and QDs. They were manufactured by emulsification polymerization and cross-linking with 3 % divinylbenzene according to the internal protocols of the company. The microspheres had a mean diameter of 10 μm with an extremely narrow size distribution. The coefficient of variation (CV) was declared to be less than 5 % (Figure 44).

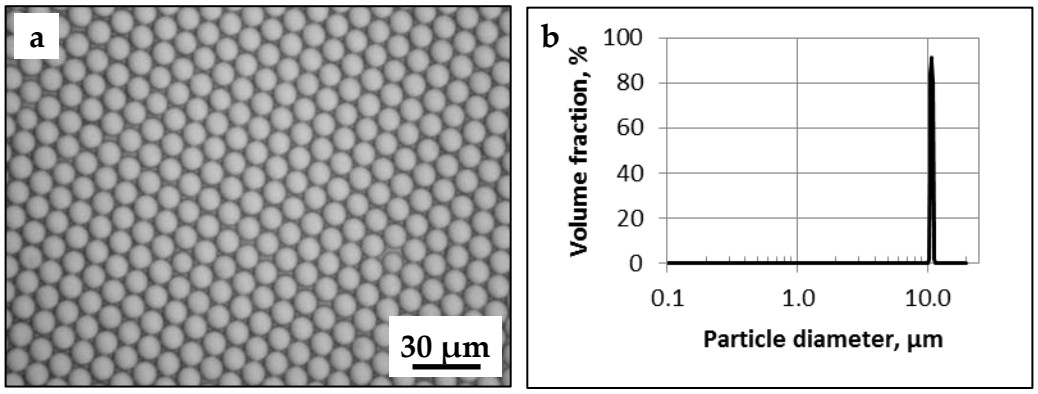

Figure 44. Cross-linked PMMA microspheres: (a) SEM image; (b) microsphere size distribution (image credit: Microbeads AS).

Amino acid derivatives

Commercially available amino acid derivatives (Merck KGaA, Bachem AG), pre-activated at their α-carboxyl group and protected at their α-amino group and side chain group (if applicable), were used as monomers in peptide synthesis. In total 20 different types of proteinogenic amino acid derivatives were tested in terms of their extraction from the microbeads and coupling to the functional layer (Appendix A1). The declared purity (HPLC) of the monomers was ≥ 98 %.

Quantum dots

Hydrophobic ZnCdSeS alloyed QDs (PlasmaChem GmbH) were used as fluorescent markers for labelling the microbeads. The core of the QDs was coated with hydrophobic organic molecules, which made them readily soluble in non-polar organic solvents. The quantum dots with the emission maximum at 470 nm, 490 nm, 500 nm, 520 nm, 530 nm, 550 nm, 560 nm, 570 nm, 580 nm, 590 nm, and 610 nm were tested. The declared accuracy of the maximum emission wavelength was +/-5 nm. The full width at half maximum (FWHM) of the QD emission spectra was 35 nm.

3.2.2 Microbead Manufacturing

The process of microbead manufacturing was developed and optimized within the scope of the present research project (Appendix A2). It consists of two stages schematically shown in Figure 45 and Figure 46.

In the first stage, the solid carriers were labelled with individual QD combinations. A 1 gram sample of cross-linked PMMA microspheres was dispersed in 10 mL of DCM. The dispersion was stirred in a closed vial for 30 min to achieve the swollen state of

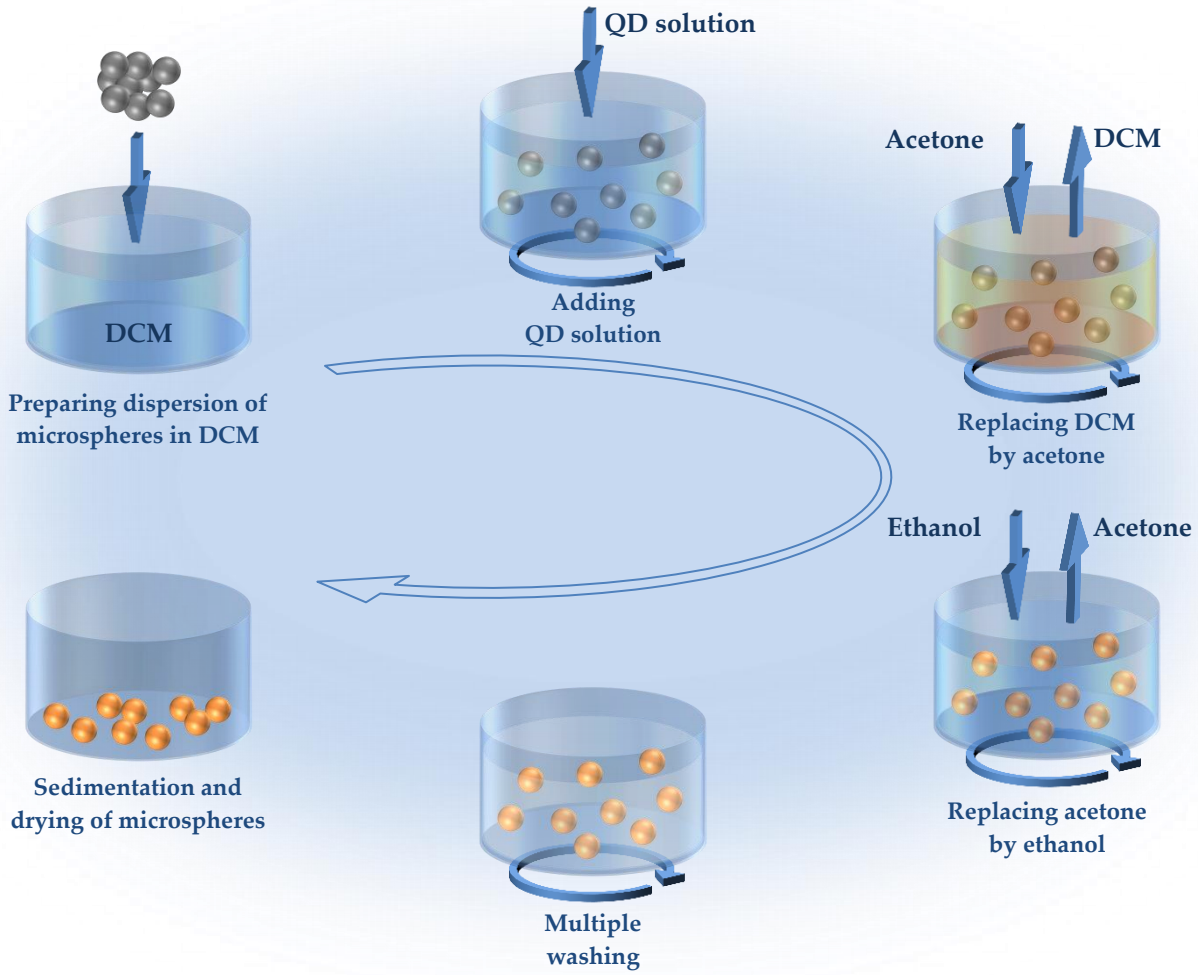

Figure 45. Schematic illustration of the microsphere labelling process. Cross-linked PMMA microspheres are dispersed in DCM and stirred to achieve swelling. The QD solution is added thereafter to the dispersion. In the next step, DCM is gradually replaced by acetone added dropwise to the dispersion. It leads to an increase in the polarity of the continuous phase, initiating precipitation of the hydrophobic QDs onto the swelled microspheres. Then acetone is gradually replaced by ethanol, initiating shrinkage of the cross-linked PMMA. After several washing steps, the labelled microspheres sediment and dry up after removal of the supernatant.

the microspheres. Thereafter, the solutions of QDs in chloroform (2.5 mg/mL) were sequentially added in equal volumes to the dispersion. To derive the optimum content of the QD labels per 1 g of solid carriers, the total volume of the QD solutions varied in the range between 50 μL and 150 μL. The mixture of the microspheres and QDs in DCM was stirred in the closed vial for another 30 min to reach the homogeneous state. While stirring, the hydrophobic QDs were distributed in the continuous phase with the relative permittivity close to that of pure DCM ($\varepsilon_r = 8.9$). On the next step, the vial was opened to initiate evaporation of DCM ($T_B = 40$ °C). During stirring, 30 mL of acetone ($\varepsilon_r = 20.7$) were added dropwise to the dispersion

from a burette. The feeding rate of acetone was adjusted in such a way so that the volume of the dispersion was kept constant and equal to approximately 11 mL. The intention was to change gradually the composition of the continuous phase since the evaporation rate of acetone (T_B = 56 °C) is smaller than the evaporation rate of DCM. As the content of acetone increased, the polarity of the continuous phase increased as well. The hypothesis was that the gradual increase of the polarity of the continuous phase induced precipitation of the hydrophobic QDs onto the microspheres that remain swollen in acetone. In the next step, 30 mL of ethanol (ε_r = 24.5) were added dropwise to the dispersion from the burette. The feeding rate was adjusted so that the volume of the dispersion remained constant. Due to the fact the evaporation rate of ethanol (T_B = 78 °C) is smaller than that of acetone and DCM, its content in the continuous phase had to increase over time. It induced a gradual contraction of the cross-linked PMMA microspheres, resulting in immobilization of the QDs within the outer polymer layer. As the stirring process was terminated, the microspheres sedimented from the continuous phase. The supernatant was carefully removed with a pipette, followed by washing of the microspheres with ethanol and acetone to eliminate excessive QDs. Finally, the microspheres were dried to remove the solvent residues.

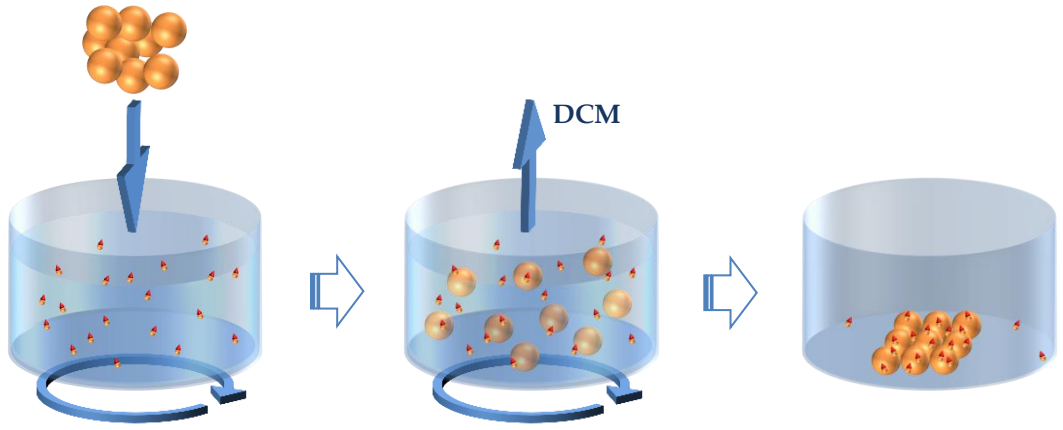

Figure 46. Schematic illustration of the amino acid embedding process. QD labelled microspheres are dispersed in a solution of amino acid derivative in DCM. Upon stirring, the volatile solvent evaporates so that a paste-like medium can form. The paste dries up slowly, followed by milling of the dry mass into a fine powder of microbeads.

On the second stage, the amino acid derivatives were introduced into the polymer matrix of the labelled solid carriers. A sample of amino acid derivatives was initially

dissolved in 10 mL of DCM. The mass of the amino acid derivatives was varied in the range between 10 mg and 50 mg with the aim to define the optimum monomer content in microbeads. The amino acid solution was added to 1 g of QD labelled microspheres. The resulting dispersion was gently stirred until a paste-like medium was obtained due to gradual evaporation of the solvent from the open vessel. The paste dried up slowly over 2 hours. The resulting dry mass of microbeads was milled in a falcon tube with several metal spheres (Ø = 5 mm) on a vortex shaker.

Three assumptions were made in favor of the method's viability. First, the microbeads swelled in DCM within a relatively short time. Second, the QDs embedded into the microspheres in a previous stage remained inside the cross-linked polymer without being extracted. Third, the amino acid derivatives gradually precipitated from the saturated solution into the swelled microbeads, while the solvent underwent evaporation.

3.2.3 Optimization and Quality Control

Within the scope of the present project, the composition of the microbeads had to be optimized in terms of the content of both the amino acid derivatives and the QDs. To control the quality of the manufactured microbeads, the samples were applied either over the flat functionalized substrate or into the microwells of the microstructured substrate. The strength and the homogeneity of the QD fluorescence signals were studied by fluorescence imaging of the microbeads followed by image analysis.

The nature and the content of the amino acid derivatives influenced their diffusion rate and the coupling yield. Under certain conditions, the amino acid derivatives were extracted from the microbeads and coupled to the functional layer, followed by acetylation of the remaining free amino groups of the substrate, Fmoc-deprotection of the amino groups of the coupled amino acids, and fluorescent labelling of those amino groups with an NHS (*N*-hydroxysuccinimide) ester dye (see Section 3.8). The fluorescence signals of the amino acid spots were considered to be proportional to the surface concentration of the coupled monomers defined by their coupling yield. The analysis of the cross-section spot profiles provided information on the diffusion of the amino acid derivatives extracted and coupled at given conditions.

3.3 Microparticle Deposition

In the initial phase of the project, various methods were tested to deposit the microbeads into the microwells of the microstructured substrate. They were based on the surface tension impact of the meniscus inside the microfluidic channel, the electrostatic properties of the solid carriers, and the mechanical forces applied to the microbeads. In the present dissertation, two methods of microbead deposition into the microwells of the substrate are considered. Both methods are based on dry-state microbead deposition using mechanical impact.

The first method was based on a manual spreading of a dry microbead mixture over the surface of the microstructured substrate by a soft lint-free tissue (Kimtech Science, Kimberly-Clark) (Figure 47a). The excess of microbeads was removed from the top surface using a compressed air flow applied under various pressures in a range of angles with respect to the substrate (Figure 47b).

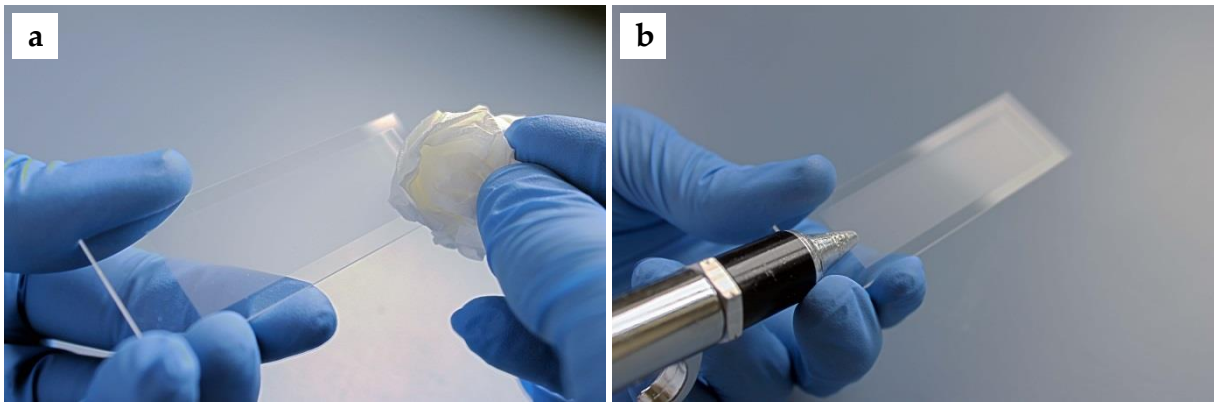

Figure 47. Two-step microbead deposition: (a) spreading the microbeads with a soft tissue; (b) removal of the microbeads from the top surface of the substrate using a compressed air blow gun.

An alternative technique was based on using a doctor blade. A mixture of microbeads was manually spread over the substrate with a plastic spatula having a fine-polished edge (Figure 48). While pushing forward the microbeads along the top surface, the blade performed a dual function: It inserted some microbeads into the vacant microwells and removed the excessive microbeads from the top surface.

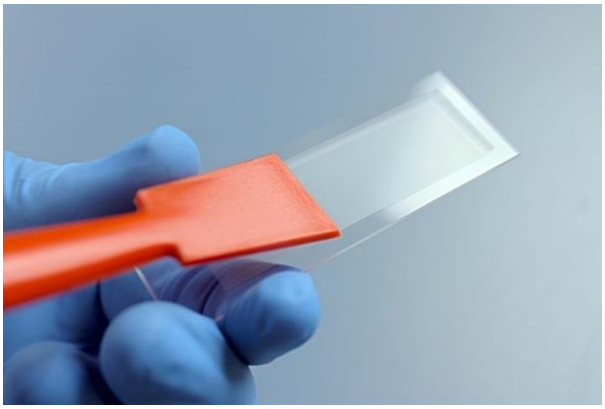

Figure 48. One-step microbead deposition. A plastic spatula is used to introduce the microbeads into the vacant microwells and remove the excessive microbeads from the top surface of the substrate.

The filling rate of the microwells, the contamination of the top surface by excessive microbeads, as well as the fragmentation of the microbeads upon deposition were inspected using optical microscopy and fluorescence scanning.

3.4 Image Acquisition

Image acquisition was performed with a confocal fluorescence scanner InnoScan 1100 AL (Innopsys) (Figure 49). The scanner was equipped with three excitation laser sources emitting at the wavelengths of 488 nm (blue channel), 532 nm (green channel), and 635 nm (red channel). Each excitation source was coupled to a high-sensitive photomultiplier tube (PMT), which enabled image acquisition in up to three optical channels simultaneously. Each optical channel was equipped with a motorized filter wheel with a customer-defined set of fluorescence filters (Semrock, Inc.): 504/12 and 520/5 filters in the blue channel; 549/15, 580/14, 582/75 and 615/20 filters in the green channel; 673/11 and 677/45 filters in the red channel. The scanner had the optical resolution of 0.5 μm/pixel and used a real-time autofocus system.

Figure 49. Fluorescence scanner InnoScan 1100 AL (image credit: Innopsys).

The images acquired with the fluorescence scanner were analyzed using Mapix software (Innopsys). A grid with predefined parameters corresponding to the layout of the microstructured substrate was applied to the image and automatically adjusted to match the microwell pattern. Each spot of the substrate underwent automatic segmentation and was analyzed in each fluorescence channel to derive the photometric feature and background values (Figure 50). The photometric data calculated for all the spots were saved in a file.

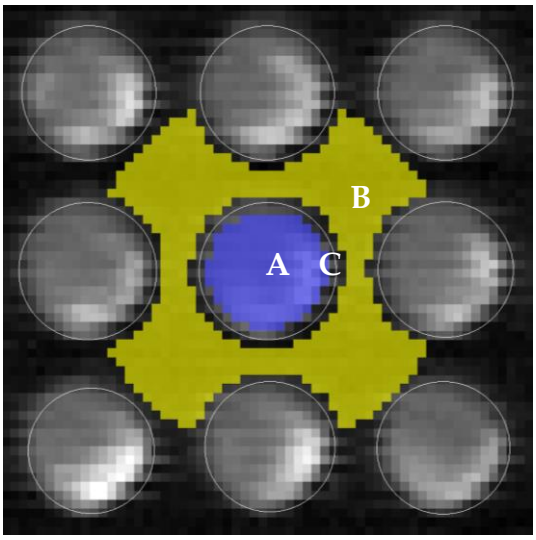

Figure 50. Automatic segmentation of the spots: (A) feature pixels; (B) background pixels; (C) excluded pixels.

In order to facilitate the automatic classification of the microbeads of various types, the combination of the fluorescence filters had to be identified that enabled the spectral resolution of the QD labels. It had to be done in a way to minimize the crosstalk of up to five different QDs in the respective fluorescence channels. The individual effective signals of different QDs in each fluorescence channel were theoretically estimated by using the formula:

$$S = \int_{\lambda_1}^{\lambda_2} E(\lambda) T(\lambda) \, \mathrm{d}\lambda \tag{20}$$

Here, $E(\lambda)$ is the emission function of a QD, $T(\lambda)$ is the transmission function of a fluorescence filter, λ_1 and λ_2 are the integration limits. The transmission values of the filters were provided by the manufacturer, whereas the emission function of the QDs was approximated by a Gaussian function with the standard deviation (SD) defined through the FWHM:

$$SD = \frac{FWHM}{2\sqrt{2\ln 2}} \tag{21}$$

To derive the optimum combination of QDs and fluorescence filters, in total 65 narrow-band Semrock filters and 17 types of QDs, emitting in a spectral range between 490 nm and 650 nm with the step of the emission maximum of 10 nm and the FWHM of 35 nm, were considered. It resulted in 1 105 effective signal values of the QDs in the respective fluorescence channels. Then, all possible combinations of

five kinds of QDs and five fluorescence filters were analyzed in terms of specificity of the QD signals in the corresponding fluorescence channels. Finally, the theoretical data was confirmed experimentally by scanning the QD labelled microbeads in selected fluorescence channels and analyzing the cross-talk between different channels.

3.5 QD Label Decoding

For automatic classification of the microbeads, special software was developed within the scope of the present project. The core algorithm was based on the principles of unsupervised machine learning. The program was created in MATLAB environment (MathWorks, Inc.) and consisted of several blocks executed sequentially (Figure 51).

In the first stage, the data was uploaded from a file generated with the Mapix software. It included the values of feature diameter, median feature signal and mean background signal calculated for each of approximately 3 million spots in each fluorescence channel.

In the next stage, identification of the microwells containing debris of various origins was carried out. For this purpose, the diameters of the spots automatically calculated during the segmentation procedure were analyzed. If the feature diameter was smaller than 8 μm, the given spot was considered to be empty. These spots were assigned "*X*" values and excluded from the data array passed on to the next stage.

Identification of the spots contaminated with relatively large impurities was performed in the following stage. In this case, the impurities were mainly lint microfibers or dust particles of a size much bigger than the pitch of the microstructures. Since these objects overlapped multiple microwells at once, their identification was based on overall analysis of the mean background values. If the mean background value of a spot was higher than a certain threshold value, the corresponding microwell was considered to be covered by an extraneous object. Due to the fact it was impossible to derive information, whether such microwells were filled with amino acid carrying microbeads and of which type, they were assigned "*?*" values and excluded from further analysis.

In the following stage, recognition of the empty microwells was performed. For this purpose, a certain threshold value of the total fluorescence signal had to be derived, which depended on the scanning parameters and the fluorescence characteristics of the microbeads. Since these parameters could differ over time, the algorithm had to enable identification of a dynamic threshold. For each microwell, the median feature values calculated in each fluorescence channel were summed up, thus resulting in the total detected signal. The microwells were arranged in groups depending on their total signal values. This step is analogous to generating a histogram with a certain bin size. In the first iteration, the bin size was assigned to the value Bin_1, whereas the threshold Thr_1 was defined as the central value of the bin having the local minimum frequency. In the next iteration, a new histogram was built for the microwells with the total signal ranging between $Thr_1 - 1.5 \cdot Bin_1$ and $Thr_1 + 1.5 \cdot Bin_1$, with a bin size of $Bin_2 = Bin_1/2$. The adjusted threshold Thr_2 was assigned the central value of the bin having the minimum frequency. The process was repeated multiple times until the histogram with a bin size $Bin_n = 1$ was generated. The value Thr_n was used as a global threshold to identify whether the microwells were filled (total fluorescence signal $\geq Thr_n$) or empty (total fluorescence signal $< Thr_n$). The empty microwells were assigned "*X*" values and excluded from the data considered on the next stage.

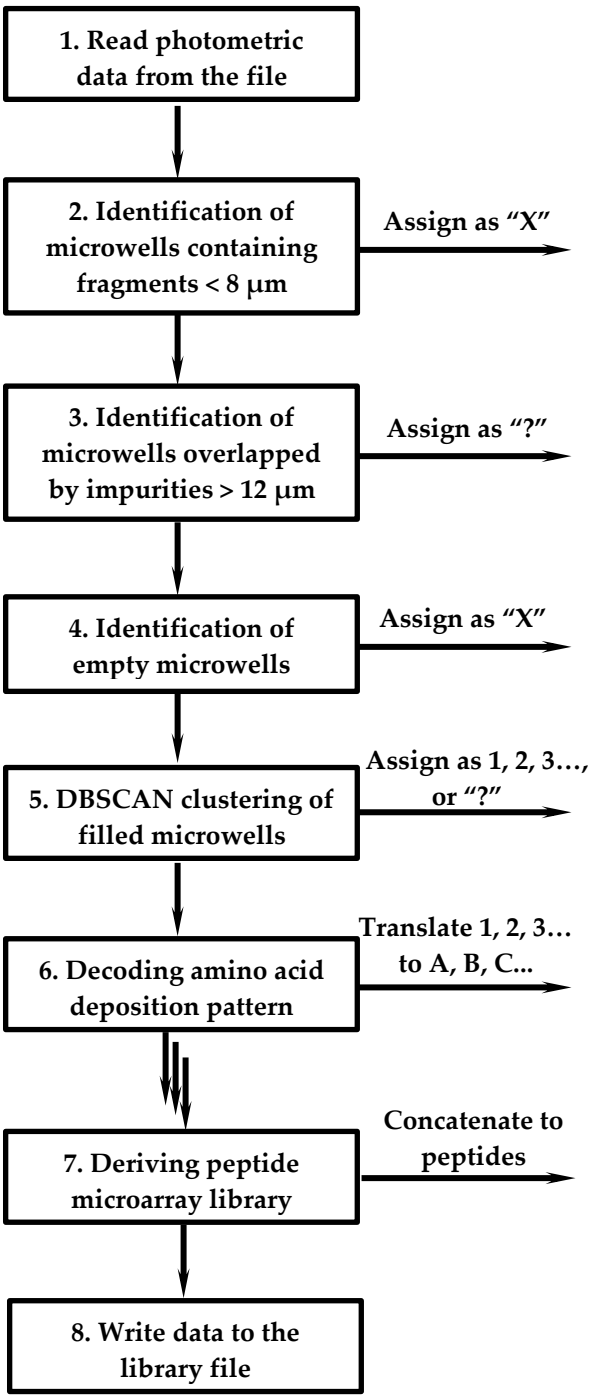

Figure 51. Simplified diagram of the amino acid deposition decoding and generation of the peptide microarray library.

The microwells, which were considered in the previous stages to be filled and non-contaminated, were classified by the DBSCAN clustering algorithm. For this purpose, the median feature values of a given spot, acquired in each fluorescence channel, were normalized with respect to the total signal. It compensated the non-homogeneity of the QDs labelling of the microbeads. As a result of code execution, the microbeads were assigned to different clusters. The judgement on which cluster the microbead corresponded to was based on a relative contribution of the QD labels to the total signal of the microbead. The microwells identified as the elements of the clusters were assigned a one-letter value representing the respective amino acid derivative. The microwells identified as outliers were assigned "*?*" values.

The amino acid patterns derived for each coupling cycle were used in the final stage to generate a file with the peptide library. For each microwell, the amino acid symbols and the "?" symbol were concatenated in the order of peptide chain elongation from C-terminus to N-terminus, whereas the concatenation was terminated if the symbol "*X*" appeared in a given peptide sequence. Thereafter, the peptide sequences were reversed to conform to the notation standard from N-terminus to C-terminus. The derived peptide library was saved in a file, which was used later on to analyze the results of a bioassay.

3.6 Amino Acid Extraction and Coupling

Within the framework of the present project, a new method for amino acid extraction in context of *in situ* solid phase peptide synthesis was proposed. The extraction process took place in a saturated vapor of organic solvent. A special metal chamber was designed to facilitate the extraction process (Figure 52). It was made of stainless steel and consisted of two movable slide holders, each accommodating up to five substrates, and two polytetrafluoroethylene (PTFE) tanks for the liquid-state organic solvent. After adding 30 mL of liquid medium to the tanks, the chamber was kept closed for 30 min to achieve the equilibrium state. Thereafter, the slide holders with the substrates were inserted into the chamber for a certain period of time. After taking the slides out of the chamber, the process was repeated several times to enhance the extraction of the amino acid derivatives from the microbeads.

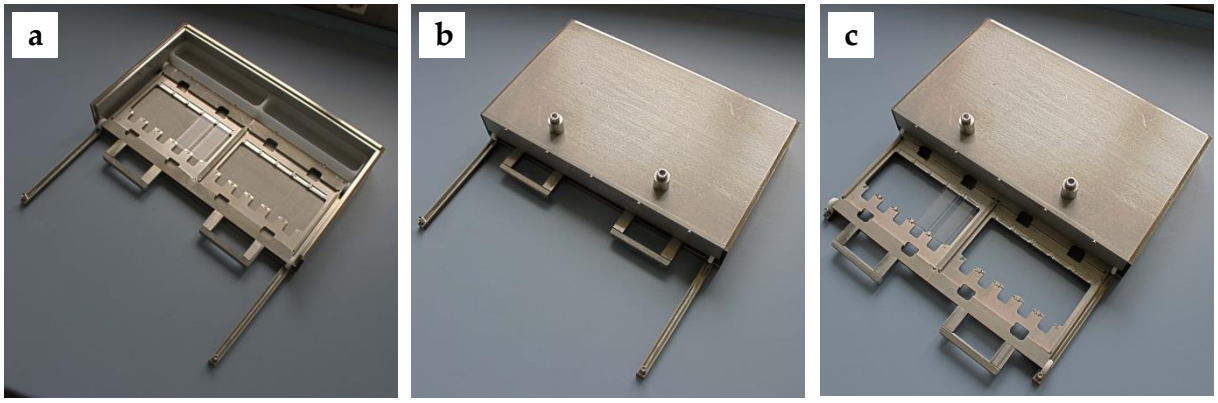

Figure 52. Extraction chamber: (a) view without a lid; (b) general view; (c) view with the slide holders outside the chamber.

The subsequent coupling step was performed for 60 min at 90 °C. For this purpose, the substrate was placed into a coupling chamber, which was filled thereafter with argon and put in the preheated oven (Figure 53). After removing the coupling chamber from the oven, it was slowly cooled down to ambient temperature.

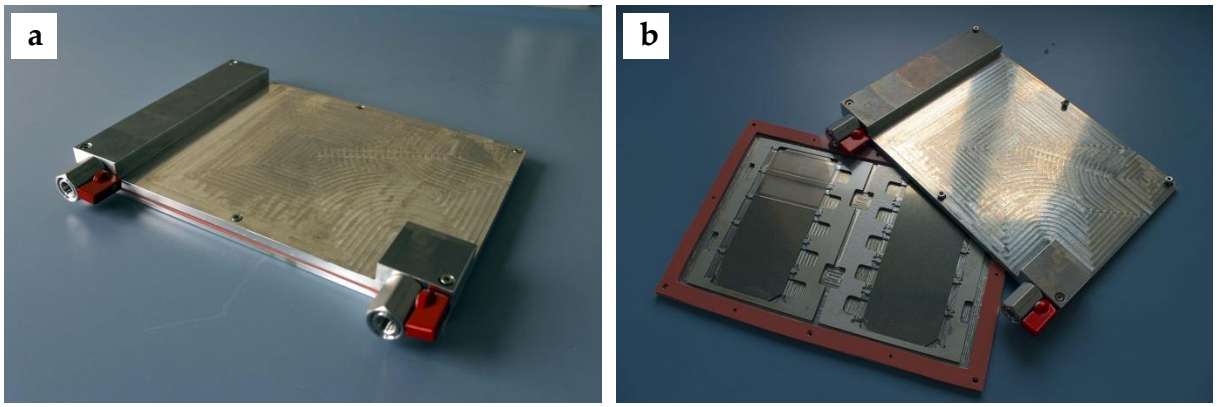

Figure 53. Coupling chamber: (a) general view; (b) view with an open lid.

The process of extraction had to be optimized with the aim to maximize the coupling yield of the amino acid derivatives, while the diffusion of the extracted monomers had to be confined to the microwells (corresponding to approximately 30 μm spots when using flat functionalized substrates). Three organic solvents, acetone, DCM, and *N*,*N*-dimethylformamide (DMF), were tested in terms of their extraction efficiency (Table 2). The duration of a single extraction cycle varied between 0.5 min and 2.0 min. The number of extraction repetitions was ranged between 3 and 15 with intermediate pauses of 1 min.

Table 2. Comparison of organic solvents for amino acid extraction from microbeads.

Parameter	Organic solvent		
	Acetone	**DCM**	**DMF**
Boiling point, °C	56.1	39.6	153.0
Vapor pressure*, kPa	30.6	57.3	0.5
Solubility of PMMA	medium	high	low
Surface wettability	medium	low	high

(*) – vapor pressure at 25 °C.

After extraction and coupling of the amino acid derivatives at certain conditions, the remaining functional groups of the substrate were acetylated, the amino groups of the coupled monomers were Fmoc-deprotected and fluorescently labelled with NHS ester dye (see Section 3.8). The resulting coupling yield and the diffusion of the amino acid derivatives were analyzed based on the images acquired by fluorescence scanning of the substrates.

3.7 Microbead Removal

Removal of the microbeads from the microwells was performed in several steps by placing the substrate in a liquid medium and exposing it to acoustic waves in an ultrasonic bath. In the first step, the substrate was placed into the falcon tube filled with a mixture of 5 % (v/v) *N*-methylethylamine (MEA) and acetone and sonicated for 2 min. MEA was used as a passivation additive to avoid contamination of the microwells with a mixture of non-coupled amino acids derivatives. In the next step, the substrate was sonicated for 2 min in pure acetone. The final sonication step was performed for 2 min in pure DCM. The microbead removal rate was analyzed by optical microscopy and scanning with the fluorescence scanner using neutral-density filters.

3.8 Chemical Steps

Manufacturing of the stochastic peptide microarrays involves standard procedures of surface acetylation and deprotection of the terminal α-amino groups (Appendix A3), as well as deprotection of the side chain groups (Appendix A4). These steps are briefly described in this section, along with the fluorescence staining of the free amino groups (Appendix A6) and immunostaining of the prototype microarray with fluorescently labelled antibodies (Appendix A5).

Fmoc-deprotection

Prior to each coupling step, the terminal α-amino groups were Fmoc-deprotected. A solution of piperidine (20 % v/v) in DMF was applied in excess over the substrate and shaken on a rotary shaker for 30 min. Thereafter, the substrate was washed two times in DMF for 5 min each and two times in methanol for 3 min each.

Blocking step

After the coupling and washing steps were carried out, the unreacted free amino groups of the functional layer were acetylated. A mixture of acetic anhydride (10 % v/v), *N*,*N*-diisopropylethylamine (DIPEA) (20 % v/v), and DMF (70 % v/v) was applied in excess over the substrate and shaken on a rotary shaker for 10 min. Thereafter, the blocking solution was replaced with a fresh one for another 40 min. Finally, the residues of the blocking solution were removed by washing the substrate two times in DMF for 5 min each and two times in methanol for 3 min each.

Side-chain group deprotection

Prior to immunostaining of the stochastic peptide microarray, the side chain groups of the peptides were deprotected. First, the substrate was incubated in DCM for 30 min. Then, a fresh mixture of trifluoroacetic acid (TFA) (51 % v/v), DCM (44 % v/v), triisobutilsilane (TIBS) (3 % v/v), and H_2O (2 % v/v) was applied over the substrate three times for 30 min each, followed by washing in DCM for 5 min. After pre-swelling in DMF for 5 min, the substrate was incubated with a mixture of DIPEA (5 % v/v) and DMF (95 % v/v) for 30 min to neutralize the acidic residues resulted from the TFA cleavage steps. Finally, the substrate was washed three times in DMF for 5 min each, two times in methanol for 3 min each and in DCM for 1 min.

Fluorescence staining with organic dyes

In several series of experiments, the amino acid derivatives coupled to the substrate surface were fluorescently labelled with TAMRA or DyLight 650 NHS ester dyes. Initially, the substrate was incubated in phosphate buffer saline with TWEEN 20 (PBS-T) for 10 min. Thereafter, a solution of a fluorescent dye in PBS-T in dilution of 1 : 10 000 was applied over the substrate for 2 h in the dark. Finally, the substrate was washed two times in PBS-T for 3 min each and then washed in Milli-Q for 1 min.

Immunostaining with fluorescently labelled antibodies

Immunostaining of the stochastic peptide microarray prototype was performed after the side-chain group deprotection. The substrate was preliminary incubated with PBS-T for 10 min. To prevent unspecific binding of the antibodies to the surface, the microarray was incubated thereafter in Rockland blocking buffer (Rockland Immunochemicals, Inc.) for 30 min. After washing the substrate in PBS-T for 1 min, the monoclonal antibodies diluted 1 : 1000 in a mixture of Rockland buffer (10 % v/v) and PBS-T (90 % v/v) were applied over the substrate for 1 h in the dark. Finally, the microarray was washed three times in PBS-T for 1 min each and rinsed with Milli-Q.

3.9 Prototype Microarray Fabrication

A proof-of-principle experiment was carried out to verify whether the proposed concept of stochastic peptide microarray manufacturing was feasible. For this purpose, a full-size prototype microarray, containing random peptides with the length of up to 9 amino acids, was fabricated. The quality of the resulting prototype was proved by immunostaining of the microarray with fluorescently labelled antibodies, followed by fluorescence scanning and data evaluation.

A microstructured fused silica slide (AMO GmbH) with the dimensions of 75 mm x 25 mm x 1 mm was used as a solid support for stochastic peptide synthesis. The microstructures had the pitch size of 20 μm, the diameter of 12 μm, and the depth of 9 μm providing nearly 3 million microwells. Prior to peptide synthesis, the slide was functionalized with a polymer layer of 10:90 poly(PEGMA-co-MMA).

Six types of microbeads containing different amino acid derivatives and QD labels were manufactured according to the established protocol (Appendix A2). The

microbeads and their composition, optimized in a series of preliminary experiments, are listed in Table 3.

Table 3. Set of microbeads for manufacturing stochastic microarray prototype.

Amino acid*	1-Letter notation	Mass fraction	QD label
Alanine	A	2 %	500 nm
Aspartic acid	D	3 %	500 nm
Lysine	K	3 %	580 nm
Proline	P	3 %	580 nm
Tyrosine	Y	3 %	580 nm
Valine	V	3 %	580 nm

(*) – Fmoc-protected, OPfp-activated.

The types of the microbeads in each synthesis cycle were selected in such a way so that the FLAG-epitope (DYKDDDDK) and the HA-epitope (YPYDVPDYA) could be stochastically generated with high probabilities. The mixtures of the microbeads applied prior to each coupling step are shown in Table 4.

Table 4. Microbead mixture compositions in each synthesis cycle.

Synthesis layer	FLAG epitope		HA epitope	
	Amino acid	QD label	Amino acid	QD label
1	Lysine (K)	580 nm	Alanine (A)	500 nm
2	Aspartic acid (D)	500 nm	Tyrosine (Y)	580 nm
3	Aspartic acid (D)	500 nm	Aspartic acid (D)	500 nm
4	Aspartic acid (D)	500 nm	Proline (P)	580 nm
5	Aspartic acid (D)	500 nm	Valine (V)	580 nm
6	Lysine (K)	580 nm	Aspartic acid (D)	500 nm
7	Tyrosine (Y)	580 nm	Tyrosine (Y)	580 nm
8	Aspartic acid (D)	500 nm	Proline (P)	580 nm
9	–	–	Tyrosine (Y)	580 nm

The prototype microarray was synthesized by repeating the sequence of the following basic process steps. Each synthesis cycle started with Fmoc-deprotection of the terminal amino groups of the functional layer. Thereafter, the microbeads were applied into the microwells using a soft lint-free tissue, followed by removal of the microbeads from the top surface with an air jet. Image acquisition of the microbead deposition pattern was performed by scanning the substrate in fluorescence channels 520/5 (corresponding to 500 nm QD labels) and 580/14 (corresponding to 580 nm QD labels). The amino acid pattern was decoded using the software described in Section 3.5. To extract the amino acid derivatives from the microbeads, the substrate was placed into the DCM extraction chamber five times for 1 min each with intermediate pauses of 1 min. The coupling was performed in the coupling chamber under an argon atmosphere at 90 °C for 60 min. The microbeads were removed from the microwells by sonicating the substrate in acetone and DCM for 2 min. Thereafter, the remaining free amino groups were acetylated according to a standard procedure.

After the peptides were synthesized, the terminal amino groups were Fmoc-deprotected and acetylated, followed by deprotection of the side-chain groups. The resulting peptide microarray was incubated with the monoclonal anti-FLAG (conjugated with Cy5 fluorescent dye) and anti-HA (conjugated with Cy3 fluorescent dye) antibodies. The microarray was scanned in fluorescence channels 582/75 (corresponding to a Cy3 fluorophore) and 677/45 (corresponding to a Cy5 fluorophore). The photometric data calculated for each microwell was compared with the peptide library and further evaluated.

4 Results and Discussion

This chapter provides an insight on how the concept of stochastic peptide microarrays manufacturing is manifested in reality. The results of multiple series of experiments on optimization of the layout of the microstructured substrate, as well as on rational design and composition of the microbeads are shown and discussed in Section 4.1 and Section 4.2, respectively. In Section 4.3, two methods for microbead deposition are compared in terms of the microwell filling rates and mechanical stability of the microbeads. The results on multiplexed labelling of the microbeads and readout of their fluorescence signals are discussed in Section 4.4, whereas the performance of the algorithm for decoding the amino acid allocation patterns is evaluated in Section 4.5. Considering the amino acid diffusion and coupling yield, the optimum conditions for their extraction are addressed in Section 4.6. Section 4.7 gives a brief overview of the problems arising during microbead removal. Finally, the results of prototype manufacturing are presented and discussed in Section 4.8.

4.1 Microstructured Substrates

4.1.1 Optimal Layout Parameters

The cross-linked PMMA microspheres with the diameter of 10 μm were deposited into the microwells of the substrate having the dimension of 20 mm x 20 mm and comprising nine microstructured fields with different layouts and the depth of 10 μm. The microbead deposition was performed using a lint-free tissue, whereas the excessive microbeads were removed from the top surface with a compressed air flow. Figure 54 depicts fragments of the images obtained by optical microscopy for different microstructured fields.

As expected, the microwells with the diameter of 25 μm (Figure 54b) and 35 μm (Figure 54c) accommodated several microspheres, whereas the microwells with the diameter of 11 μm (Figure 54f), 12 μm (Figure 54e) and 13 μm (Figure 54d) were filled with not more than one microsphere. The microwells with the intermediate diameter of 15 μm (Figure 54a) contained quite frequently two microspheres, one

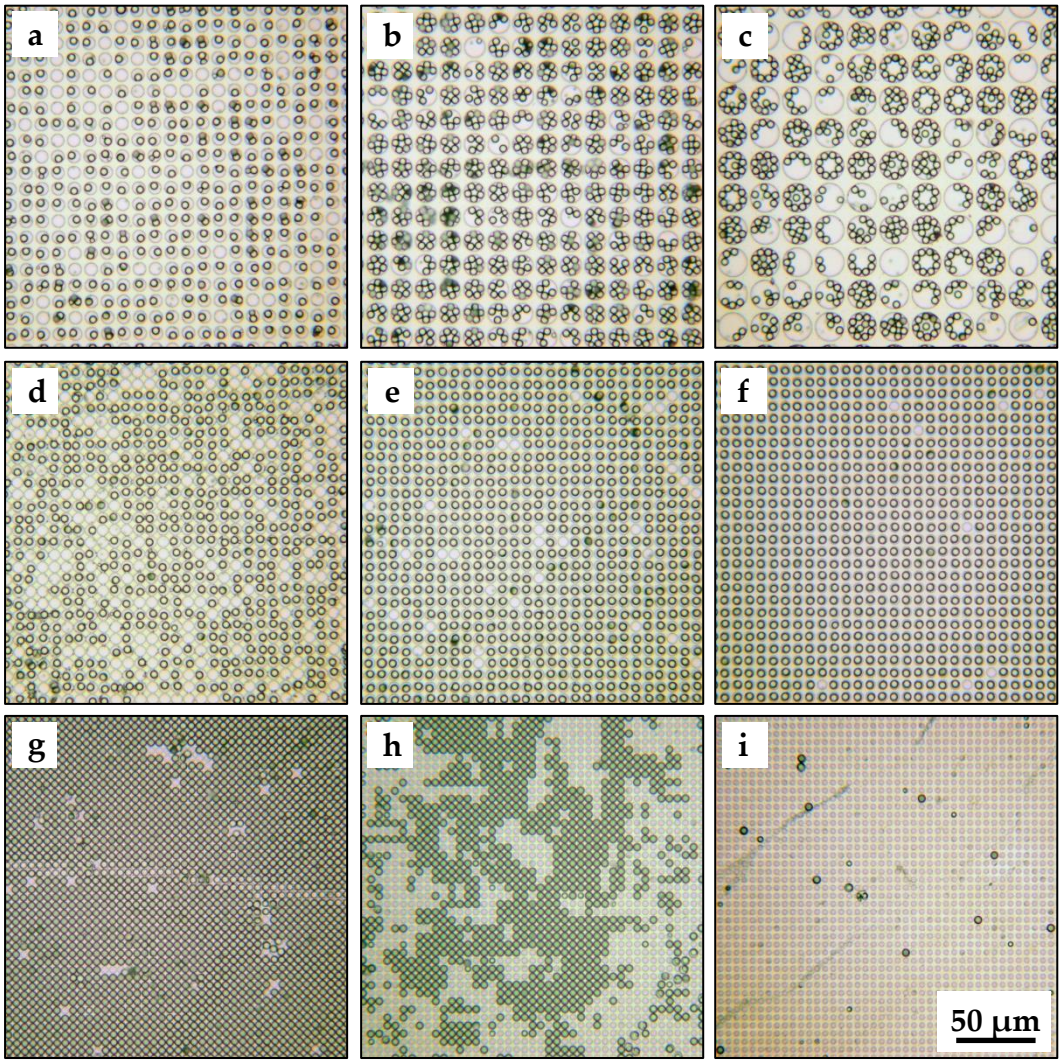

Figure 54. Filling of the microwells with polymer microspheres (Ø 10 µm): (a) P20 D15; (b) P30 D25; (c) P40 D35; (d) P15 D13; (e) P15 D12; (f) P15 D11; (g) P10 D8; (h) P10 D7; (i) P10 D6.

shifted slightly above another. The microstructures with the diameter of 6 µm (Figure 54i), 7 µm (Figure 54h) and 8 µm (Figure 54g) were rather sealed by the microspheres sitting upon the edge of the microwells and rarely contained fine-fraction microbeads with the diameter smaller than 10 µm (Figure 54i).

The principle "one microwell – one peptide" implies that in each synthesis step the microwells are filled with not more than one microbead carrying an individual amino acid derivative. In case of using the microspheres with the diameter of 10 µm, this requirement was satisfied for the microstructures with the diameter of 11 µm, 12 µm, and 13 µm. Therefore, the optimum ratio of the diameter of the microwells to the diameter of the microspheres ranges between 1.1 and 1.3.

The microstructures with the diameter of 11 μm, 12 μm and 13 μm and the depth of 9 μm and 10 μm were compared in terms of their filling rates after depositing the microspheres with the diameter of 10 μm. The deposition of the microspheres was performed by using a lint-free tissue, followed by removal of the excessive microspheres with an air flow. The results derived from the analysis of the acquired images are shown in Table 5.

Table 5. Filling rates of various microstructures with microspheres (Ø 10 μm).

Diameter of the microwells	**Depth of the microwells**	
	9 μm	**10 μm**
11 μm	96.9 %	98.4 %
12 μm	90.2 %	96.3 %
13 μm	42.5 %	75.5 %

The microstructures with the depth of 10 μm and the diameter of 11 μm had the highest filling rate of 98.4 %. The filling rate of the microstructures with a similar depth gradually decreased to 96.3 % for the 12 μm microwells and fell down to 75.5 % for the 13 μm microwells. The microstructures with a depth of 9 μm demonstrated on the whole lower filling rates: 96.9 %, 90.2 %, and 42.5 % for the microwells with the diameters of 11 μm, 12 μm, and 13 μm, respectively.

The fact that the filling rates were lower than 100 % can be explained by the removal of the microspheres from the microwells under the impact of the compressed air flow. Air swirls could originate in the microwells due to partial deflections of the main air stream pushing the microspheres out of the microstructures. At the same time, the microspheres from the top surface could capture the microspheres from the microwells and pull them out. A closer fitting of the microspheres and the microwells restricted origination of the air swirls inside of the microstructures, whereas the geometric constraints prevented movements of the deposited microspheres. Therefore, the maximum filling rates can be achieved when the depth and the diameter of the microstructures approach the diameter of the microbeads.

Another factor, which had to be taken into account when deciding on the optimal parameters of the microstructures, was the microbead removal rate. The close

geometric matching of the non-soluble polymer microspheres to the microwells resulted in extremely low rates of their removal. If the size of the microsphere matched the diameter of the microwell, it was almost impossible to remove this microsphere without deforming or destroying it. Although the cross-linked PMMA microspheres had a mean size of 10 μm, the coefficient of variation of their diameter was declared to be 5 %. It implies that roughly 1 % of the microspheres had a diameter ranging from 10.9 μm to 11.0 μm (assuming normal size distribution) that could potentially block thousands of microwells with the diameter of 11 μm in each step of microbead deposition.

Taking into account the results obtained in a series of experiments, the decision was made to continue the experimental work with the full-size microstructured substrates (75 mm x 25 mm x 1 mm) having the pitch size of 20 μm, the microwell diameter of 12 μm and the depth of 9 μm.

4.1.2 Full-Size Microstructured Substrates

The full-size substrates were investigated in terms of their quality and compliance with the declared parameters. Figure 55 depicts fragments of the microstructured substrate imaged by scanning electron microscopy (SEM).

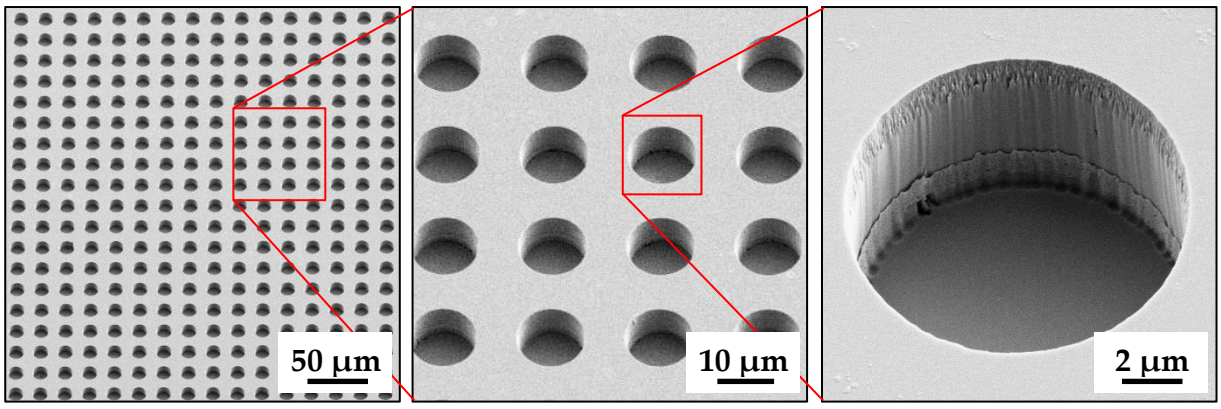

Figure 55. SEM images of the full-size microstructured substrate.

As can be seen, the microstructures were extremely homogenous. No visible defects both at the top surface and at the bottom of the microwells were identified. In order to derive quantitative characteristics of the microstructures, the substrate was investigated by white light interferometry (Figure 56).

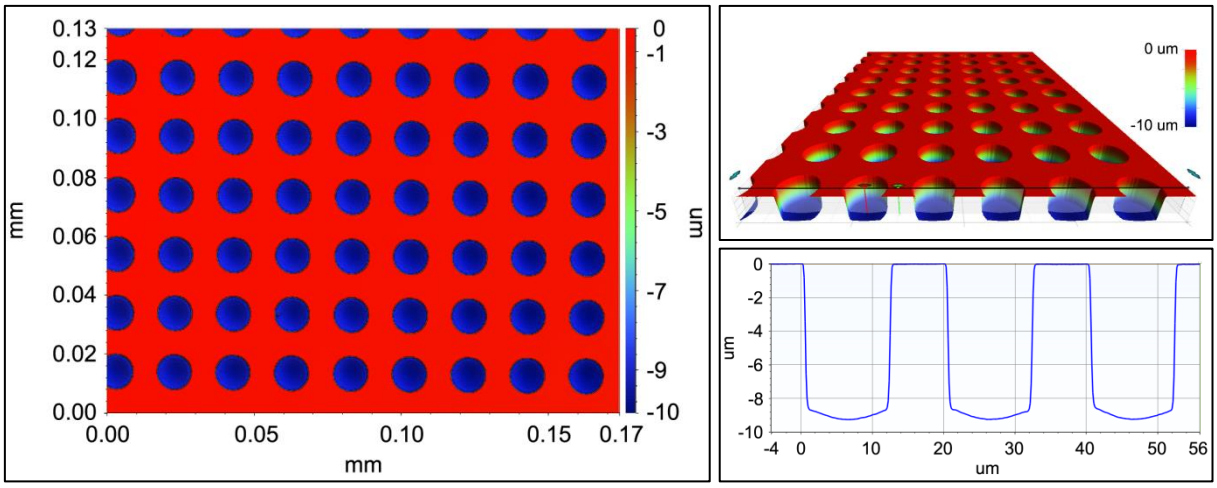

Figure 56. Topology of the microstructured substrate derived by white light interferometry: (left) 2D reconstruction of the microstructured surface; (upper right) 3D reconstruction of the microstructured surface; (bottom right) fragment of the cross-section profile of the microwells.

As can be seen from the image, the microwells had a shape close to cylindrical with nearly vertical walls and slightly convex bottom. The analysis of the cross-section profile of the microstructures resulted in the measured values of the pitch size to be 20.0 μm, the diameter of 12.0 μm (measured at the top of the microwells), and the depth of 9.0 μm (averaged over the convex bottom of the microwell). The parameters of the microstructures were constant throughout the substrate and complied with the declared values. In general, the obtained results confirmed the quality of microstructuring outsourced to the external company.

4.1.3 Substrate Functionalization

The full-size substrate, functionalized with a layer of 10:90 poly(PEGMA-co-MMA) copolymer, was stained with amine-reactive TAMRA fluorescent dye. Figure 57 depicts fragments of the image acquired by scanning the substrate in the 532 nm excitation channel with the fluorescence filter 582/75.

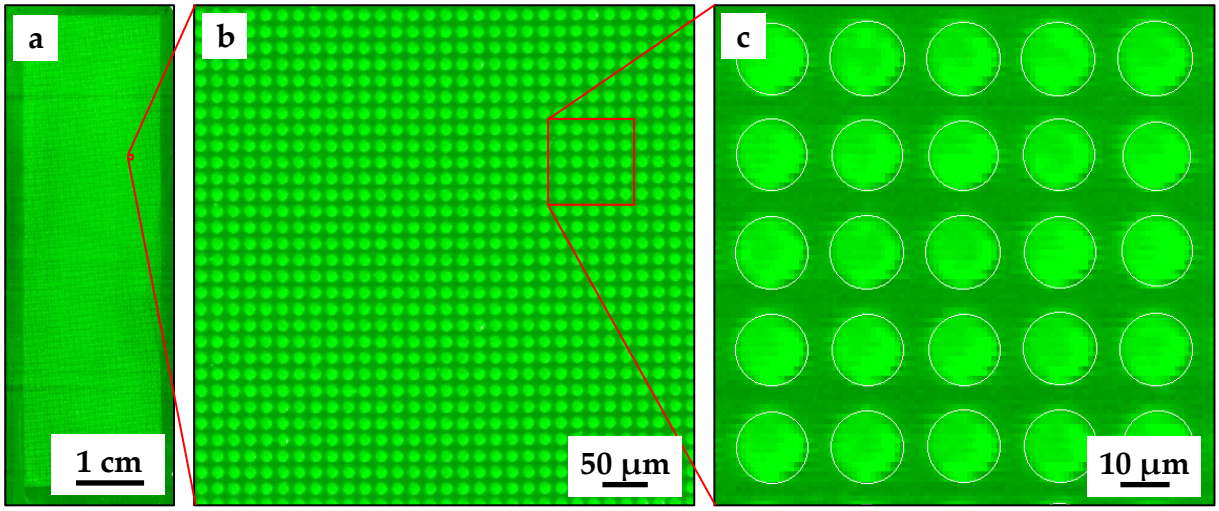

Figure 57. Fluorescence image of the microstructured substrate stained with TAMRA: (a) full-size image; (b) (c) image fragments.

Visually, one can judge on the homogeneity of the functional layer from the intensity profile of the fluorophore molecules coupled to the free amino groups of the substrate. For quantitative analysis, the standard deviation and the mean signal in the microwells and on the top surface were calculated based on the median feature values and the mean background values obtained for approximately 3 million microwells. The results of the statistical analysis are shown in Table 6.

Table 6. Signal characteristics derived by fluorescent scanning of the functionalized microstructured substrate stained with TAMRA.

Parameters of the signal	**Localization of the signal**	
	Microwells	**Top surface**
Mean, 10^3 x a.u.	24.3	13.8
SD, 10^3 x a.u.	2.8	1.5
CV	0.115	0.109

The signal value in the microwells was estimated to be $24.3 \cdot 10^3 \pm 2.8 \cdot 10^3$ a.u., whereas the coefficient of variation was 0.115. These results indicate that the distribution of the amino groups over the microwells of the functionalized substrate was fairly homogeneous. The average signal from the top surface was $13.8 \cdot 10^3 \pm 1.5 \cdot 10^3$ a.u. with the coefficient of variation of 0.109. In both cases, the signal variation can be explained by heterogeneities of the functional layer, as well as by the shifts of the

focal plane during scanning (which can be seen in Figure 57a as horizontal dark stripes). The noticeable difference in signal between the microwells and the top surface can be explained by the various thickness of the functional layer resulted from the siATRP process.

4.2 Microbead Manufacturing

4.2.1 Morphology of Solid Carriers

The cross-linked PMMA microspheres were investigated in terms of their morphology using SEM (Figure 58) and AFM (Figure 59).

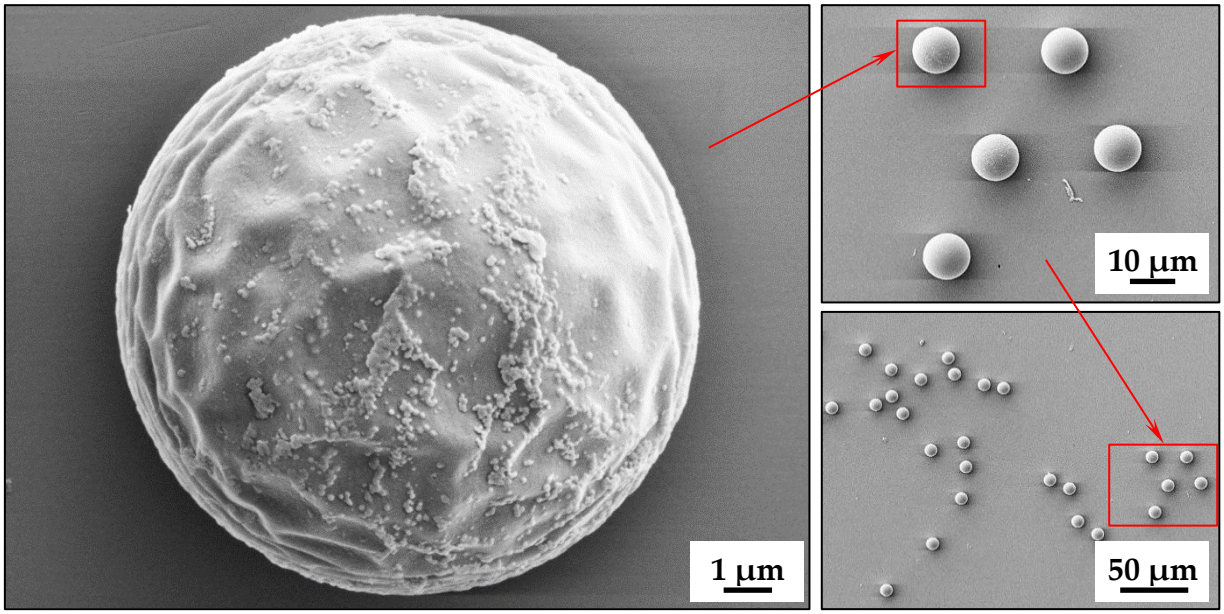

Figure 58. SEM images of cross-linked PMMA microspheres.

The images acquired with SEM confirmed an extremely narrow size distribution of the microspheres having the median diameter of 10 µm, which complied with the data provided by the manufacturer (Figure 44). As can be seen from Figure 58, the surface of the microspheres was not ideally smooth. It rather resembled the Moon's surface with quite frequent grooves and elevations, which could result from emulsion polymerization and cross-linking of PMMA.

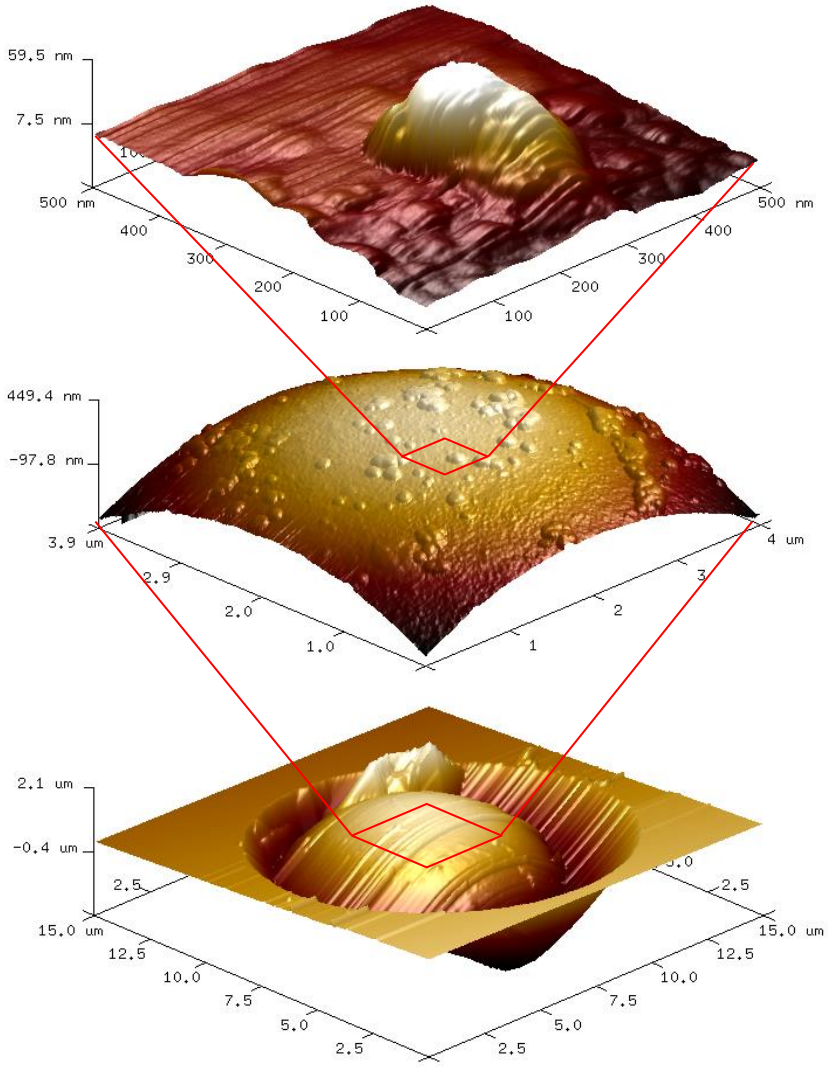

Figure 59. AFM images of a cross-linked PMMA microsphere in a microwell.

Cross-section profile measurements performed with AFM revealed that the height of the elevations did not exceed 100 nm. Therefore, the surface of the microspheres could be considered sufficiently smooth in micrometer scale. It is important to note that no micropores were visualized on the surface of the microspheres. It left open the question on possible localization sites of the amino acid derivatives and QDs during microbeads manufacturing.

4.2.2 QD Labelling of Microspheres

Figure 60 depicts QD labelled microspheres randomly deposited onto the flat microscope slide. Labelling of the microspheres was performed by QDs emitting at 580 nm according to the optimized protocol (Appendix A2). The image was acquired by scanning the slide in the fluorescence channel 580/14.

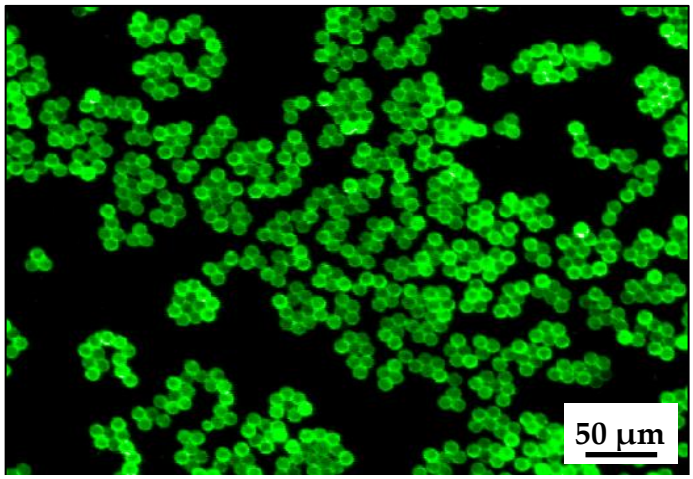

Figure 60. QD labelled microspheres. Labelling was performed by 580 nm QDs according to the optimized protocol. The images were acquired in the fluorescence channel 580/14 (green channel).

As can be seen, each microsphere was homogeneously labelled with QDs, whereas the signals from various microspheres slightly differed from each other. In order to understand the reasons for such variations, the mechanism of fluorescent labelling had to be investigated. For this purpose, several samples of dispersion were taken in different steps of the labelling process and imaged afterward with the fluorescence scanning technique (Figure 61).

Figure 61a depicts a fluorescence image of the sample of 580 nm QD solution in DCM after solvent evaporation. As can be seen, the QD stain demonstrates a strong and homogeneous signal over the central region. A narrow fluorescence ring can be visualized around the stain, which corresponds to the perimeter of the initial sample droplet. During evaporation of the volatile solvent, the QD solution shrank to the center of the droplet leaving a ring of QD residues at its original edge. This phenomenon is known as the coffee ring effect. Figure 61b illustrates the fluorescence of the dispersion of the cross-linked PMMA microspheres in the QD solution after solvent evaporation. Even though the dispersion was quite thick, only a small fraction of particles, mainly located at the perimeter of the spot, demonstrated slight fluorescence, whereas the majority of the microspheres remained non-labelled. We assume that the hydrophobic QDs, being readily soluble in chlorinated solvents, tend to stay in the continuous phase rather than precipitate on the swelled PMMA microspheres. The minor signal of the microspheres located at the edge of the spot can be explained by precipitation of the QDs from the continuous phase during evaporation of the volatile solvent. Figure 61c represents the sample of the dispersion

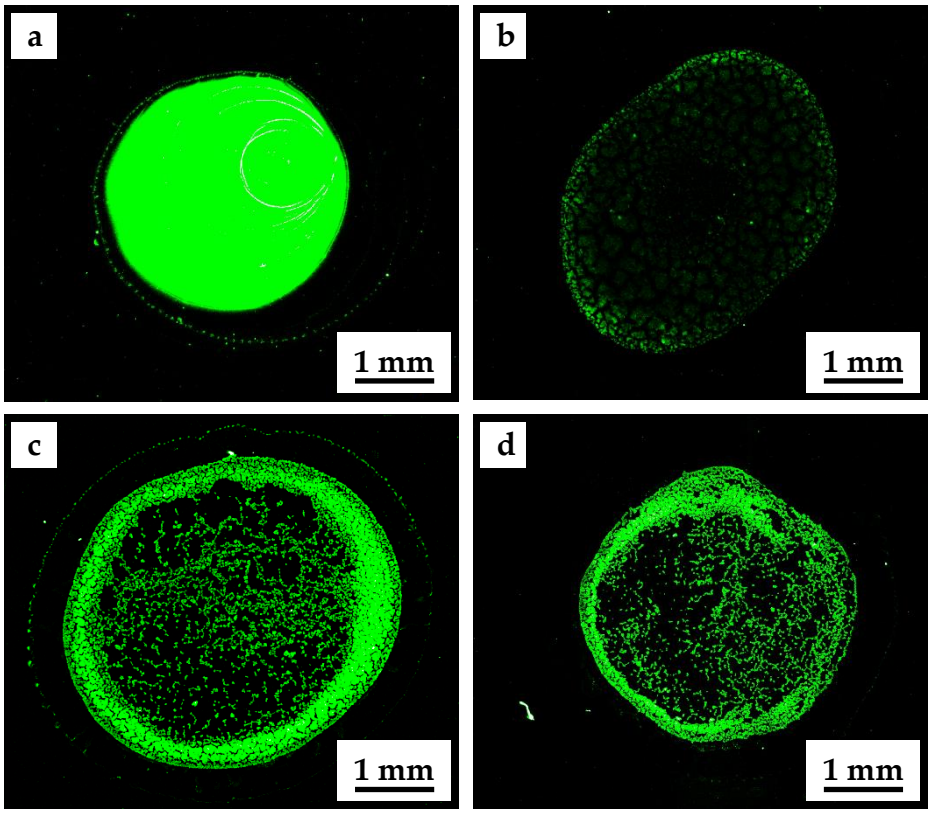

Figure 61. Fluorescence images of the samples taken in different steps of the labelling process: (a) solution of 580 nm QD in DCM; (b) dispersion of cross-linked PMMA microspheres in the QD solution in DCM; (c) dispersion of microspheres after replacing DCM with acetone; (d) dispersion of microspheres after adding ethanol. The images were acquired in the fluorescence channel 580/14.

after replacing DCM with acetone. The image was taken after evaporation of the solvent. As can be seen, the fluorescence signal mainly originates from the microspheres constituting the spot. We suppose that the QDs tend to precipitate on the swelled microspheres while the polarity of the continuous phase gradually increases due to the replacement of DCM ($\varepsilon_r = 8.9$) by acetone ($\varepsilon_r = 20.7$). The residual amount of QDs in the liquid phase is negligible and manifested in the coffee ring effect at the perimeter of the initial droplet. Figure 61d demonstrates the sample of the dispersion after adding ethanol. The image was taken after the volatile components completely evaporated. The fluorescence signal of the microspheres remained as it was after replacing DCM with acetone, which means that the QDs were not "washed out" from the microspheres after exposure to the additional solvent. At the same time, the coffee ring effect was not visualized for the sample, which enabled us to conclude that the QDs completely precipitated from the continuous phase after partial replacement of acetone by ethanol ($\varepsilon_r = 24.5$).

When the labelling process was performed by gradual replacement of DCM by ethanol, the fluorescence signal of individual microspheres was extremely inhomogeneous. We assume that ethanol initiates shrinkage of the cross-linked PMMA before the QDs precipitate from the continuous phase. It explains why the labelling process has to be performed in three steps. First, the microspheres should undergo swelling in DCM, which is an appropriate solvent for hydrophobic QDs. Second, precipitation of the QDs has to be initiated by replacing DCM with polar acetone, whereas the microspheres should remain swollen. Third, the microspheres are to be washed with ethanol, which induces their shrinkage and results in a complete precipitation of the QDs from the continuous phase.

The variation in signal between different microspheres can be explained by the fact that the labelling process is nonequilibrium. The polarity of the continuous phase changes unevenly in time and space due to the fact that the additive solvents are introduced into the dispersion dropwise from a burette. Rapid local changes of the properties of the continuous phase have a greater impact on those microspheres which happened to be in the place of the droplet hitting the dispersion, thus inducing an inhomogeneous precipitation of the QDs on the microspheres.

4.2.3 Embedding of Amino Acid Derivatives

The function of the microbeads as carriers of the amino acid derivatives is demonstrated in Figure 62. The microbeads were labelled with 580 nm QDs and loaded with Fmoc-glycine pentafluorophenyl ester (Fmoc-Gly-OPfp) according to the protocol (Appendix A2). After random deposition of the microbeads on the flat functionalized substrate, they were imaged in the fluorescence channel 580/14 corresponding to the emission maximum of the QD labels (Figure 62a). Thereafter, the amino acid derivatives were extracted from the microbeads and coupled to the functional layer of the substrate. After microbead removal, surface acetylation and Fmoc-deprotection, the coupled amino acids were fluorescently stained with DyLight 650 NHS ester dye. It made it possible to visualize the coupled monomers in the fluorescence channel 677/45 corresponding to the emission of the fluorescent dye (Figure 62b).

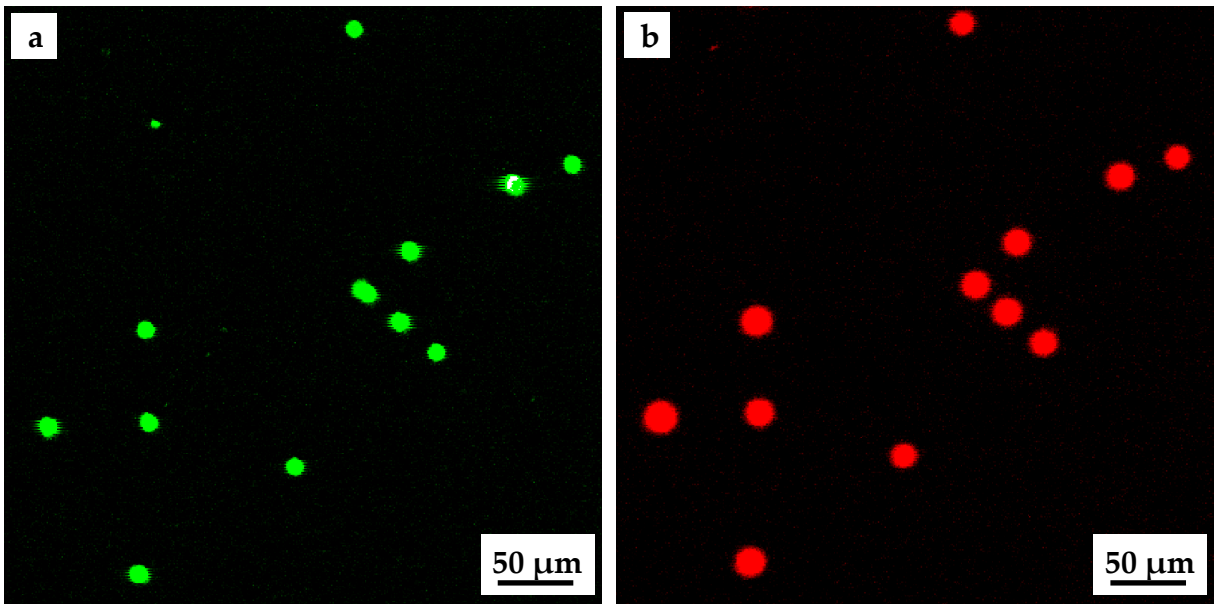

Figure 62. Coupling results of the microbeads labelled with 580 nm QDs and loaded with Fmoc-Gly-OPfp: (a) random pattern of the QD labelled microbeads deposited onto a flat functionalized substrate. The image was acquired in the fluorescence channel 580/14 (green channel); (b) fluorescently labelled amino acids extracted from the microbeads and coupled to the functional surface. The image was acquired in the fluorescence channel 677/45 (red channel).

The fluorescence pattern of the coupled amino acids corresponds to the initial deposition of the microbeads. Each microbead carried a certain amount of amino acid derivatives that were extracted under certain conditions and coupled to the functional layer. Even though the source of the amino acid derivatives were the contact points of the microbeads and the substrate, the diameter of the amino acid spots was around 20 µm due to diffusion of the released monomers over the surface.

One of the major tasks was to derive the maximum content of the amino acid derivatives per solid carrier microspheres. On the one hand side, the higher content of the monomers should lead to higher extraction and coupling yields. On the other hand side, there should be a limit of the microsphere's carrying capacity, exceeding which may lead to adverse effects. In order to identify this limit, twelve samples of microbeads were manufactured and tested in terms of the coupling behavior of the embedded amino acid residues. Two components, Fmoc-Gly-OPfp and *N*,*N*-diphenylformamide (DPF), were loaded in different ratios into the cross-linked PMMA microspheres. Due to its relatively low melting point (73.5 °C), DPF was used as an additive to facilitate extraction of the amino acid residues at elevated temperatures. Within the scope of this experiment, DPF can be considered as a

"ballast" component occupying vacant space within the microspheres. With respect to the mass of the solid carrier, the amino acid derivatives were used in mass fractions of 2 % (m/m), 5 % (m/m), and 8 % (m/m), whereas the DPF content varied in mass fractions of 0 % (m/m), 3 % (m/m), 6 % (m/m), and 9 % (m/m), resulting totally in twelve possible combinations. The individual samples were locally spread over the surface of the flat functionalized substrate using a soft lint-free tissue. Figure 63 depicts fragments of the images acquired for two out of twelve samples, which illustrate fluorescently stained amino acids coupled to the surface after their extraction from the microbeads.

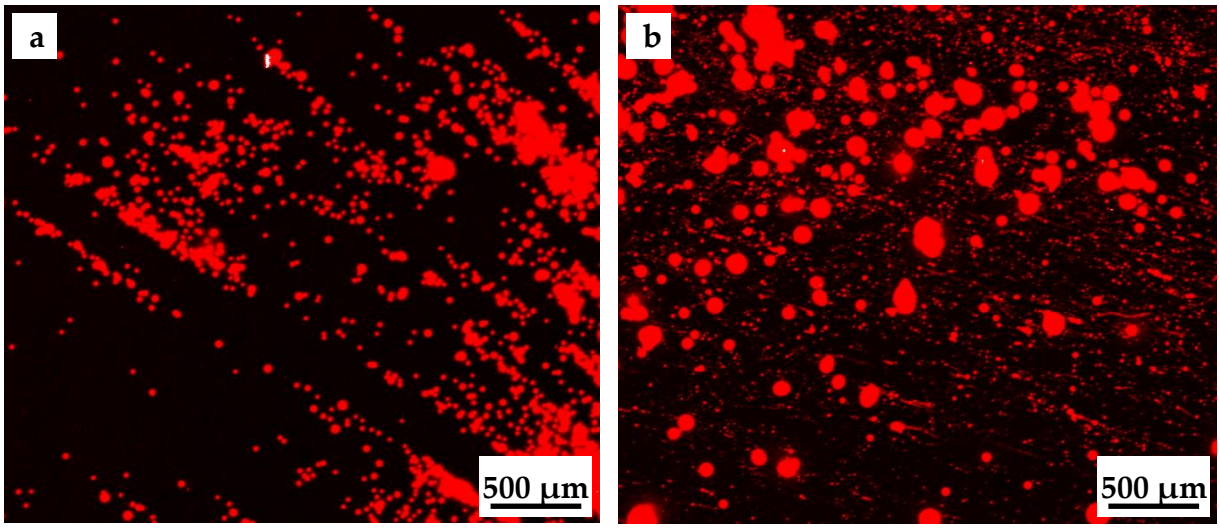

Figure 63. Coupling patterns of amino acid derivatives extracted from the microbeads of various composition: (a) microbeads carrying 2% (m/m) of Fmoc-Gly-OPfp; (b) microbeads carrying 8 % (m/m) of Fmoc-Gly-OPfp. In both cases, the content of DPF was 6 % (m/m).

As can be seen in Figure 63a, the amino acid spots obtained for the microbeads with 2 % (m/m) of Fmoc-Gly-OPfp and 6 % (m/m) of DPF were well defined, whereas their global pattern resembled the lines of the microbeads from their spreading with a tissue. Despite the fact the microbeads were subjected to the mechanical impact and rubbing against the surface of the substrate, they kept the embedded amino acid residues and did not produce any contaminations over the surface. In contrast to this, the sample with 8 % (m/m) of Fmoc-Gly-OPfp and 6 % (m/m) of DPF was characterized by numerous impurities of the amino acid derivatives in form of scratch-like lines and non-circular spots with the size of several micrometers.

The results of a qualitative analysis performed for all twelve samples of the microbeads with varied content of Fmoc-Gly-OPfp and DPF are listed in Table 7.

Table 7. Contaminating tendency of the microbeads with the varied content of Fmoc-Gly-OPfp and DPF.

Fmoc-Gly-OPfp, % (m/m)	DPF, % (m/m) 0	3	6	9
2	No impurities	No impurities	No impurities	Low impurities
5	No impurities	No impurities	Low impurities	High impurities
8	No impurities	Low impurities	High impurities	High impurities

As soon as the total mass fraction of the embedded components exceeds 8 % (m/m), the microbeads tend to contaminate the surface with the residues of amino acid derivatives. We assume that these impurities originate from the excessive amino acids and DPF crystallized on the surface of the microbeads during their manufacturing due to the fact the outer thin layer of the cross-linked PMMA matrix is already occupied by these substances. From the qualitative data shown in Table 7, we can conclude that the cross-linked PMMA microbeads can incorporate 8 % (m/m) of Fmoc-Gly-OPfp without generating any impurities during their deposition.

Similar experiments were performed for the remaining 19 types of proteinogenic amino acids, whereas only the content of the monomers was varied in mass fractions of 2 % (m/m), 3 % (m/m), 4 % (m/m), 6 % (m/m), and 8 % (m/m). The microbeads with the highest content of the amino acid derivatives, which did not demonstrate any visible traces of impurities upon their deposition over the substrate, were considered the most preferred for the stochastic peptide microarray manufacturing. The mass fractions of the monomers in these microbeads are listed in Table 8.

Table 8. Optimal content of amino acid derivatives in microbeads.

Amino acid*	1-Letter notation	Mass fraction	Amino acid*	1-Letter notation	Mass fraction
Alanine	**A**	2 %	**Leucine**	**L**	2 %
Arginine	**R**	2 %	**Lysine**	**K**	3 %
Asparagine	**N**	2 %	**Methionine**	**M**	3 %
Aspartic acid	**D**	3 %	**Phenylalanine**	**F**	3 %
Cysteine	**C**	2 %	**Proline**	**P**	3 %
Glutamic acid	**E**	2 %	**Serine**	**S**	3 %
Glutamine	**Q**	2 %	**Threonine**	**T**	3 %
Glycine	**G**	3 %	**Tryptophan**	**W**	3 %
Histidine	**H**	2 %	**Tyrosine**	**Y**	3 %
Isoleucine	**I**	2 %	**Valine**	**V**	3 %

(*) – Fmoc-protected, OPfp-activated.

As can be seen in Table 8, the cross-linked PMMA solid carriers could accommodate the amino acid derivatives in mass fractions of 2 % (m/m) and 3 % (m/m), which is far lower than 8 % (m/m) derived for Fmoc-Gly-OPfp. To compensate the difference in amino acid diffusion, the content of Fmoc-Gly-OPfp was reduced to 3 % (m/m).

4.2.4 Morphology of Microbeads

An attempt was made to determine the localization of the amino acid derivatives and QDs on the surface of the microbeads manufactured according to the established procedure. For this purpose, the microbeads containing 5 % (m/m) of Fmoc-Gly-OPfp and QDs emitting at 580 nm were investigated using AFM (Figure 64).

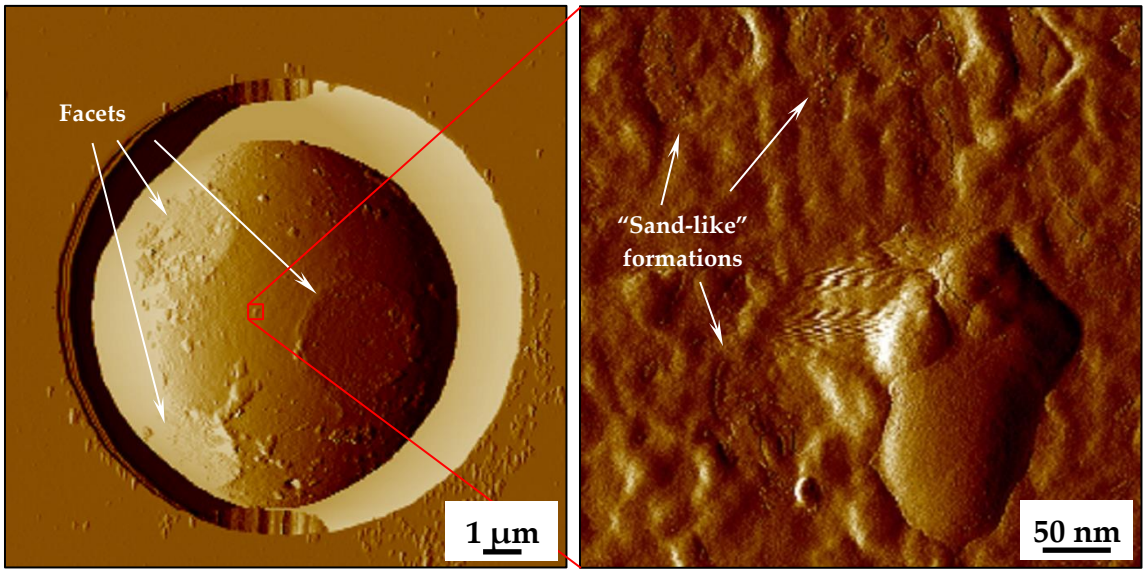

Figure 64. AFM images of a microbead loaded with 5 % (m/m) of Fmoc-Gly-OPfp and 580 nm QDs.

On the left image, three characteristic facets can be identified on the surface of the spherical microbead. These facets result from the final step of the amino acid embedding process. As the continuous phase of the dispersion evaporates, the swelled microspheres are being brought in contact with each other forming a paste-like medium. After the paste is dry, it becomes a single bulk piece composed of many microbeads "glued" to each other. After the dry paste is ground in a mill into a fine powder of microbeads, the former contact regions between the microbeads convert into the facets on their surface.

On the right image, the surface of a microbead loaded with QDs and amino acid derivatives appears relatively smooth and similar to the surface of the pure PMMA microspheres (Figure 59). No microcrystalline formations were identified on the surface of the microbead. The slight difference was in sporadic "sand-like" patterns of an undefined origin spread over the surface of the microbead. The size of the features was at the resolution limit of AFM. The obtained results allowed us to conclude that the monomers and the fluorescent labels were either embedded into the outer thin layer of the polymer microsphere or deposited as nanometer clusters onto the surface of the solid carrier.

4.3 Microbead Deposition

4.3.1 Self-organization of Microbeads

Self-organization of the microbeads in the microwells of the microstructured substrate is one of the fundamental principles of the stochastic peptide microarray manufacturing. Figure 65 depicts how this principle is manifested in practice.

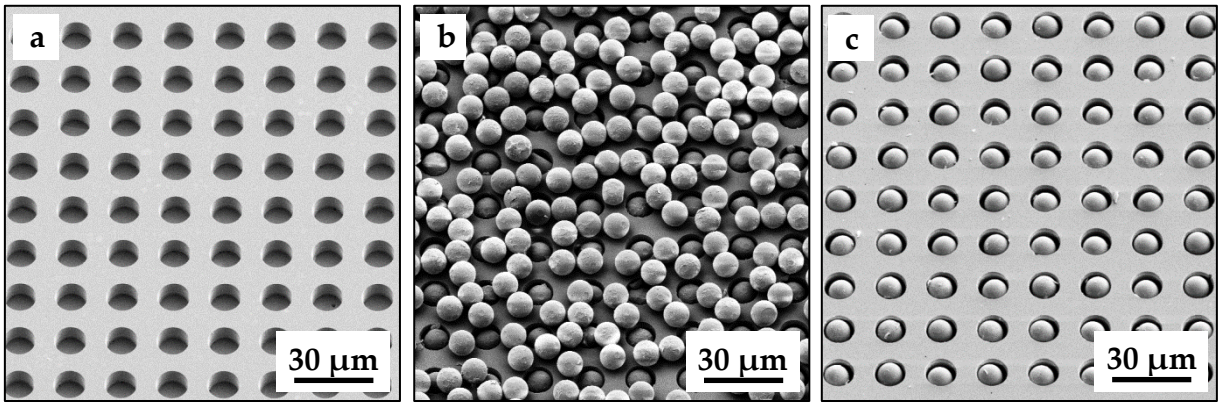

Figure 65. SEM images of a microstructured substrate demonstrating the principle of self-organization of the microbeads: (a) initial empty microstructures; (b) microstructures after spreading the microbeads with a soft tissue; (c) microstructures after applying a tangential flow of compressed air.

The deposition of the microbeads was performed in two steps. First, the dry mixture of the microbeads was spread over the surface of the microstructured substrate with a soft lint-free tissue (Figure 65b). Although the microstructures were completely filled with the microbeads, the top surface of the substrate still contained a monolayer of excessive microbeads. This excess was removed in the second step with the flow of compressed air applied tangentially to the surface of the substrate (Figure 65c). As can be seen, the air flow totally removed the excessive microbeads from the top surface, whereas the microwells remained filled. These images demonstrate the effect of the geometric constraints the microbeads inside the microwells are subjected to.

Microbead deposition into the microwells of the substrate was prone to various errors. The most frequent cases of deposition errors are illustrated in Figure 66.

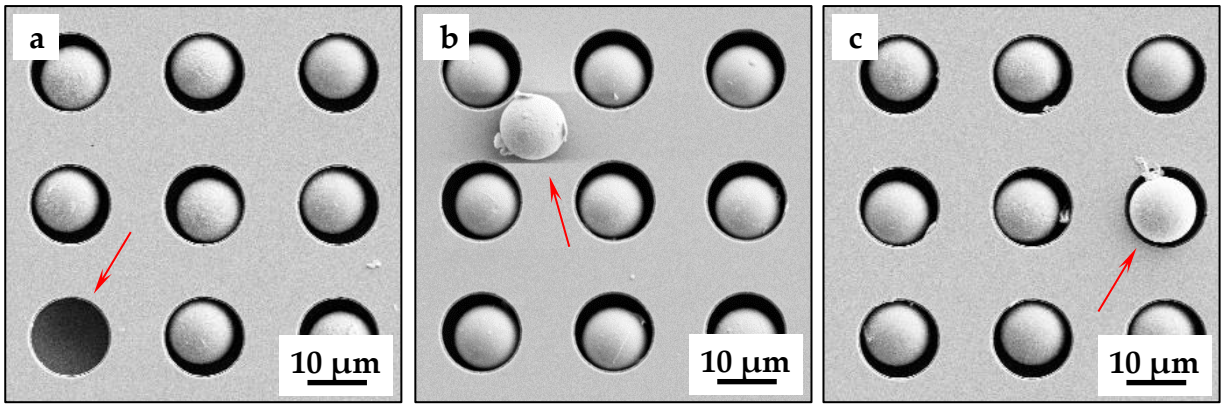

Figure 66. Microbead deposition errors: (a) an unfilled microwell; (b) a microbead left on the top surface of the substrate; (c) a microbead not touching the bottom of a microwell.

Unfilled microwells (Figure 66a) lead to the termination of peptide synthesis due to the absence of monomers in a certain step of peptide chain elongation. It results in a reduction of the number of fully-synthesized peptides. In case of the microbeads left on the top surface of the substrate (Figure 66b), the major adverse effect is the contamination of the neighboring microwells by arbitrary amino acid derivatives extracted from the residual microbeads. It locally affects the quality of the synthesized peptides and can lead to false positive signals in biological applications. The most difficult case of a deposition error in terms of recognition and prevention is depicted in Figure 66c. The microbead, "hanging" on the side wall of the microwell and not touching its bottom, is only partially introduced into the microwell. The monomer source point is shifted outside of the area where the peptides are supposed to be synthesized leading to an extremely low coupling yield at the bottom of the microwell. Eventually, it may result in false negative signals when implementing a peptide microarray in bioassays.

The defects of the first type and the second type can be easily identified from fluorescence images of the substrate filled with QD labelled microbeads (Figure 67). Empty microwells are identified based on their low median feature values, whereas the microwells with the neighboring microbeads on the top surface can be identified from their higher mean background values. This enables taking these two types of deposition errors into account when deriving a peptide microarray library. In contrast to that, partially filled microwells cannot be identified from fluorescence images. This makes it impossible to take this type of error into account in a microarray library.

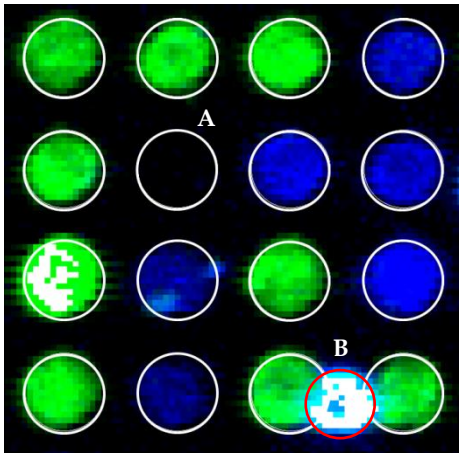

Figure 67. Deposition errors derived from fluorescence imaging: (A) an unfilled microwell; (B) a microbead on the top surface.

4.3.2 Comparison of Microbead Deposition Methods

Maximizing the filling rate of the microstructures is the primary requirement for the microbead deposition methods. Figure 68 depicts fluorescence images of the substrate stochastically filled with a mixture of microbeads labelled by 500 nm QDs and 580 nm QDs. Microbead deposition was performed using a soft lint-free tissue with subsequent removal of excessive microbeads by a flow of compressed air. The fluorescent scanning was performed in the fluorescence channels 520/5 and 580/14.

Figure 68 gives an impression on the number of microbeads deposited on a substrate and the quality of deposition using a soft tissue in combination with a compressed air flow. The filling rate of the microstructures was lower than 100 %, whereas the microbeads on the top surface were extremely rare. As for the microbeads deposited into the microwells, they could be easily differentiated in terms of their QD labels demonstrating sufficiently homogenous and strong signals.

The acquired images were analyzed by applying a grid, aligning it to the microwell pattern on the substrate and calculating the photometric values of each spot. The calculated data was further processed by the software developed within this project, particularly, to derive the filling rate of the microstructures. Using this approach, two methods of microbead deposition were compared. The combination of a soft tissue-

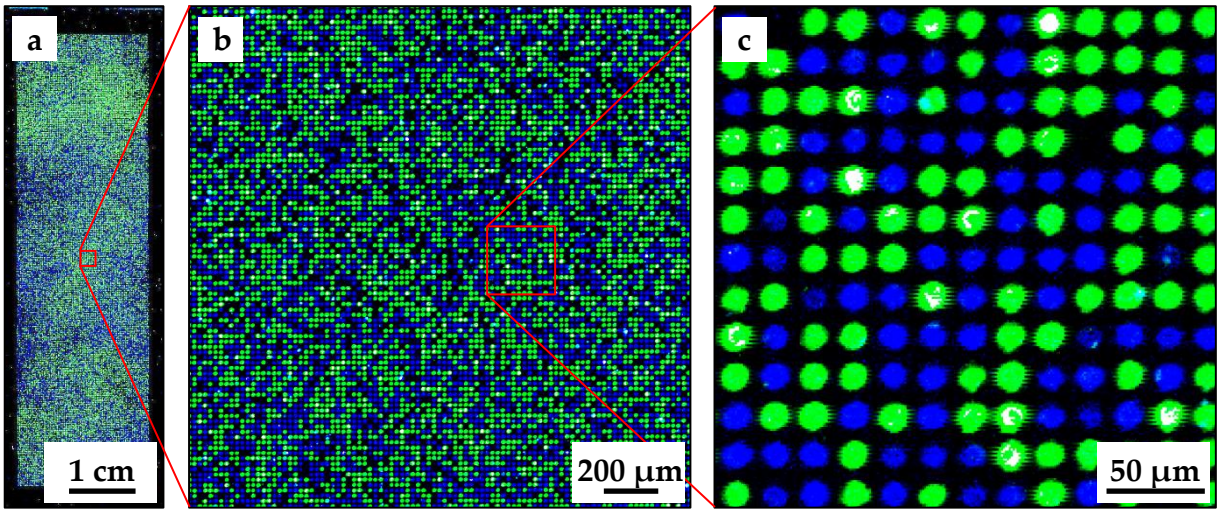

Figure 68. Deposition pattern of microbeads labelled by 500 nm QDs (shown in blue) and 580 nm QDs (shown in green) in the microwells of the microstructured substrate. The microbead deposition was performed using a soft lint-free tissue and a compressed air flow: (a) full-size image; (b) (c) image fragments.

based deposition with subsequent removal of the excessive microbeads by a compressed air flow resulted in an average filling rate of 92.6 % compared to 97.7 % achieved with the doctor blade technique. A lower filling rate in the first case could result from spontaneous removal of the microbeads by microscale air swirls originating in the microwells from the tangential flow of compressed air. While being removed from the top surface, excessive microbeads could pull out the deposited microbeads from the microwells due to their initial contact or random collisions.

Despite the fact the doctor blade approach resulted in a higher filling rate of the microwells, it had one significant drawback. Figure 69 illustrates the deposition pattern of the same microbeads labelled by 500 nm QDs and 580 nm QDs and stochastically spread over the substrate with a plastic spatula. The parameters of the fluorescence scanning were identical to those used for the microbeads deposited with a lint-free tissue.

The appearance of the microbeads in the microwells is completely different in comparison to the first trial. The cyan color of the microbeads indicates that they emit in green and blue fluorescence channels at the same time. Excessive friction of the microbeads with each other and with the surface of the substrate resulted in cross-contamination of the QDs between the microbeads of both types. The results of this experiment demonstrate the dilemma of microbead deposition: A low mechanical impact leads to insufficient filling rates or high contamination of the top surface with

excessive microbeads, whereas great mechanical forces damage the microbeads making them not applicable for the stochastic peptide microarray manufacturing.

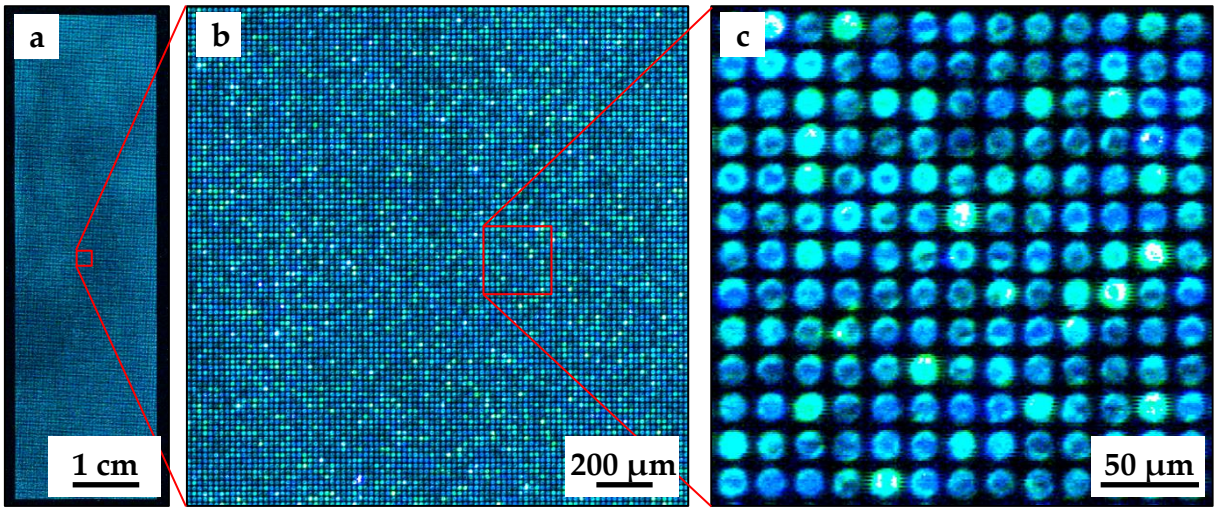

Figure 69. Deposition pattern of microbeads labelled by 500 nm QDs and by 580 nm QDs in the microwells of the microstructured substrate. The microbead deposition was performed using the doctor blade technique: (a) full-size image; (b) (c) image fragments.

Figure 70 depicts the microbeads that were severely damaged by excessive force intentionally applied during microbead deposition with the plastic spatula. As can be seen, the cross-linked PMMA microspheres underwent irreversible deformations and even destructions being exposed to great mechanical forces. In peptide microarray manufacturing, it could lead to contamination of the microwells by arbitrary amino acids from the fragments of the destroyed microbeads. The obtained results testify to the microbead deposition method based on spreading of the microbeads with a soft lint-free tissue followed by removal of the excessive microbeads from the top surface with a compressed air flow.

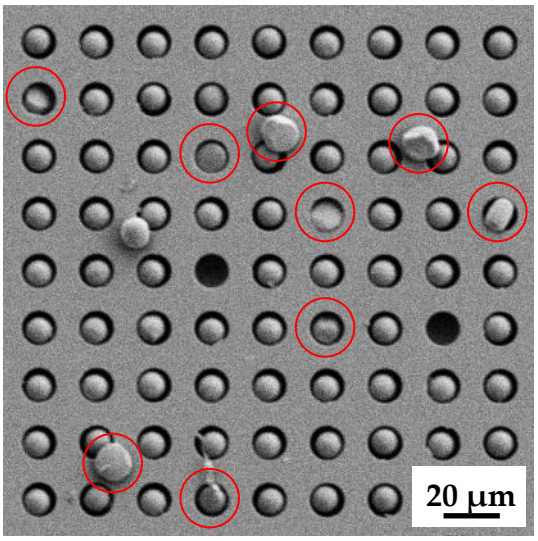

Figure 70. Damaged microbeads due to excessive forces applied during their deposition.

4.4 Image Acquisition

4.4.1 Multiplexed Labelling and Decoding

The concept of multiplexed QD labelling of the microspheres and their decoding from fluorescence images acquired in multiple fluorescence channels is illustrated in Figure 71. Three kinds of microspheres, labelled by 500 nm QDs, 610 nm QDs, and the combination of 500 nm QDs and 610 nm QDs, were deposited into the microstructures and scanned in the fluorescence channels 520/5 and 615/20.

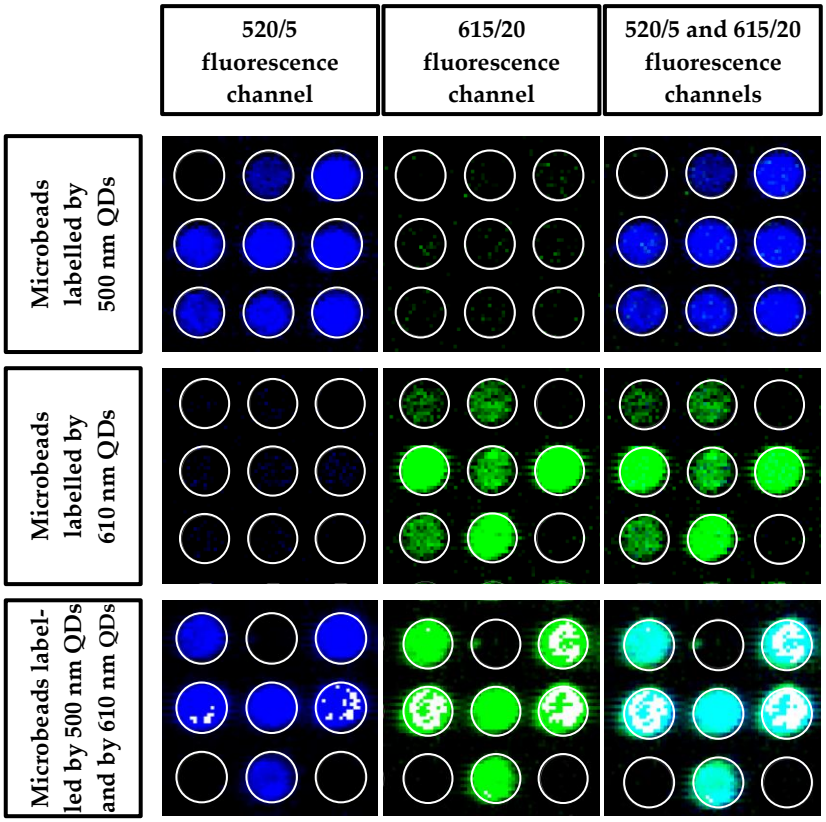

Figure 71. Fluorescence images of QD labelled microbeads. Three types of microbeads were deposited into the microwells: (from top to bottom row-wise) 500 nm QD labelled microbeads, 610 nm QD labelled microbeads, and 500 nm QD + 610 nm QD labelled microbeads. The images were acquired: (from left to right column-wise) in 520/5 channel (blue), in 615/20 channel (green), and in combination of 520/5 and 615/20 channels.

As can be seen in Figure 71, the microbeads labelled by 500 nm QDs demonstrate high signal in the channel 520/5 and nearly no signal in the channel 615/20. In contrast to this, the microbeads labelled by 610 nm QDs demonstrate strong signal in the channel 615/20 and absolutely no signal in the channel 520/5. When the

microbeads are labelled by a combination of the QDs, they shine well in both fluorescence channels at the same time. These results comply with the initial idea that the microbeads labelled with different combinations of QDs can be differentiated from each other by their unique "fingerprints" acquired in multiple fluorescence channels. It implied that certain combinations of QDs and fluorescence filters had to be selected in such a way so that each type of QDs could be detected in a corresponding unique fluorescence channel.

4.4.2 Set of QDs and Fluorescence Filters

A set of basic QDs and fluorescence filters was derived in several iterations according to the procedure described in Section 3.4. Table 9 presents a theoretically derived optimal set of QDs and fluorescence filters with the respective effective signal values.

Table 9. Effective signal values of a theoretically derived optimal set of QDs and fluorescence filters (in a.u.).

QDs, nm	Fluorescence filter				
	520/5	**549/15**	**580/14**	**615/20**	**673/11**
500	**2.4**	0.1	0.0	0.0	0.0
550	0.5	**17.1**	3.1	0.0	0.0
580	0.0	2.9	**17.2**	1.7	0.0
610	0.0	0.0	3.1	**8.3**	0.0
650	0.0	0.0	0.0	0.4	**4.0**

The data structure in Table 9 resembles the arrangement of the images in Figure 71. When considering the numeric values row-wise, one can get an impression on how strong the microbeads labelled with a certain type of QDs would shine in each fluorescence channel. Although the highest signal of the QDs should be obtained for the corresponding fluorescence filter with the closest central transmission wavelength (marked in bold), one can also expect significant signal values in the neighboring fluorescence channels. By changing the loading of the microbeads by a certain type of QDs, the signal values are expected to change proportionally in each channel. Considering the numeric values column-wise provides an understanding of

how different the signals of the microbeads, labelled with various QDs, would be when obtained in a certain fluorescence channel. Despite the fact the transmission bandwidth of the filters ranged between 5 nm and 20 nm, it was still possible to detect tail signals of the QDs with emission maximum located relatively far away from the central transmission wavelength of a given filter. By changing the PMT settings in a certain fluorescence channel, the QD signals are expected to change proportionally. Hence, for a given pair of a QD and a fluorescence filter, it is not probable to augment or decrease the effective signal value without changing the effective signals of the dependent pairs. However, it should be feasible to enhance the detection specificity of a certain QD type by optimizing the concentration of the QD labels in the microbeads and the PMT settings in each channel.

In the next iteration, a set of microbeads labelled with individual types of QDs with emission maximum wavelengths ranging between 490 nm and 650 nm were manufactured and scanned in the fluorescence channels defined in the previous step. The mean and the standard deviation of the median feature values were estimated for each type of QD labelled microbeads in every fluorescence channel based on 200 sample spots. The optimal set of QD labels for the respective fluorescence channels was defined based on detection specificity (Table 10).

Table 10. Effective signal values of an experimentally derived optimal set of QDs in various fluorescence channels (in 1 000 x a.u.).

QDs, nm	Fluorescence filter				
	520/5	**549/15**	**580/14**	**615/20**	**673/11**
500	**26.2 ± 10.1**	5.9 ± 1.5	5.2 ± 1.1	12.3 ± 2.7	2.6 ± 0.6
550	3.7 ± 0.9	**40.7 ± 12.0**	19.6 ± 5.9	11.4 ± 2.5	1.7 ± 0.5
580	1.4 ± 1.1	8.0 ± 4.1	**27.0 ± 11.8**	18.6 ± 8.9	1.2 ± 0.5
610	2.1 ± 0.4	6.9 ± 1.8	10.6 ± 2.9	**23.5 ± 5.5**	1.8 ± 0.4
650	0.8 ± 0.4	1.7 ± 0.5	2.1 ± 0.6	6.9 ± 2.2	**5.7 ± 6.7**

As can be seen in Table 10, the theoretically derived optimal set of basic QDs was experimentally confirmed for the selected fluorescence channels. However, the observed specificity of the QD signals was lower than it was theoretically predicted.

In other words, the signals of individual QD labels were less confined to the corresponding fluorescence channels with the closest central transmission wavelength and spread considerably to the neighboring fluorescence channels. Such a difference could be explained by the fact that the emission spectrum of individual QDs was broader than the theoretical approximation with a Gaussian function with FWHM of 35 nm. Moreover, the actual wavelength of the QD emission maximum was declared by the manufacturer with the accuracy of ± 5 nm. It means that the emission spectrum of the QDs could shift considerably towards shorter or longer wavelength regions, thus leading to a redistribution of the signals between the fluorescence channels. The ratio of the standard deviation to the mean signal for the given pair of matching QDs and fluorescence filters characterized the homogeneity of the fluorescence labelling. The results obtained for the QDs emitting at 650 nm were not acceptable: The majority of the respective microbeads were hardly labelled with QDs while rarely shining microspheres were inhomogeneous in their appearance. The decision was made to exclude 650 nm QDs from the labelling palette and proceed with four types of QD labels. In total 14 different microbeads could be labelled with the final set of QDs (Table 11).

Table 11. Possible combinations of basic QDs for microbead labelling.

QDs	QD combinations													
	1	**2**	**3**	**4**	**5**	**6**	**7**	**8**	**9**	**10**	**11**	**12**	**13**	**14**
500	x	-	-	-	x	x	x	-	-	-	x	x	-	x
550	-	x	-	-	x	-	-	x	x	-	x	x	x	x
580	-	-	x	-	-	x	-	x	-	x	x	-	x	x
610	-	-	-	x	-	-	x	-	x	x	-	x	x	x

The results of classification of the microbeads labelled with various combinations of basic QDs are discussed in the next section.

4.5 Decoding of Amino Acid Deposition Pattern

4.5.1 Filled and Empty Microwells

Whether the microwells were filled or empty, they were differentiated based on their total signal acquired in all fluorescence channels. A mixture of microbeads, labelled by 500 nm QDs and by 580 nm QDs, was stochastically deposited into the microstructures of a full-size substrate. The distribution of approximately 3 million microwells according to their sum feature values obtained in the fluorescence channels 520/5 and 580/14 is depicted in Figure 72.

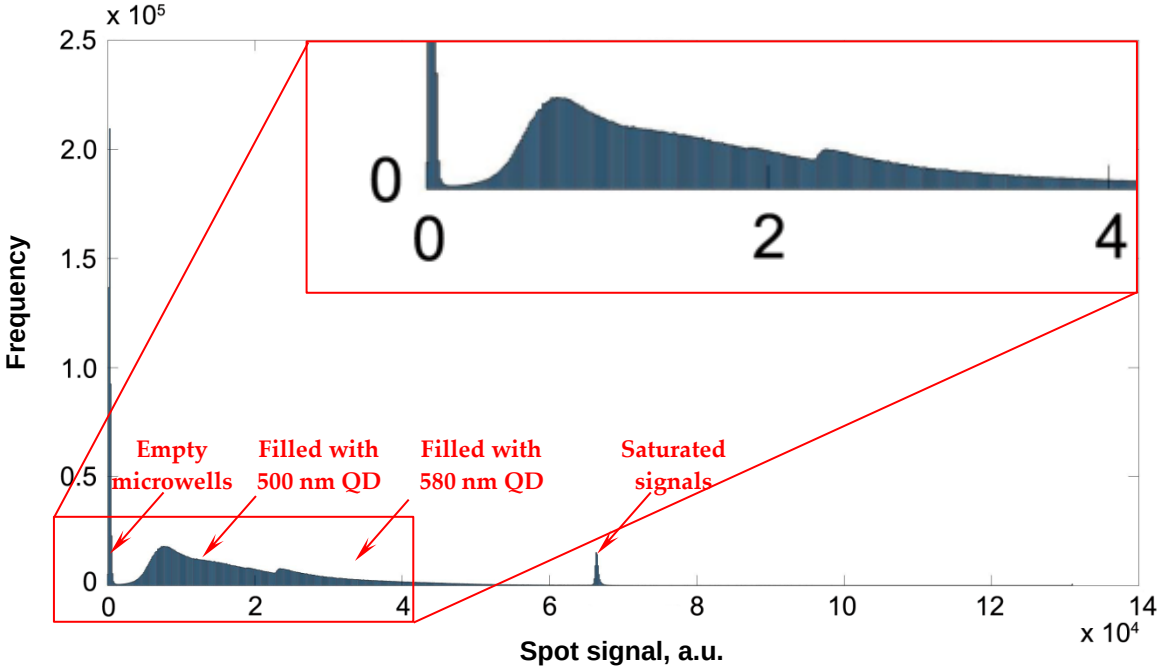

Figure 72. Distribution of the microwells filled by a mixture of QD labelled microbeads according to their total signal acquired in the fluorescence channels 520/5 and 580/14.

Empty microwells, characterized by low signal values, constitute the sharp peak close to the origin of the histogram. Two overlapping peaks with long tails correspond to the microwells filled with the 500 nm QD labelled microbeads and with the 580 nm QD labelled microbeads. The shape of these peaks indicates that the microbeads of the same type had a broad signals distribution due to inhomogeneous labelling with QDs. An additional peak is located close to 65 535 a.u. (maximum pixel value for a 16-bit image); it represents the microwells with saturated signals in either of the two fluorescence channels.

As can be seen from the histogram, the peaks of the empty and the filled microwells overlap with each other. It means that the signals of the "brightest" empty microwells were higher than the signals of the "dimmest" filled microwells. In this case, an error-free differentiation of the filled and empty microwells based on their total feature value was practically impossible. Any threshold signal value would result in a certain fraction of filled microwells being identified as empty and a certain number of empty microwells being identified as filled. A threshold value assigned to the local minimum of the function, describing the microwell distribution depending on their total feature value, was intended to minimize these errors.

Based on the sum feature values of approximately 3 million microwells, a threshold value for differentiating between empty and filled microwells was calculated according to the algorithm described in Section 3.5. This threshold was applied to a sample of 900 microwells out of 3 million, while their state of being filled or empty was "manually" defined in advance. The estimated error rates are shown in Table 12.

Table 12. Estimated error rates of identifying filled and empty microwells.

Identified	**Defined**		**Total**
	Filled	**Empty**	
Filled	758	5	763
Empty	0	137	137
Total	758	142	900
Error rate	0.0 %	3.5 %	**0.6 %**

The error of identifying filled microwells as empty was 0 %, whereas the error of identifying empty microwells as filled was 3.5 %. The total error rate of microwell differentiation was 0.6 %. When performing bioassays with stochastic peptide microarrays, the first type of error may lead to false positive signals, whereas the second type of error may result in false negative signals. However, the total accumulated error rate over up to 10 synthesis layers is relatively low and expected not to exceed 5 %.

4.5.2 Microbead Clustering

Figure 72 demonstrates the principle of the DBSCAN algorithm applied for three types of microbeads labelled with individual QDs, emitting at 500 nm, 550 nm, and 610 nm, and imaged in three fluorescence channels (520/5, 549/15, and 615/20).

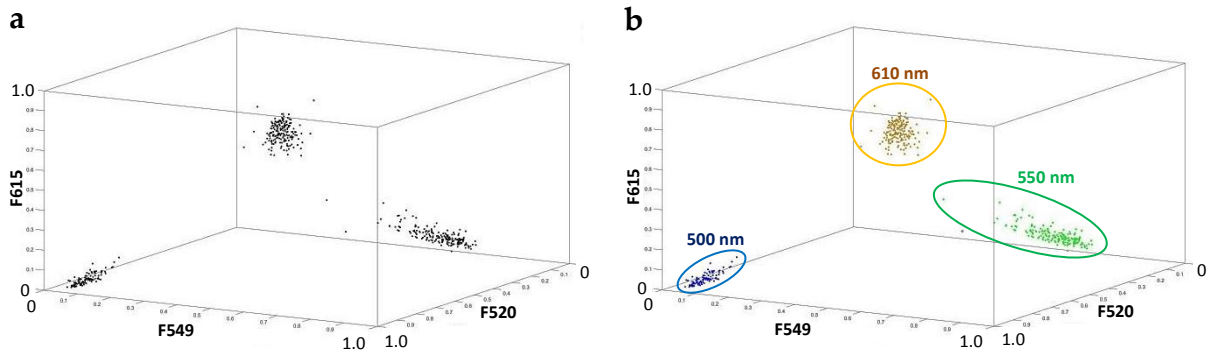

Figure 73. DBSCAN clustering of three types of QD labelled microbeads: (a) allocation of data points according to the microbead signals normalized for three fluorescence channels; (b) three clusters of microbeads automatically assigned to the respective QD labels.

Each black point in Figure 73a represents a single microbead labelled with one out of three types of QDs. The coordinates of each point correspond to the normalized signals obtained for the respective microbead in three fluorescence channels. The microbeads with similar signals will be assigned to the same cluster depending on how close their mutual position is in 3D space. Three clusters can be easily visualized on the diagram, each corresponding to a certain type of microbeads. The clusters are characterized by their size and position in space. The size of the cluster gives an idea on how similar the distribution of the relative fluorescence signals is in three fluorescence channels, or, in other words, how homogeneous the QD loading was among the microbeads. The position of the cluster in the diagram reveals the type of QDs used for the microbead labelling. As can be seen from Figure 73b, nearly all microbeads were successfully assigned by DBSCAN algorithm to one out of three clusters without any preliminary information on characteristic signal values for each type of microbeads. One microbead was assigned as an outlier due to the fact its normalized signals differed too much from the other microbeads.

Figure 74 demonstrates DBSCAN clustering results on an expanded set of QD labelled microbeads. Three types of microbeads labelled with individual basic QDs were supplemented by four types of microbeads labelled with QD combinations.

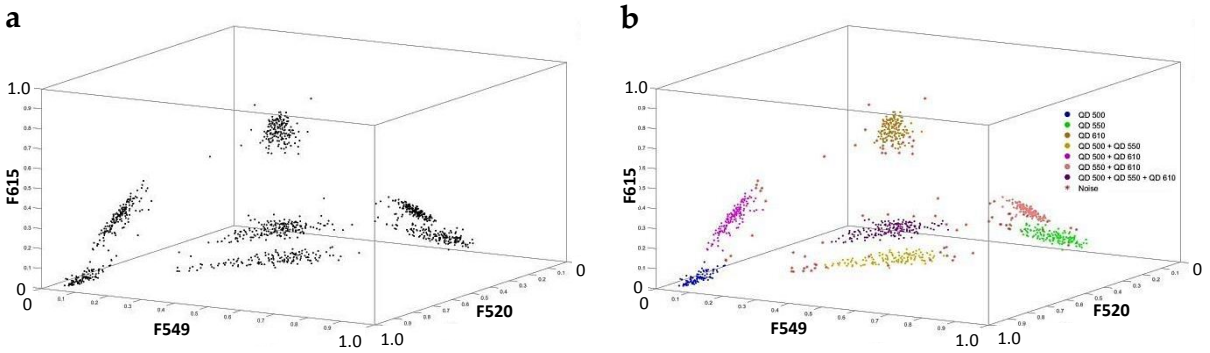

Figure 74. DBSCAN clustering of seven types of QD labelled microbeads: (a) allocation of data points according to the microbead signals normalized for three fluorescence channels; (b) seven clusters of microbeads automatically assigned to the respective QD labels.

As can be seen from Figure 74, four additional clusters fit in well between the clusters of the mono-labelled microbeads. Moreover, each cluster of the multi-labelled microbeads is located between the clusters of the microbeads labelled with the corresponding basic QDs. Since each data point represents the microbead signal normalized for three fluorescence channels, the clustering problem becomes two-dimensional. To confirm this, one can see that all seven clusters are located on the major diagonal plane (F520 + F549 + F615 = 1).

By using four types of basic QDs, in total 14 types of QD labelled microbeads were manufactured (Table 11). After scanning these microbeads in the corresponding fluorescence channels, the maximum number of microbeads resolved by DBSCAN was identified to be 11. Figure 75a depicts the allocation of the considered data points, whereas the microbead clustering results are shown in Figure 75b.

As can be seen in Figure 75, eleven microbead clusters are packed quite dense with respect to each other. The lack of free space accompanied by the extended size of the clusters imposed a restriction on the maximum number of microbeads, which could be resolved by DBSCAN. This limitation can be overcome in two ways. First, the QD labelling process can be further optimized to enable more homogeneous loading of the microspheres with QDs. It should result in a narrower distribution of the signals, thus making the clusters smaller. Another approach implies that the microbeads are

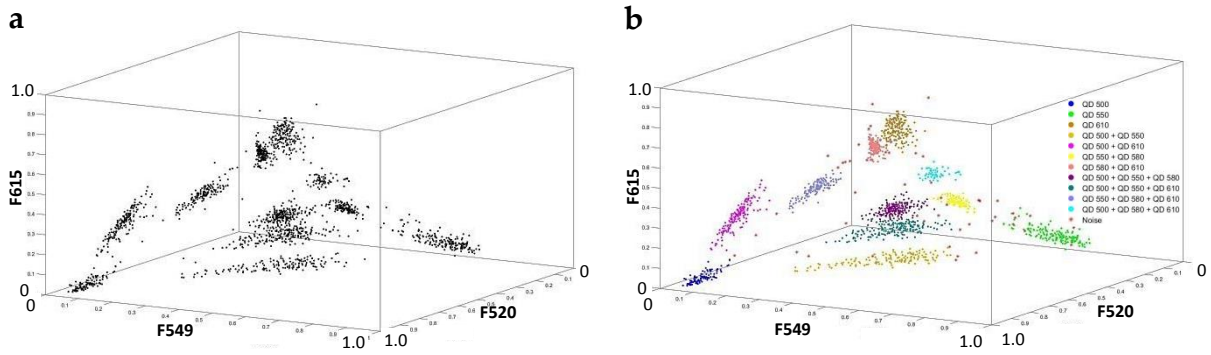

Figure 75. DBSCAN clustering of eleven types of QD labelled microbeads: (a) allocation of data points according to the microbead signals normalized for three fluorescence channels; (b) eleven clusters of microbeads automatically assigned to the respective QD labels.

considered in a space of a higher dimensionality. In other words, an additional fluorescence channel can be implemented to resolve the neighboring clusters.

The performance of the clustering algorithm was analyzed on a data set of in total 2 000 microbeads of 11 different types. The experiment was planned in such a way so that the types of the microbeads were known in advance. It enabled an estimation of the error rates of identifying the microbeads as outliers, as well as the error rates of identifying the microbeads as of another type (Table 13).

Table 13. Error rates of DBSCAN clustering.

QD label	Error rate of identifying as noise	Error rate of identifying as a wrong label
QD 500	0.9 %	0.0 %
QD 550	6.7 %	0.0 %
QD 610	5.3 %	0.0 %
QD 500 + QD 550	3.5 %	0.7 %
QD 500 + QD 610	1.1 %	0.0 %
QD 550 + QD 580	2.0 %	0.7 %
QD 580 + QD 610	1.6 %	0.0 %
QD 500 + QD 550 + QD 580	2.3 %	0.0 %
QD 500 + QD 550 + QD 610	2.9 %	0.5 %
QD 500 + QD 580 + QD 610	5.8 %	0.0 %
QD 550 + QD 580 + QD 610	0.5 %	0.0 %

As can be seen in Table 13, the error rates of identifying the microbeads as outliers were significant and ranged between 0.5 % and 6.7 %. These microbeads would be assigned "?" values when generating a peptide library, which means that the type of the amino acid derivative in a given position is not defined. At the same time, the error rates of identifying the microbeads as of another type were relatively low (0.2 %). The error rates could considerably decrease by improving the homogeneity of the QD labelled microbeads, by implementing an additional fluorescence filter, or by decreasing the number of microbead types.

4.6 Extraction and Coupling

4.6.1 Amino Acid Spot Profile

Analysis of amino acid spots was essential for interpretation of the experimental results on the monomer extraction from the microbeads and their coupling to the functionalized substrate. Each spot was characterized by two parameters that were derived from its cross section profile measurement (Figure 76).

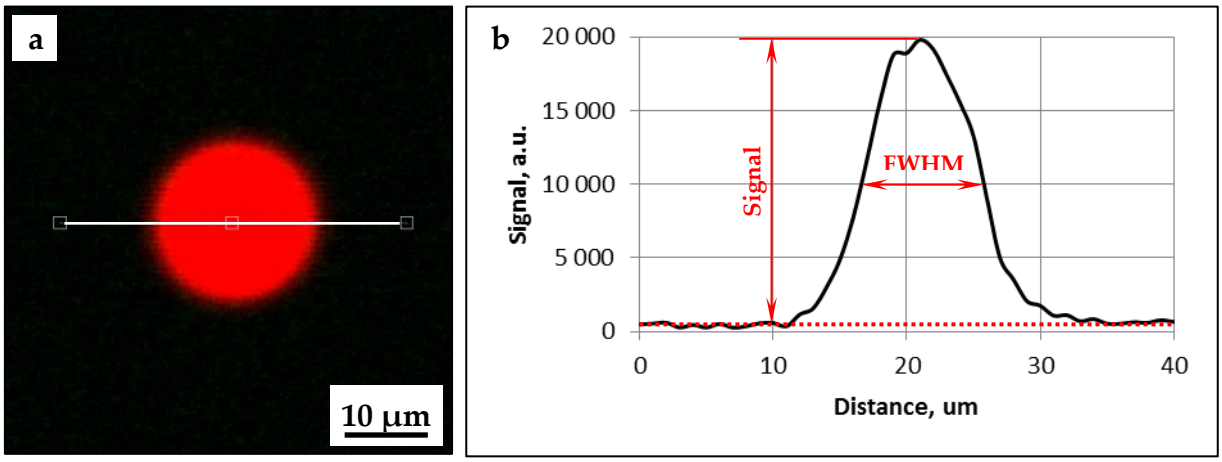

Figure 76. Cross section profile of an amino acid spot: (a) fluorescence image of an amino acid spot with a cross section line; (b) a cross section profile of the amino acid spot.

In most cases, the spot profile had a bell curve shape and could be approximated by a Gaussian function. The height of the background-corrected bell curve was treated as a spot signal and was considered proportional to the surface concentration of the coupled amino acids. The higher coupling yields were associated with stronger spot signals, provided that other factors remained the same. The coupling yield was

estimated as the ratio between the spot signal and the reference signal associated with an excessive amount of monomers coupled from their solution in DMF. Another characteristic value, the diameter of the amino acid spot, was assigned to the FWHM of the background-normalized bell curve. The spot diameter defined the degree of amino acid diffusion during their extraction and coupling.

4.6.2 Optimum Solvent for Amino Acid Extraction

Microbeads containing 5 % (m/m) of Fmoc-Gly-OPfp were used in a series of experiments to identify the most suitable organic solvent for amino acid extraction. The samples were deposited onto flat functionalized substrates and exposed to the saturated vapor of three individual organic solvents (acetone, DCM, and DMF) five times for 1 min each with intermediate pauses of 1 min. Amino acid coupling was performed in the oven at 90 °C for 60 min. The coupled amino acids were fluorescently labelled with NHS ester dye. The mean spot signals and the mean spot diameters were estimated upon fluorescence scanning of the substrates (Table 14).

Table 14. Effect of organic solvent nature on amino acid diffusion and coupling.

Solvent	Spot intensity, 1000 x a.u.	Spot diameter, μm	Spot intensity/ diameter ratio
DMF	15.0 ± 3.8	18.0 ± 2.0	0.8
Acetone	21.4 ± 1.9	18.1 ± 1.9	1.2
DCM	30.4 ± 2.9	17.8 ± 1.5	1.7

As can be seen from Table 14, the mean spot intensity ranged between $15.0 \cdot 10^3$ a.u. and $30.4 \cdot 10^3$ a.u. depending on the organic solvent used for amino acid extraction from the microbeads. The highest mean signal of $30.4 \cdot 10^3$ a.u. was obtained in case the amino acid extraction was performed in DCM vapor, whereas the amino acid mean signals due to extraction in acetone and DMF were $21.4 \cdot 10^3$ a.u. and $15.0 \cdot 10^3$ a.u., respectively. The difference in spot intensity can be explained by various extraction rates of the monomers from the microbeads of a similar composition. Two aspects mainly define whether the solvent is suitable for the amino acid extraction. First, the cross-linked PMMA matrix has to swell to release the embedded amino acid derivatives. Second, the solubility of the amino acid derivatives has to be good

enough to enable their diffusion to the functionalized surface. DCM meets both requirements to a greater extent compared to acetone and DMF.

The solvent nature did not cause a big difference in amino acid spot diameters, which ranged on average between 17.8 μm and 18.1 μm. It was expected that the organic solvents with an expressed tendency to wet the surface (DMF) would enhance the diffusion of the extracted monomers, resulting in larger amino acid spots. However, the extraction process time was not sufficient to observe this effect.

The amino acid spot intensity and diameter are defined not only by the nature of the organic solvent, but they also depend on the extraction duration. The aim of this series of experiments was to select such a solvent, which enables the highest spot signals within limited amino acid diffusion. Therefore, the ratio of the spot signal to the spot diameter was used as the criteria to select a proper solvent for the monomer extraction. As can be seen in Table 14, DCM demonstrated the best performance and was considered to be the optimum solvent.

4.6.3 Optimum Duration of Amino Acid Extraction

In the next series of experiments, the process duration was optimized for amino acid extraction in saturated DCM atmosphere. As in the previous series, the microbeads containing 5 % (m/m) of Fmoc-Gly-OPfp were applied onto a flat functionalized substrate. Amino acid extraction was performed five times for the periods of 0.5 min, 1.0 min and 2.0 min each with intermediate pauses of 1 min. Thereafter, the substrate was placed in the oven at 90 °C for 60 min to enhance the amino acid coupling to the surface. Staining of the coupled amino acids was performed with NHS ester dye. After fluorescence scanning, the mean spot signals and spot diameters were estimated (Table 15).

Table 15. Effect of extraction process duration on amino acid diffusion and coupling.

Duration, min	Spot intensity, 1000 x a.u.	Spot diameter, μm	Spot intensity/ diameter ratio
0.5	42.5 ± 4.5	5.4 ± 0.4	7.9
1.0	33.2 ± 1.4	20.0 ± 0.9	1.7
2.0	28.5 ± 1.7	49.6 ± 2.9	0.6

The data shown in Table 15 contradicts to the hypotheses that the longer extraction times result in higher coupling yields and larger spot diameters. Indeed, the mean spot diameter increases as the extraction period becomes longer, whereas the spot intensity gradually abates. The longer the substrate remains in the saturated gas atmosphere, the larger amount of organic solvent condensates at the contact point of the microbead to the surface. It enhances the swelling of the microbead, the release of the amino acid derivatives, as well as their diffusion over the functional layer. Due to their spreading over the functional layer, the surface concentration of the amino acid derivatives decreases, resulting in a lower spot intensity. In fact, the integral signal over the spot area, associated with the total amount of the extracted and coupled monomers, increases as the process duration becomes longer. Therefore, shorter process durations are preferable if the diameter of the amino acid spots ranges between 15 μm and 30 μm. The spot size constraints are due to the fact that the monomers, extracted from the microbeads, should homogeneously spread over the bottom of the microwell and not diffuse to the neighboring microstructures. This requirement was met in case the amino acid extraction period was 1 min.

4.6.4 Optimum Scheme of Amino Acid Extraction

In order to enhance the coupling of the amino acid derivatives, it was suggested to perform the extraction process multiple times for 1 min each. Microbeads with 5 % (m/m) of Fmoc-Gly-OPfp were deposited onto several flat functionalized substrates, which were independently placed into the extraction chamber 3, 5, 7, 10, and 15 times for 1 min each with their intermediate removal for 1 min. The resulting mean spot signals and diameters were measured and listed in Table 16.

Table 16. Effect of extraction scheme on amino acid diffusion and coupling.

Scheme, 1 min x repetitions	Spot intensity, 1000 x a.u.	Spot diameter, μm	Spot intensity/ diameter ratio
1 min x 3	24.3 ± 1.5	15.3 ± 0.9	1.6
1 min x 5	34.4 ± 2.9	21.9 ± 1.1	1.6
1 min x 7	31.6 ± 4.0	25.4 ± 1.4	1.2
1 min x 10	28.9 ± 4.4	28.9 ± 1.3	1.0
1 min x 15	27.8 ± 2.6	30.1 ± 1.9	0.9

The initial hypothesis was that in each iteration, an additional amount of amino acids derivatives could be extracted from the microbeads, resulting in a higher coupling yield without considerable spreading of the monomers. The data shown in Table 16 indicates that the correlation between the spot signal and the number of process repetitions is more complex than the direct relationship between the spot diameter and the number of process cycles. By increasing the number of repetitions from 3 to 15, the spot diameter gradually increased from 15.3 μm to 30.1 μm, whereas the spot intensity first increased from $24.3 \cdot 10^3$ a.u. to $34.4 \cdot 10^3$ a.u. for 5 repetitions and then slowly decreased to $27.8 \cdot 10^3$ a.u. Starting from 5 repetitions, the spot signal decreased due to the fact the extracted amino acid derivatives diffused over a larger area defined by the spot diameter. In case of 3 repetitions, the amino acid extraction rate was not yet sufficient to result in a high surface density of the monomers. Hence, the optimum confinement of the amino acid derivatives within the microwells could be achieved by extracting the monomers 5 times for 1 min each.

4.6.5 Extraction in Microstructures

The optimum extraction parameters were tested on microbeads with 5 % (m/m) of Fmoc-Gly-OPfp deposited into the microwells of the microstructured functionalized substrate. Extraction of the amino acid derivatives was performed in the chamber with saturated DCM atmosphere for 1 min periods repeated 5 times with intermediate removal of the substrate for 1 min. The coupling, fluorescence staining and imaging were performed according to the standard procedures. The resulting fluorescence pattern is depicted in Figure 77.

The filing rate of the microstructures was intentionally kept low to verify whether the amino acid derivatives diffused to the neighboring microwells during extraction and coupling steps. The qualitative analysis of the fluorescence image indicates that the extracted amino acids were confined to the microwells, whereas their diffusion over the top surface was prevented. The spot signals were strong and homogeneous. These results confirm that the parameters of the amino acid extraction optimized for the flat functionalized substrates were also suitable for the microstructured surfaces.

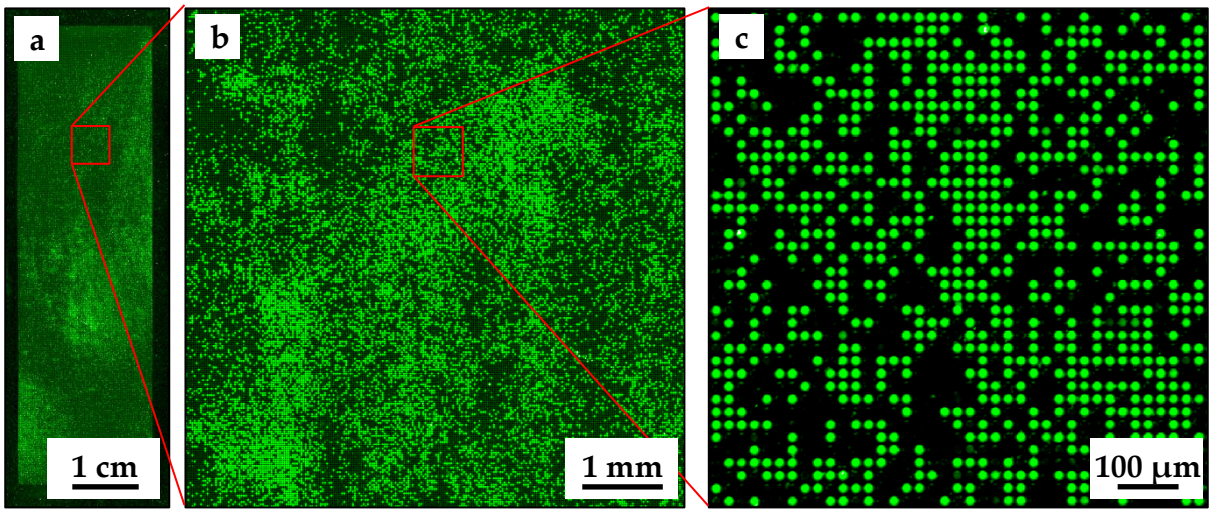

Figure 77. Fluorescence pattern generated by stochastic deposition of microbeads carrying Fmoc-Gly-OPfp and subsequent extraction and coupling of the monomers in the microwells of a microstructured substrate, followed by fluorescence staining with TAMRA: (a) full-size image; (b) (c) image fragments. The fluorescence signal is proportional to the surface concentration of the coupled amino acid derivatives. The filling rate was reduced on purpose to verify the events of amino acid diffusion into the neighboring empty microwells.

In a similar way, the optimum extraction conditions were confirmed for all 20 types of microbeads carrying different proteinogenic amino acid derivatives. The microbead samples with the amino acid content defined in Table 8 were individually deposited into the microwells of the microstructured substrate. Amino acid extraction was performed in DCM chamber 5 times for 1 min each with intermediate removal of the substrate from the chamber for 1 min. The coupling, staining, and fluorescence imaging resulted in amino acid spots confined to the microwells of the microstructured substrate, which enabled us to conclude that the optimum extraction parameters were in general suitable for the stochastic peptide microarray manufacturing.

4.7 Microbead Removal

4.7.1 Microbead Residues

The most efficient method of microbead removal was based on sonication of the microstructured substrate in an organic solvent. The removal rate depended on the nature of the organic solvent, sonication power and process duration. The removal

rate of nearly 100 % was achieved when performing the process in DCM for 5 min three times. However, every time less than 0.01 % of the microwells were blocked by the microbeads regardless of the removal process parameters (Figure 78).

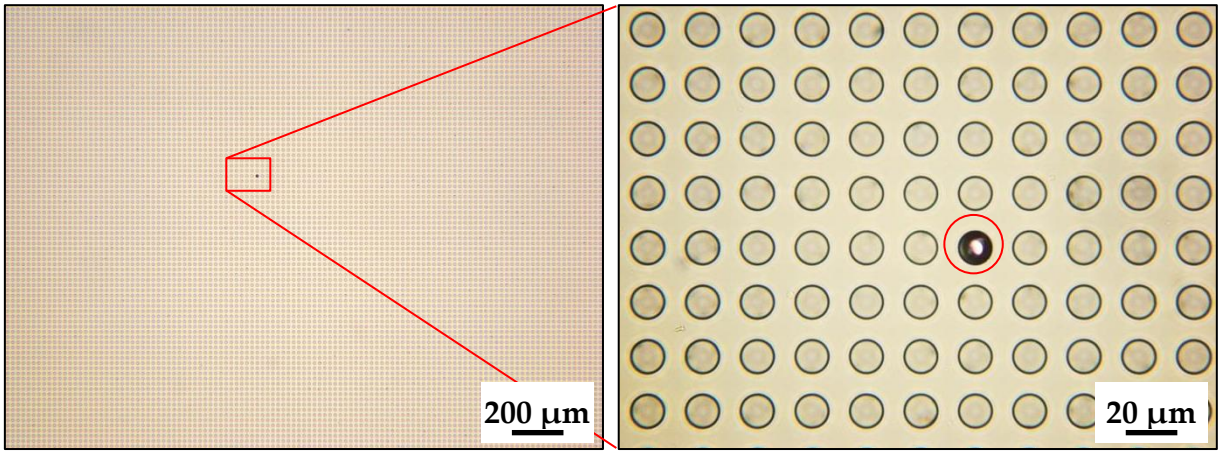

Figure 78. Microbead residues after washing the substrate in organic solvent in ultrasonic bath. Due to the fact the fine fraction of the microspheres had diameters bigger than 12 µm, they got stuck in the microwells without being able to be removed.

Even though the microbeads were based on the cross-linked PMMA microspheres with extremely narrow size distribution, their fine fraction had a size matching the diameter of the microwells. During their deposition, the microbeads with the size of 12 µm were pushed into the microwells by mechanical force. Later on, it was impossible to remove these microbeads from the microwells by any of the tested methods. In case of sonication, the adhesion of the microbeads to the walls of the microwells was higher than the mechanical impact of the acoustic waves.

In case some microwells are blocked by microbeads in a certain process step, the synthesis of the respective peptides undergoes termination. These microwells are considered to be empty in the next process iterations since the blocking microbeads become deprived of any QD labels during multiple washing steps in DCM. Therefore, the peptide sequences in the library file should match the amino sequence in the respective microwells.

4.7.2 Microstructure Stability

An attempt to increase the sonication power improved the microbead removal rates to a certain extent. However, starting from a certain level of sonication power, the microstructures underwent multiple destructions (Figure 79).

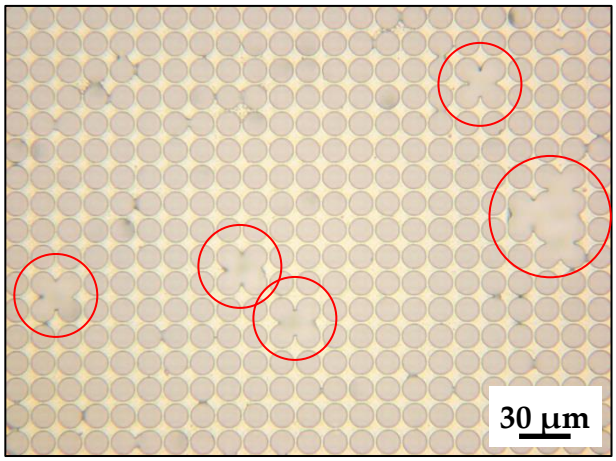

Figure 79. Multiple defects of the microstructures due to the mechanical impact of the ultrasonic waves. The stability of the microstructures depends on the thickness of the walls forming the microwells, as well as on the power of the ultrasonic waves and the process duration.

The stability of the microstructures mainly depends on the spacing between two microwells. The thicker the walls of the microwells were, the more stable they were against the mechanical impact of ultrasonic waves. For a given type of microstructures, the parameters of the microbead removal were optimized in such a way so that the microwells remained intact.

4.8 Prototype Microarray

4.8.1 Immunostaining

After the stochastic peptide microarray prototype was incubated with fluorescently labelled anti-HA antibodies (conjugated with Cy3 dye) and anti-FLAG antibodies (conjugated with Cy5 dye), it was scanned in the corresponding fluorescence channels 582/75 (green channel) and 677/45 (red channel). Figure 80 depicts fragments of the acquired fluorescence image.

The majority of the spots contain randomly synthesized peptides of various length. Some of these peptides demonstrate a certain affinity to the fluorescently labelled antibodies. The spots containing such peptides will be characterized by a fluorescence signal in the respective channel, which depends on the concentration of the peptides in the microwell and their affinity to the antibodies. Black spots represent the microwells that either do not contain any peptides or contain peptides with no affinity to the analyte molecules.

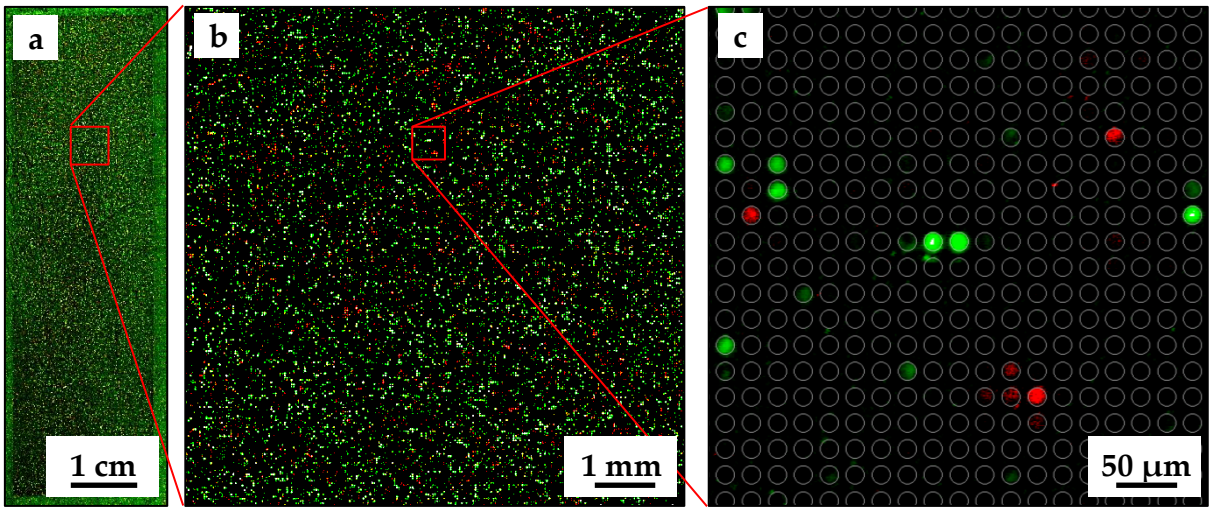

Figure 80. Fluorescence image of the prototype microarray incubated with fluorescently labelled anti-FLAG antibodies (conjugated with Cy5) and anti-HA antibodies (conjugated with Cy3): (a) full-size image; (b) (c) image fragments. The fluorescence signal depends on the concentration of the peptides in the microwell and their affinity to the antibodies.

A qualitative analysis of the image indicates that the prototype microarray contains stochastically synthesized peptides demonstrating an affinity for both types of antibodies. The fluorescence spot signals are confined to the respective microwells, whereas the shape of the fluorescence spots is nearly circular. It means that the manufacturing of the prototype microarray can be considered successful in terms of generating biologically relevant random peptides on the substrate. However, an additional quantitative analysis is required to characterize the microarray manufacturing process.

4.8.2 Characteristics of Manufacturing Process

The peptide library of the prototype microarray originates from a stochastic microbead deposition prior to each step of amino acid coupling. Brief statistics on the filling rates of the microstructures is shown in Table 17.

The filling rate in each synthesis cycle was intentionally kept low to enable truncated analysis of the target epitopes. It ranged between 66.6 % and 84.9 % for the first eight layers. For the last layer, the filling rate was intentionally reduced to nearly 50 % to balance the synthesis probabilities of the target FLAG-epitope (consisting of only eight amino acid residues) and HA-epitope (consisting of nine amino acid residues).

Table 17. General statistics on microbead deposition during manufacturing process.

Synthesis layer	Microwells			
	filled with "blue" μ-beads	filled with "green" μ-beads	empty	undefined
1	44.0 %	39.4 %	17.9 %	0.3 %
2	39.8 %	34.6 %	25.2 %	0.3 %
3	81.2 %	0.0 %	18.6 %	0.1 %
4	39.5 %	35.4 %	25.0 %	0.1 %
5	32.1 %	34.1 %	33.8 %	0.1 %
6	33.4 %	33.1 %	33.4 %	0.1 %
7	0.0 %	70.5 %	29.5 %	0.1 %
8	42.1 %	42.8 %	15.1 %	0.1 %
9	0.0 %	47.2 %	52.6 %	0.2 %

In each synthesis cycle that implied deposition of two types of microbeads the ratio between the "green" and the "blue" microbeads was close to one-to-one with minor differences in the first, second, and fourth layers. It could potentially lead to various frequencies of the peptides stochastically synthesized on the substrate. As can be seen in Table 17, not all microbeads could be differentiated by the DBSCAN algorithm. The number of undefined microwells was relatively low and ranged between 0.1 % and 0.3 %.

Since the filling rate in each synthesis cycle was fairly low, a multitude of truncated peptides was synthesized on the microarray. The overall statistics on the number of peptides of a variable length is shown in Table 18. In general, the results comply with the data on the filling rates listed in Table 17. For instance, 17.9 % of the microwells did not contain any peptides due to the lack of the microbeads already in the first coupling iteration. Eventually, only 5.3 % of the microwells contained 8-mer peptides, whereas 9-mer peptides were synthesized in 4.8 % of the microwells.

Table 18. General statistics on peptide chains stochastically synthesized on the prototype microarray.

Peptide length*	Absolute number of sequences	Relative number of sequences
0	498 212	17.9 %
1	560 361	20.1 %
2	305 667	11.0 %
3	354 631	12.7 %
4	365 349	13.1 %
5	237 167	8.5 %
6	137 022	4.9 %
7	50 139	1.8 %
8	147 283	5.3 %
9	134 169	4.8 %
Total	2 790 000	100 %

(*) – in number of amino acid residues.

As a result of stochastic peptide synthesis, in total 64 types of 9-mer peptides had to be synthesized on the substrate (2^7 sequences, where 7 is the number of synthesis cycles involving two types of amino acid derivatives). In an ideal stochastic process, the output frequencies of the peptides synthesized in various microwells on the substrate would be equal. In a real process, an unequal ratio of the microbeads of various types applied onto the substrate in a mixture can influence the probabilities of various peptides synthesized. Figure 81 illustrates the resulting frequency distribution of 64 types of defined 9-mer peptides stochastically synthesized on the prototype microarray. The peptides were assigned indices according to the descending order of their frequencies.

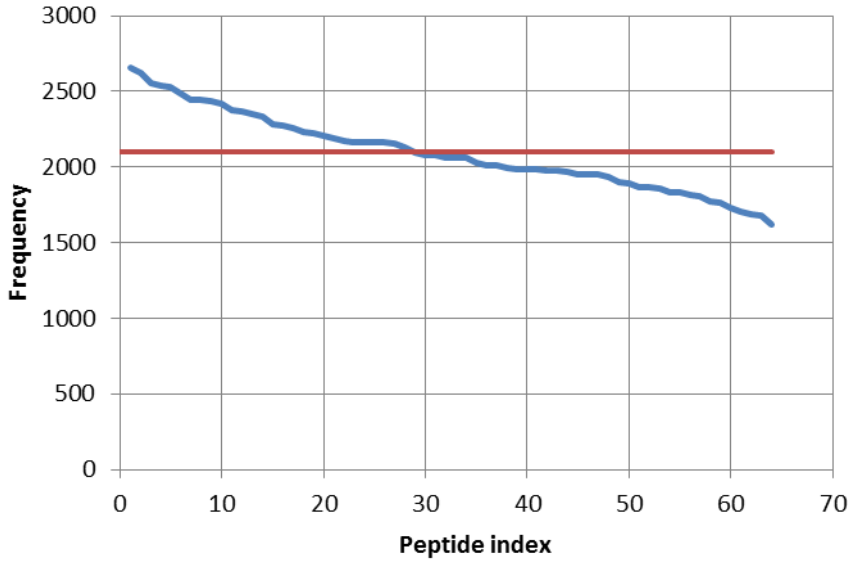

Figure 81. Frequency distribution of 9-mer peptides stochastically synthesized on a prototype microarray. The blue line corresponds to the actual frequency distribution, whereas the red line represents an ideal stochasticity of the synthesis process.

Various 9-mer peptides were synthesized on a prototype microarray with different output frequencies. The ratio of the most frequent random sequence to the rarest was approximately 1.7. The shift in frequencies was due to the non-equal distribution of the microbeads of two different types in the respective synthesis cycles (see Table 17). These results enable us to conclude that the stochasticity can be controlled to a certain extent by changing the ratio of the microbeads of various types applied over the substrate in each synthesis cycle.

4.8.3 Distribution of Spot Signals

In total 4 278 microwells with stochastically synthesized FLAG peptides were identified in the prototype microarray library. The signals of these microwells were normalized with respect to the maximum value, sorted in descending order and plotted in a diagram (Figure 82). Similar curves were observed for nearly all biologically relevant peptides and are not shown here to avoid redundancy.

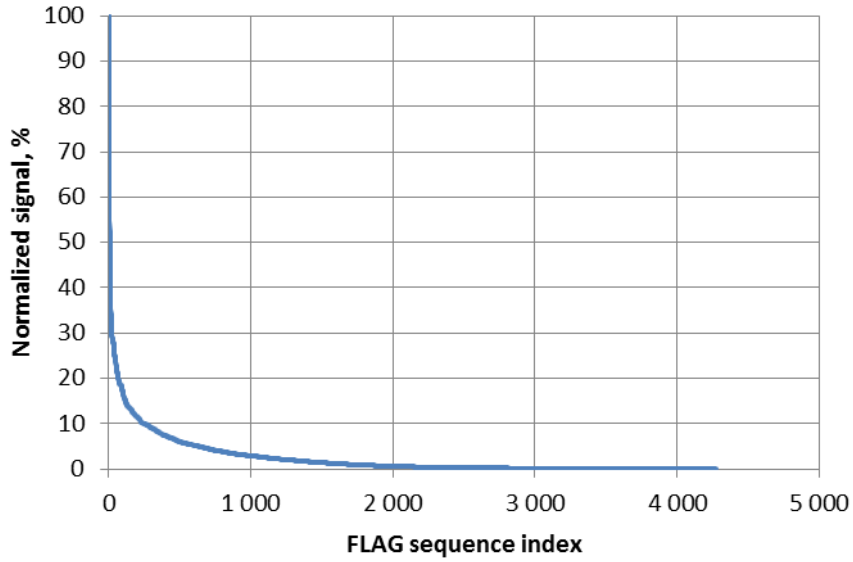

Figure 82. Normalized fluorescence signal of the microwells containing FLAG peptide. In total 4 278 microwells with FLAG peptides were assigned indices according to the descending order of their signals acquired in the fluorescence channel 677/45.

Although the considered microwells were supposed to contain the same type of peptide, their signals ranged between 0 % (absence of signal) and 100 % (strong binding). Moreover, the signal distribution was not in favor of "good" spots: 94 % of the microwells demonstrated normalized signals below 10 %. Since the signal depends not only on the affinity of the peptides to the antibodies but also on their surface concentration, we conclude that the peptide output was extremely low in the majority of the microwells. Such results could be explained by several reasons. First, the coupling yield of every type of amino acid derivatives, extracted from the microbeads, was not perfectly uniform. The variation in the coupling yield could accumulate over nine synthesis cycles, resulting in a significant difference in the product output. Second, after their deposition into the microstructures, the microbeads could be attached to the walls of the microwells without touching their bottom (see Figure 66c). In this case, the amino acid diffusion profiles would have their maximum on the side surface of the microwells, whereas the bottom of the microwells would not be covered completely by a sufficient amount of the monomers. It would result in an extremely low coupling yield in the respective microwells in a given synthesis cycle, if not in a complete termination of the peptide synthesis. Unfortunately, it was impossible to identify the localization of the contact point between the microbeads and the substrate surface from the fluorescence

images. Therefore, this hypothesis remains unproven. Other circumstances, such as an inhomogeneity of the functional layer or its local destruction due to mechanical impact of the microbeads or ultrasonic waves, as well as errors in microbead decoding could contribute to the broad distribution of fluorescence signals obtained for the identical peptide spots.

4.8.4 Characteristic Signals of Synthesized Peptides

In order to derive relevant information from the generated set of experimental data, it was suggested to characterize each type of peptide by the median signal value calculated for the sixteen "brightest" spots. It enabled us to remove from consideration those peptide spots, which were subjected to adverse effects during prototype manufacturing. In each fluorescence channel, these median values were normalized for all 9-mer sequences, sorted in the descending order and plotted in diagrams (Figure 83 and Figure 84).

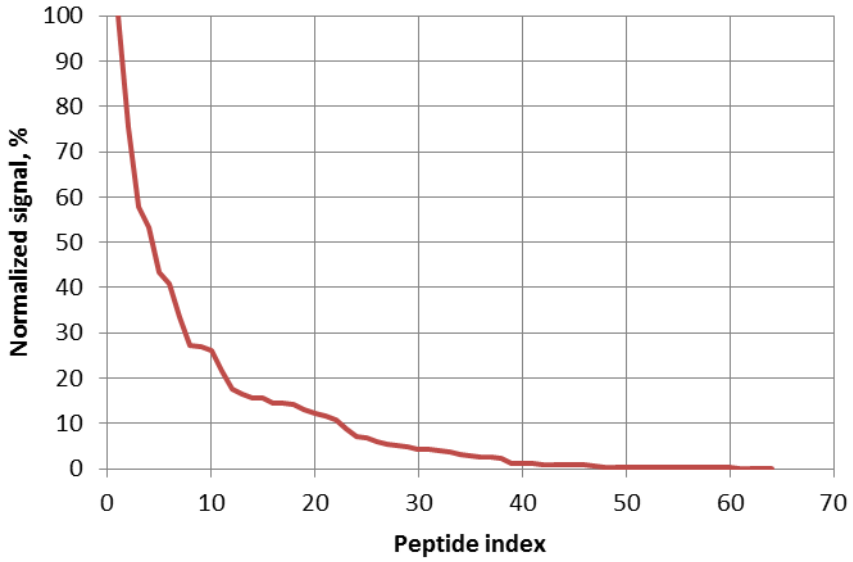

Figure 83. Normalized signal distribution of 64 types of 9-mer peptides synthesized on the prototype microarray in the fluorescence channel 677/45 corresponding to Cy5 conjugated anti-FLAG antibody.

As can be seen from Figure 83, the fluorescence signal exponentially decays while moving from the peptides with the highest affinity to the anti-FLAG antibody to the peptides with no affinity to the antibody. As expected, the majority of stochastically synthesized peptides did not interact with the analyte. Ten peptide sequences with the highest spot signals in the respective fluorescence channel are listed in Table 19.

Table 19. Peptide sequences with the highest affinity to the anti-FLAG antibody.

Peptide index	Amino acid sequence	Normalized signal
1	YDYKDDDYK	100.0 %
2	YDYKDDDYA	75.5 %
3	YDYKDDDDA	57.9 %
4	YDYKVDDYK	53.2 %
5	YPYKDDDYK	43.3 %
6	**YDYKDDDDK**	**40.9 %**
7	YDYKVDDYA	33.5 %
8	YPYKDDDYA	27.1 %
9	YPYKVDDYK	27.1 %
10	YDYKDPDYK	26.2 %

The FLAG peptide with the normalized signal of 40.9 % is marked in bold. One can clearly see that the sequences with the highest affinity to the anti-FLAG antibody had common fragments "DYK" in either of the two ends of the chain. Moreover, the sequence with the highest signal contained two DYK fragments.

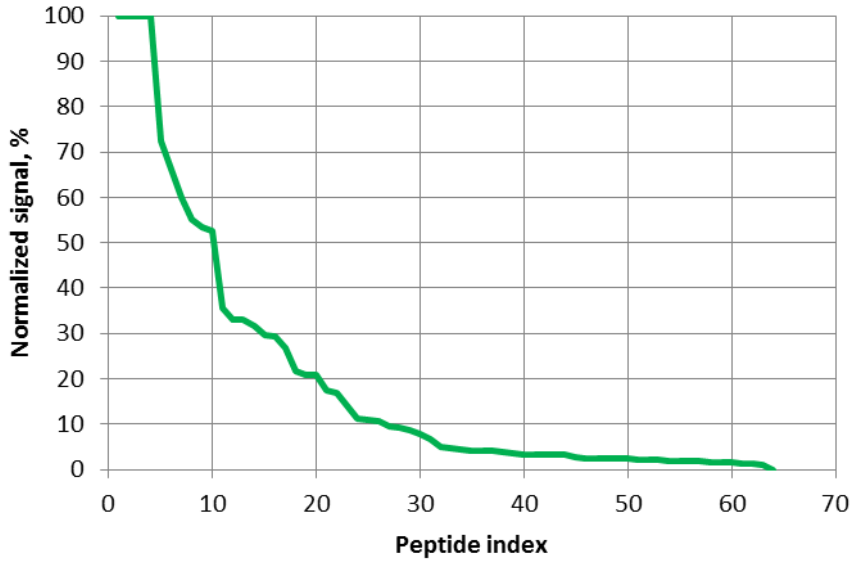

Figure 84. Normalized signal distribution of 64 types of 9-mer peptides synthesized on the prototype microarray in the fluorescence channel 582/75 corresponding to Cy3 conjugated anti-HA antibody.

The diagram, representing the normalized signals of 64 types of 9-mer peptides acquired in the channel 582/75 and sorted in descending order, resembles the diagram with the sorted signals of the same peptides in the channel 677/45. The majority of the random sequences did not demonstrate any affinity to the respective antibodies, whereas four sequences had a similar normalized signal of 100 % due to saturation during fluorescence scanning. Ten peptides with the highest signals in the respective channel are listed in Table 20.

Table 20. Peptide sequences with the highest affinity to the anti-HA antibody.

Peptide index	Amino acid sequence	Normalized signal
1	**YPYDVPDYA**	**100.0 %**
2	YDYDVPDYA	100.0 %
3	YPYDDPDYA	100.0 %
4	YDYDDPDYA	100.0 %
5	YPYDVDDYA	72.5 %
6	YDYDVDDYA	66.1 %
7	YDYKVPDYA	59.8 %
8	YPYKVPDYA	55.2 %
9	YPYDVPDDA	53.5 %
10	YDYDVPDDA	52.5 %

As expected, the target HA peptide demonstrated the highest signal in the fluorescence channel corresponding to the anti-HA antibody. As can be seen, the peptides with the highest spot signals had a common fragment of “DxxDYA”. As soon as any of these relevant amino acids were randomly substituted for another one, the affinity of the peptide considerably decreased.

5 Conclusions and Outlook

Within the scope of the present work, a novel microbead-based stochastic method for manufacturing low-cost high-density peptide microarrays was proposed and developed. It has several distinctive features compared to the other known methods.

First, the underlying principle of self-organization of the microbeads in the microwells of a microstructured substrate does not require the use of expensive high-precision equipment for the amino acid pattern generation. The accuracy and repeatability of the amino acid deposition are ensured by matching the size and shape of the microbeads, carrying the monomers, and the microwells, representing individual spots of the microarray. As a result, the manufacturing capital costs are potentially lower than in case of the alternative manufacturing methods.

Second, each step of peptide synthesis is carried out simultaneously for several million spots on a microarray. By using a mixture of different microbeads, up to 20 types of amino acid derivatives can be distributed into the microwells in a single process step. Moreover, the monomers in each microwell undergo extraction and subsequent coupling at the same time. These factors make the manufacturing time independent of the number of peptides to be simultaneously synthesized.

Third, the suggested method is scalable in terms of the number of peptides that can be displayed on a single microarray. By changing the diameter and pitch of the microstructures and adapting the size of the microbeads, a broad range of peptide spot densities can be achieved. For instance, decreasing the pitch to 10 μm would result in a spot density of 10^6 spots/cm^2, which corresponds to 11 million spots on a standard size substrate. Such extremely high spot densities enable representation of all possible 5-mer peptides (20^5) on a single substrate.

In order to implement the proposed manufacturing concept in practice, several process steps were elaborated and optimized. In most cases, it required resolving inherent physical and technical contradictions caused by an inverse dependence of the process parameters. In the following, these contradictions and their solutions are summarized.

The layout of the microstructured substrate was optimized to facilitate the deposition and removal of microbeads with a diameter of 10 μm. The closer the geometric matching between the microwells and the microbeads was, the higher filling rates could be achieved. However, it impaired the microbead removal from the microwells. The optimum filling and removal rates were obtained for the microstructures with the pitch of 20 μm, the depth of 10 μm and the microwell diameter of 12 μm.

A new architecture of the amino acid carrying microbeads was proposed and implemented. The microbeads had to be rigid enough to survive their deposition to the microwells while being exposed to a mechanical force. At the same time, they had to be soft enough to release amino acid derivatives under certain conditions. This contradiction was resolved by implementing cross-linked PMMA microspheres as solid carriers of amino acid derivatives. Their capacity enabled loading of the monomers in mass fraction of 2 % (m/m) to 3 % (m/m).

The microbead deposition method had to be efficient in terms of reaching high filling rates, which could be achieved by implementing higher mechanical force on the microbeads. At the same time, the method had to be gentle enough not to damage the microbeads during their deposition. This contradiction was resolved by using a soft lint-free tissue to deposit the microbeads into the microwells, while the excessive microbeads were removed from the top surface with a compressed air flow. With this approach, the average filling rate of 92.6 % was achieved.

A straightforward approach of decoding the microbead deposition pattern required their sequential deposition with intermediate optical imaging of the substrate. At the same time, the microbead deposition had to be fast and uniform, which implied that the microbeads of different types had to be applied as a mixture at once. This contradiction was resolved by multiplexed encoding of the microbeads with QD labels introduced into the cross-linked PMMA microspheres. A set of four basic QDs and four basic fluorescence filters enabled encoding of 14 types of microbeads.

Special software was developed to enable fast and automatic decoding of the amino acid deposition pattern. It made it possible to identify contaminated microwells, differentiate between filled and empty microwells, as well as classify the microbeads

of various types depending on their unique QD labels. In total 11 types of microbeads could be differentiated with an error rate of 0.2 %.

A new method of amino acid extraction from the microbeads was proposed and optimized. On the one hand, it had to enable a maximum extraction rate to achieve high coupling yields. On the other hand, the diffusion of the extracted amino acid derivatives to the neighboring microwells had to be prevented. The problem was solved by simultaneous and precise deposition of an organic solvent in each microwell due to its capillary condensation from the saturated gas. The process was performed in a special chamber with a saturated DCM atmosphere five times for 1 min each with intermediate removal of the substrate for 1 min.

After the process steps were optimized, the proposed concept was verified in a proof-of-principle experiment. A prototype microarray with 2.79 million spots was manufactured and incubated with the fluorescently labelled anti-FLAG and anti-HA antibodies. The resulting fluorescence pattern confirmed that the peptides demonstrating an affinity to the respective antibodies were stochastically synthesized on the substrate.

A detailed evaluation of the staining results revealed an extremely inhomogeneous distribution of the spot signals representing the same amino acid sequence. Presumably, the extracted amino acid derivatives could not efficiently spread over the bottom of certain microwells due to the fact the microbeads were attached to the sidewalls instead of touching the bottom of the microstructures. Confirming the actual reasons requires further studies.

The proof-of-principle experiment demonstrated that the process stochasticity can be controlled by adjusting the ratio of the microbeads in the mixture applied onto the substrate. By doing so, the probabilities of generating certain amino acid sequences can be shifted in either direction. By employing such an approach of directed stochasticity, one can generate application-specific peptide libraries on the substrate.

Although the suggested approach of peptide microarray manufacturing is conceptually feasible, it requires further improvements and adjustments. In the short term, the microbead manufacturing procedure has to be further optimized to enable a homogenous labelling of the microbeads with QDs. It can be done by implementing an automated pipetting system with a controlled feeding rate of the liquid medium.

At the same time, an additional pair of a QD and a fluorescence filter can be introduced to expand the set of microbeads that can be differentiated by DBSCAN.

The microbead deposition approach can be further elaborated to achieve higher filling rates of the microwells. For this purpose, paramagnetic nanoparticles can be introduced into the cross-linked PMMA microspheres, which should enable microbead deposition in a dynamic magnetic field. The microbeads will be exposed to a limited force exceeding their adhesion to the surface, thus eliminating the risk of their fracture of cross-contamination.

In the long-term, the proposed manufacturing procedure can be scaled up. Currently, it takes approximately 2 weeks to manufacture one stochastic microarray with 10-mer peptides. To increase the annual manufacturing throughput from 25 microarrays to 250 microarrays, the process steps have to be carried out in parallel for a set of 10 substrates. It can be done by implementing special chemical chambers that can accommodate multiple slides. At the same time, the microbead deposition process has to be intensified and automated. The remaining bottle-neck step of fluorescence scanning can be performed by multiple scanners in parallel.

The scope of biological applications can be further expanded by implementing cyclic peptide libraries and post-translationally modified peptide libraries. The first task can be solved by adapting the known protocols of peptide cyclization to the current procedure of peptide synthesis in a microarray format. The second task can be addressed by implementing modified amino acid derivatives as individual monomers. For this purpose, new types of monomer carrying microbeads have to be designed and optimized.

The concept for bacteria and cell assays can be developed to enable high-throughput studies of their interactions with randomly synthesized peptides. Each microwell of a stochastic microarray, representing a certain peptide spot, can be treated as an individual reaction chamber. By applying cells of various types into the microwells and cleaving the peptides from the functional surface, the impact of various peptides on the cell cycle can be investigated.

Appendix

A1 List of Amino Acid Derivatives

Amino acid derivative	Molecular weight (g/mol)	Amino acid derivative	Molecular weight (g/mol)
Fmoc-Ala-OPfp	477.88	Fmoc-Leu-OPfp	519.46
Fmoc-Arg(Pbf)-OPfp	814.82	Fmoc-Lys(Boc)-OPfp	634.59
Fmoc-Asn(Trt)-OPfp	762.72	Fmoc-Met-OPfp	537.50
Fmoc-Asp(O*t*Bu)-OPfp	577.50	Fmoc-Phe-OPfp	553.48
Fmoc-Cys(Trt)-OPfp	751.76	Fmoc-Pro-OPfp	503.42
Fmoc-Glu(O*t*Bu)-OPfp	591.52	Fmoc-Ser(*t*Bu)-OPfp	549.49
Fmoc-Gln(Trt)-OPfp	776.75	Fmoc-Thr(*t*Bu)-OPfp	563.51
Fmoc-Gly-OPfp	463.35	Fmoc-Trp(Boc)-OPfp	692.63
Fmoc-His(1-Trt)-OPfp	785.77	Fmoc-Tyr(*t*Bu)-OPfp	625.58
Fmoc-Ile-OPfp	519.46	Fmoc-Val-OPfp	505.43

A2 Microbead Manufacturing

QD labelling of microspheres

1. Disperse 1 g of cross-linked PMMA microspheres in 10 mL of DCM in a 20 mL vial. Close the vial with a cap to prevent evaporation of DCM. Gently stir the dispersion for 30 min to achieve swelling of the microspheres.

2. Add 100 μL of QD solution in chloroform (2.5 mg/mL). Stir the dispersion in the closed vial for 30 min. Replace the dispersion from the vial to a 25 mL beaker.

3. Add 30 mL of acetone dropwise from a burette. Adjust the feeding rate so that the liquid level remains constant (i.e. overcomes the evaporation rate of the solvents).

4. Add 30 mL of ethanol dropwise from a burette. Adjust the feeding rate so that the liquid level remains constant or slowly increases.

5. Stop stirring and let the microspheres sediment. Remove the supernatant with a pipette.

6. Add 20 mL of ethanol and stir the dispersion for 2 min. Stop stirring and let the microspheres sediment. Remove the supernatant with a pipette. Repeat the washing step with ethanol two times.

7. Add 20 mL of acetone and stir the dispersion for 2 min. Stop stirring and let the microspheres sediment. Remove the supernatant with a pipette. Repeat the washing step with acetone two times

Embedding amino acid derivatives into microspheres

8. Add 4 mL of amino acid derivative solution in DCM. The mass per volume fraction (%, m/v) has to be adjusted for each type of monomer (see Table 8).

9. Gently stir the dispersion until a paste-like medium is obtained. Stop stirring and let the paste dry out completely.

10. Transfer the dry particle agglomerates to a falcon tube with 2 steel beads (Ø 5 mm). Perform milling using a vortex shaker until a fine powder is obtained. Place the powder into a falcon tube or a glass vial.

Storage of microbeads

11. Fill the vessel with argon, seal it with Parafilm, and store in a freezer.

A3 Peptide Synthesis

Fmoc deprotection

1. Wash the substrate in DMF for 5 min.
2. Apply a solution of 20 % (v/v) piperidine in DMF for 30 min.
3. Wash two times in DMF for 5 min each.
4. Wash two times in methanol for 3 min each.
5. Wash in DCM for 1 min.

Microbead deposition and image acquisition

6. Apply a mixture of microbeads onto the substrate and spread it with a lint-free tissue over the surface. Remove the excessive microbeads from the top surface using a compressed air flow. Perform intermediate control of microstructure's filling rate using optical microscopy.

7. Perform fluorescence scanning of the substrate in the fluorescence channels corresponding to the QD labels.

Amino acid extraction and coupling

8. Place the substrate into the extraction chamber with pre-saturated DCM atmosphere five times for 1 min each with intermediate removal of the substrate from the chamber for 1 min.

9. Place the substrate into the coupling chamber, fill it with argon and place it in the preheated oven for 60 min at 90 °C.

10. Remove the chamber from the oven and let it cool down to room temperature.

Microbead removal

11. Wash in a solution of 5 % (v/v) MEA in acetone for 2 min in an ultrasonic bath.

12. Wash in acetone for 3 min in an ultrasonic bath.

13. Wash in DCM for 2 min in an ultrasonic bath.

14. Dry the substrate and control the microbead removal rate using optical microscopy.

Capping free amino groups

15. Wash in DMF for 5 min.

16. Apply a solution of 10 % (v/v) acetic anhydrate and 20 % (v/v) DIPEA in DMF for 10 min. Repeat the step with a fresh solution for 10 min.

17. Wash two times in DMF for 5 min.

18. Wash two times in methanol for 3 min.

19. Wash in DCM for 1 min.

In case of the peptide synthesis, repeat the steps 1 – 19 multiple times.

Fmoc deprotection

20. Wash the substrate in DMF for 5 min.

21. Apply a solution of 20 % (v/v) piperidine in DMF for 30 min.

22. Wash two times in DMF for 5 min each.

Capping free amino groups

23. Apply a solution of 10 % (v/v) acetic anhydrate and 20 % (v/v) DIPEA in DMF for 10 min. Repeat the step with a fresh solution for 40 min.

24. Wash two times in DMF for 5 min.

25. Wash two times in methanol for 3 min.

26. Wash in DCM for 1 min.

A4 Side-Chain Group Deprotection

1. Wash the substrate in DCM for 30 min.

2. Apply a mixture of TFA (51 % v/v), DCM (44 % v/v), TIBS (3 % v/v), and H_2O (2 % v/v) three times for 30 min each.

3. Wash in DCM for 5 min.

4. Wash in DMF for 5 min.

5. Apply a solution of 5 % (v/v) DIPEA in DMF for 30 min.

6. Wash three times in DMF for 5 min.

7. Wash two times in methanol for 3 min.

8. Wash in DCM for 1 min.

A5 Immunostaining with anti-FLAG and anti-HA Antibodies

1. Wash the substrate in PBS-T for 10 min.

2. Incubate in Rockland blocking buffer for 30 min.

3. Wash three times in PBS-T for 1 min each.

4. Incubate in the staining solution of anti-FLAG and anti-HA antibodies diluted 1 : 1000 in a mixture of Rockland buffer (10 % v/v) and PBS-T (90 % v/v) for 1 h in the dark.

5. Wash three times in PBS-T for 1 min each.

6. Rinse with Milli-Q.

A6 Fluorescence Staining of Terminal Amino Groups

1. Wash in PBS-T for 10 min.

2. Incubate in the staining solution of TAMRA or DyLight NHS ester in PBS-T in dilution of 1 : 10 000 for 2 h in the dark.

3. Wash two times in PBS-T for 3 min each.

4. Wash in Milli-Q for 1 min.

5. Wash two times in DMF for 5 min each.

6. Wash two times in methanol for 3 min each.

7. Wash in DCM for 1 min.

Bibliography

[1] J. A. DiMasi, H. G. Grabowski and R. W. Hansen, "Innovation in the pharmaceutical industry: New estimates of R&D costs," *J Health Econ.,* vol. 47, p. 20–33, 2016.

[2] BIO, Biomedtracker, Ampilon, "Clinical development success rates 2006-2015," June 2016. [Online]. Available: https://www.bio.org/sites/default/files/Clinical Development Success Rates 2006-2015 - BIO, Biomedtracker, Amplion 2016.pdf. [Accessed January 2017].

[3] D. Scott, A. Bayly, C. Abell and J. Skidmore, "Small molecules, big targets: Drug discovery faces the protein-protein interaction challenge," *Nat Rev Drug Discov.,* vol. 15, pp. 533-550, 2016.

[4] L. Brocchieri and S. Karlin, "Protein length in eukaryotic and prokaryotic proteomes," *Nucleic Acids Res.,* vol. 33, no. 10, p. 3390–3400, 2005.

[5] P. Faccioli, "Investigating biological matter with theoretical nuclear physics methods," *J. Phys.: Conf. Ser,* vol. 336, 2011.

[6] M. Z. Atassi, "The complete antigenic structure of myoglobin: Approaches and conclusions for antigenic structures of proteins," in *Immunochemistry of Proteins. Volume 2*, New York, Plenum Press, 1977, pp. 77-176.

[7] J. M. Bujnicki, Prediction of Protein Structures, Functions, and Interactions, John Wiley & Sons Ltd., 2008.

[8] IUPAC, Compendium of Chemical Terminology, 2nd ed. (the "Gold Book"). Compiled by A. D. McNaught and A. Wilkinson, Oxford: Blackwell Scientific Publications, 1997.

[9] H. Andresen, K. Zarse, C. Grötzinger, J.-M. Hollidt, E. Ehrentreich-Förster, F. F. Bier and O. J. Kreuzer, "Development of peptide microarrays for epitope mapping of antibodies against the human TSH receptor," *J. Immunol. Methods,*

vol. 315, pp. 11-18, 2006.

[10] S. Buus, J. Rockberg, B. Forsströ̈m, P. Nilsson, M. Uhlén and C. Schafer-Nielsen, "High-resolution mapping of linear antibody epitopes using ultrahigh-density peptide microarrays," *Mol. Cell. Proteomics,* vol. 11, no. 15, pp. 1790-1800, 2012.

[11] B. Forsströ̈m, B. B. Axnäs̈, K.-P. Stengele, J. Bu̇hler, T. J. Albert, T. A. Richmond, F. J. Hu, P. Nilsson, E. P. Hudson, J. Rockberg and M. Uhlén, "Proteome-wide epitope mapping of antibodies using ultra-dense peptide arrays," *Mol. Cell. Proteomics,* vol. 13, no. 6, pp. 1585-1597, 2014.

[12] M. Hecker, P. Lorenz, F. Steinbeck, L. Hong, G. Riemekasten, Y. Li, U. K. Zettl and H.-J. Thiesen, "Computational analysis of high-density peptide microarray data with application from systemic sclerosis to multiple sclerosis," *Autoimmun. Rev.,* vol. 11, no. 3, pp. 180-190, 2012.

[13] M. Hecker, B. Fitzner, M. Wendt, P. Lorenz, K. Flechtner, F. Steinbeck, L. Schroder, H. J. Thiesen and U. K. Zettl, "High-density peptide microarray analysis of IgG autoantibody reactivities in serum and cerebrospinal fluid of multiple sclerosis patients," *Mol. Cell. Proteomics,* vol. 15, no. 4, pp. 1360-1380, 2016.

[14] M. Schutkowski, U. Reineke and ReimerU., "Peptide arrays for kinase profiling," *ChemBioChem,* vol. 6, p. 513–521, 2005.

[15] B. T. Houseman, J. H. Huh, S. J. Kron and M. Mrksich, "Peptide chips for the quantitative evaluation of protein kinase activity," *Nat Biotechnol.,* vol. 20, pp. 270-274, 2002.

[16] C. Katz, L. Levy-Beladev, S. Rotem-Bamberger, T. Rito, S. G. D. Rüdiger and A. Friedler, "Studying protein–protein interactions using peptide arrays," *Chem. Soc. Rev.,* vol. 40, pp. 2131-2145, 2011.

[17] R. B. Merrifield, "Solid phase peptide synthesis. I. The synthesis of a tetrapeptide," *J. Am. Chem. Soc.,* vol. 85, no. 14, p. 2149–2154, 1963.

[18] S. A. Kates and F. Albericio, Solid-Phase Synthesis: A Practical Guide, New York: Marcel Dekker, 2000.

[19] R. Frank, "Spot-synthesis: An easy technique for the positionally addressable, parallel chemical synthesis on a membrane support," *Tetrahedron,* vol. 48, no. 42, pp. 9217-9232, 1992.

[20] R. Volkmer, "Synthesis and application of peptide arrays: Quo vadis SPOT technology," *ChemBioChem,* vol. 10, no. 9, p. 1431–1442, 2009.

[21] R. Frank, "The SPOT-synthesis technique. Synthetic peptide arrays on membrane supports - principles and applications," *J. Immunol. Methods,* vol. 267, no. 1, pp. 13-26, 2002.

[22] V. Stadler, T. Felgenhauer, M. Beyer, S. Fernandez, K. Leibe, S. Guttler, M. Groning, K. Konig, G. Torralba, M. Hausmann, V. Lindenstruth, A. Nesterov, I. Block, R. Pipkorn, A. Poustka, R. Bischoff and F. Breitling, "Combinatorial synthesis of peptide arrays with a laser printer," *Angew. Chem. Int. Ed.,* vol. 47, pp. 7132-7135, 2008.

[23] C. Schirwitz, F. F. Loeffler, T. Felgenhauer, V. Stadler, F. Breitling and F. R. Bischoff, "Sensing immune responses with customized peptide microarrays," *Biointerphases,* vol. 7, pp. 1-9, 2012.

[24] "Peptide Laser Printer," PEPperPRINT GmbH, [Online]. Available: https://www.pepperprint.com/technology/peptide-laser-printer/. [Accessed 2 November 2017].

[25] S. Fodor, J. Read, M. Pirrung, L. Stryer, A. Lu and D. Solas, "Light-directed, spatially addressable parallel chemical synthesis," *Science,* vol. 251, no. 4995, pp. 767-773, 1991.

[26] J. B. Legutki, Z.-G. Zhao, M. Greving, N. Woodbury, S. A. Johnston and P. Stafford, "Scalable high-density peptide arrays for comprehensive health monitoring," *Nat. Commun.,* vol. 5, 2014.

[27] D. S. Shin, K. N. Lee, B. W. Yoo, J. Kim, M. Kim, Y. K. Kim and Y. S. Lee, "Automated maskless photolithography system for peptide microarray synthesis on a chip," *J. Comb. Chem.,* vol. 12, no. 4, p. 463–471, 2010.

[28] S. P. Fodor, L. Stryer, J. L. Read and M. C. Pirrung, "Arrays of materials attached

to a substrate". United States Patent US5744305, 6 June 1995.

[29] V. Stadler, R. Kirmse, M. Beyer, F. Breitling, T. Ludwig and F. R. Bischoff, "PEGMA/MMA copolymer graftings: Generation, protein resistance, and a hydrophobic domain," *Langmuir,* vol. 24, no. 15, pp. 8151-8157, 2008.

[30] B. Münster, Entwicklung von Mikropartikeln für die hochdichte kombinatorische Peptidarraysynthese durch laserbasierte Verfahren, Dissertation, Karlsruhe Institute of Technology, Karlsruhe, 2015.

[31] M. A. Walling, J. A. Novak and J. R. E. Shepard, "Quantum dots for live cell and in vivo imaging," *Int. J. Mol. Sci.,* vol. 10, no. 2, pp. 441-491, 2009.

[32] M. Han, X. Gao, J. Z. Su and S. Nie, "Quantum-dot-tagged microbeads for multiplexed optical coding of biomolecules," *Nat Biotechnol.,* vol. 19, no. 7, pp. 631-635, 2001.

[33] H.-Q. Wang, J.-H. Wang, X.-Q. Li, T.-C. Liu, Z.-L. Huang and Y.-D. Zhao, "Multi-color encoding of polystyrene microbeads with CdSe/ZnS quantum dots and its application in immunoassay," *J. Colloid Interface Sci.,* vol. 316, no. 2, pp. 622-627, 2007.

[34] M. Marechal, M. Hermes and M. Dijkstra, "Stacking in sediments of colloidal hard spheres," *J. Chem. Phys.,* vol. 135, no. 3, p. 034510, 2011.

[35] Y. Yin, Y. Lu, B. Gates and Y. Xia, "Template-assisted self-assembly: A practical route to complex aggregates of monodispersed colloids with well-defined sizes, shapes, and structures," *J. Am. Chem. Soc.,* vol. 123, pp. 8718-8729, 2001.

[36] S. S. Shevkoplyas, A. C. Siegel, R. M. Westervelt, M. G. Prentiss and G. M. Whitesides, "The force acting on a superparamagnetic bead due to an applied magnetic field," *Lab Chip,* vol. 7, no. 10, pp. 1294-1302, 2007.

[37] I. S. M. Khalil, J. D. Keuning, L. Abelmann and S. Misra, "Wireless magnetic-based control of paramagnetic microparticles," in *Proceedings of the IEEE RAS/EMBS International Conference on Biomedical Robotics and Biomechatronics (BioRob)*, Rome, Italy, 2012.

[38] V. Bykovskaya, Microstructure-assisted particle pattern generation for high

density peptide arrays, Dissertation, Karlsruhe Institute of Technology, Karlsruhe, 2016.

[39] C. von Bojnicic-Kninski, Entwicklung von optischen Systemen für die kombinatorische Materialablagerung und die großflächige Detektion im Rahmen von Hochdurchsatzverfahren, Dissertation, Karlsruhe Institute of Technology, Karlsruhe, 2018.

[40] A. D. Zimon, Adhesion of Dust and Powder, Consultants Bureau, 1982.

[41] H. Masuda, K. Higashitani and H. Yoshida, Powder Technology: Fundamentals of Particles, Powder Beds, and Particle Generation, CRC Press, 2006.

[42] P. Michler, Single Semiconductor Quantum Dots, Springer Science & Business Media, 2009.

[43] C. D. M. Donega, Nanoparticles: Workhorses of Nanoscience, Springer Berlin Heidelberg, 2014.

[44] C. D. M. Donega, "Synthesis and properties of colloidal heteronanocrystals," *Chem. Soc. Rev.*, vol. 40, no. 3, pp. 1512-1546, 2011.

[45] M. Ester, H.-P. Kriegel, J. Sander and X. Xu, "A density-based algorithm for discovering clusters in large spatial databases with noise," in *Proceedings of the Second International Conference on Knowledge Discovery and Data Mining (KDD-96)*, Portland, 1996.

[46] J. Han and M. Kamber, Data Mining: Concepts and Techniques, Elsevier, 2012.

[47] M. Soustelle, Thermodynamics of Surfaces and Capillary Systems, John Wiley & Sons, 2016.

[48] K. A. Dill and S. Bromberg, Molecular Driving Forces: Statistical Thermodynamics in Chemistry & Biology, Garland Science, 2003.

[49] C. Schirwitz, Purification of peptides in high-complexity arrays, Dissertation, Ruprecht-Karls-Universität, Heidelberg, 2012.

Acknowledgements

I would like to take this opportunity to thank all those who contributed to this work. Without their help, it would not have been possible to achieve the results covered in the present dissertation and left beyond its scope.

For his insights and mentorship, I express my gratitude to Prof. Alexander Nesterov-Müller, who came up with the idea of manufacturing stochastic peptide microarrays. I am also grateful to Prof. Frank Breitling for encouraging an independent thinking and sharing his creative ideas on microarray fabrication.

Many thanks go to the present and former members of the Peptide Array group. In particular, I am grateful to Clemens von Bojnicic-Kninski whom I spent many hours with discussing the concepts of stochastic microarray manufacturing, Dr. Girish Karadka Shankara for his enormous help in surface functionalization and process optimization, Dr. Daniela Mattes for her advice on the chemical aspects of the project, Dr. Valentina Bykovskaya for sharing her experience in generating random particle patterns, Dr. Bastian Münster for sharing his experience in spray drying, Dr. Tobias Förtsch for introducing the dip coating technique, Dr. Felix Löffler, Dr. Laura Weber and Andrea Palermo for their expertise in immunostaining, Dr. Barbara Ridder and Dr. Jakob Striffler for their chemical expertise, Karin Herbster for her assistance in ordering materials and tools.

Special thanks go to the members of the Institute of Microstructure Technology. In particular, I am thankful to Richard Thelen for white light interferometry and atomic force microscopy of various samples, Abrar Faisal for scanning electron microscopy of the microbeads and the microstructured substrates, Dr. Andrey Turshatov for introducing emulsification concept for microbead fabrication.

I would like to thank numerous student assistants who contributed to the project: Gero Käser for experiments on capillary condensation and SPG emulsification, Enrique Llanito for microparticle fabrication using spray drying technique and microbead deposition using a microfluidic channel, Mikhail Gavrish for his attempts to implement the algorithm for image processing and photometric data acquisition,

Manmeet Singh for his experiments on the multiplexed encoding of the microbeads, Pramit Barua for implementing the algorithm of decoding the microbead deposition pattern, Sabbir-Bin Hossain for deriving the photometric data and molecular library of the prototype microarray.

Last but not least, I thank my parents and my family members for their constant support. An especially big thank you goes to my wife Olesya and my daughter Milana who inspire me with their love.

List of Publications

Publications

C. von Bojnicic-Kninski, **R. Popov**, E. Dörsam, F. F. Loeffler, F. Breitling and A. Nesterov-Mueller, "Combinatorial particle patterning," *Adv. Funct. Mater.*, vol. 27, no. 42, 2017.

F. Löffler, T. C. Foertsch, **R. Popov**, D. S. Mattes, M. Schlageter, M. Sedlmayr, et al. "High-flexibility combinatorial peptide synthesis with laser-based transfer of monomers in solid matrix material," *Nat Commun.*, vol. 7, 2016.

C. von Bojnicic-Kninski, V. Bykovskaya, F. Maerkle, **R. Popov**, A. Palermo, D. S. Mattes, L. K. Weber, B. Ridder, T. C. Foertsch, A. Welle, F. F. Loeffler, F. Breitling and A. Nesterov-Mueller, "Selective functionalization of microstructured surfaces by laser-assisted particle transfer," *Adv. Funct. Mater.*, vol. 26, no. 39, pp. 7067–7073, 2016.

Patents

A. Nesterov-Müller, V. Bykovskaya, C. M. von Bojnicic-Kninski, F. F. Löffler, **R. Popov**, B. Ridder, F. Breitling and D. S. Althuon, "Ultra-hochdichte Oligomerarrays und Verfahren zu deren Herstellung". German Patent DE102015117567, 15 October 2015.